

INFORMATION TO USERS

This manuscript has been reproduced from the microfilm master. UMI films the text directly from the original or copy submitted. Thus, some thesis and dissertation copies are in typewriter face, while others may be from any type of computer printer.

The quality of this reproduction is dependent upon the quality of the copy submitted. Broken or indistinct print, colored or poor quality illustrations and photographs, print bleedthrough, substandard margins, and improper alignment can adversely affect reproduction.

In the unlikely event that the author did not send UMI a complete manuscript and there are missing pages, these will be noted. Also, if unauthorized copyright material had to be removed, a note will indicate the deletion.

Oversize materials (e.g., maps, drawings, charts) are reproduced by sectioning the original, beginning at the upper left-hand corner and continuing from left to right in equal sections with small overlaps. Each original is also photographed in one exposure and is included in reduced form at the back of the book.

Photographs included in the original manuscript have been reproduced xerographically in this copy. Higher quality 6" x 9" black and white photographic prints are available for any photographs or illustrations appearing in this copy for an additional charge. Contact UMI directly to order.

UMI

A Bell & Howell Information Company
300 North Zeeb Road, Ann Arbor, MI 48106-1346 USA
313/761-4700 800/521-0600



**EVALUATION OF FLEXIBLE HULL TYPES FOR VERY
LARGE FLOATING STRUCTURES**

**A DISSERTATION SUBMITTED TO THE GRADUATE DIVISION OF
THE UNIVERSITY OF HAWAII IN PARTIAL FULFILLMENT
OF THE REQUIREMENTS FOR THE DEGREE OF**

**DOCTOR OF PHILOSOPHY
IN
OCEAN ENGINEERING**

DECEMBER 1995

**By
Suqin Wang**

Dissertation Committee:

**R. Cengiz Ertekin, Chairman
Kwok F. Cheung
H. Ronald Riggs
Manley St. Denis
Patrick K. Takahashi**

UMI Number: 9615562

UMI Microform 9615562
Copyright 1996, by UMI Company. All rights reserved.

**This microform edition is protected against unauthorized
copying under Title 17, United States Code.**

UMI
300 North Zeeb Road
Ann Arbor, MI 48103

ACKNOWLEDGEMENTS

I would like to express my deepest appreciation to those who have supported and helped me develop the skill to perform this research.

I would like to thank Professor R. Cengiz Ertekin, my advisor and committee chairman, for his guidance and help whenever I needed it. His support will never be forgotten.

I am grateful to Professor H. Ronald Riggs for his constructive suggestions and kind help. I had learnt a lot through the many fruitful discussions with him.

I would like to thank the other members of my committee: Professor Manley St. Denis, for his encouragement during the study and his precious help in shaping my dissertation. The time he spent on the manuscript is highly appreciated. Professor Patrick K. Takahashi, for his kind help in providing me an opportunity of doing research in the area of utilization of ocean resources. Professor Kwork F. Cheung, for his comments and suggestions on this manuscript.

I wish to acknowledge Professor Ludwig H. Seidl, who introduced me to the field of hydrodynamics. I also wish to acknowledge Professors Yingzhong Liu and Yousheng Wu for their advice, suggestions and kind help during their visit of the department of Ocean Engineering.

I would also like to acknowledge my indebtedness to Dr. C. J. Reddy, NASA-Langley Research Center, for his providing me with the iterative solver for the full matrix case.

I also appreciate the assistance I have received from my fellow students, Arvind Tangirala, Qiao Jin, Pascal Ferier, Sander van Stiphout, Balakrishna Padmanabhan and Hari Sundararaghavan, and from Dr. Xiling Che.

Thanks are also due to Edith Katada, Secretary of the Department of Ocean Engineering, for her thoughtful help during my studentship at the University.

Special thanks are given to my husband Feng Guo and my daughter Xinmiao for their support and encouragement, understanding and patience.

The financial support, in the form of research assistantship, from the U.S. National Science Foundation under Grant Nos. BES-9200655 and BCS-8958346, is gratefully acknowledged, as is the financial support received from the Hawaii Natural Energy Institute.

ABSTRACT

In this study, Very Large Floating Structures (VLFS) of different hull forms (semi-submersible and mat-like) are evaluated on the basis of their hull motions and structural responses. Some suggestions and recommendations are provided for selecting a configuration. The theory of linear hydroelasticity is applied to the analysis. The success of such an analysis of VLFS by means of available computers rests on the development of three efficient hydroelastic analysis methods that significantly reduce the CPU time and the required computational storage.

The first method employs the modified Morison's equation and linear structural dynamic theory. The hydrodynamic coefficients in the modified Morison's equation, are obtained using the extended MacCamy & Fuchs' method for the columns and the strip theory for the pontoons, respectively. The method predicts better results at higher wave frequencies than does the Morison's equation method.

In the second method, the simplified zero-draft Green function is employed in the hydrodynamic analysis and in the structural analysis a mat-like floating body is modeled as an equivalent floating plate. These two efforts result in significant CPU savings.

The mathematical model of the last method employs a three-dimensional hydroelasticity theory. Two techniques are introduced to increase the computational efficiency of this method. One is related to the convergency of the Green function and the other involves the use of an iterative sparse solver for the linear system of

equations. This method is especially efficient for the analysis of a VLFS in terms of CPU and storage. Hence, it has been possible to analyze the hydroelastic response of a VLFS with the available computer resources.

TABLE OF CONTENTS

	<u>Page</u>
ACKNOWLEDGEMENTS	iii
ABSTRACT	v
LIST OF TABLES	xii
LIST OF FIGURES	xiii
LIST OF SYMBOLS	xvii
CHAPTER 1 INTRODUCTION	1
1.1 Background	1
1.2 Hydroelasticity Concept	3
1.3 Review of the previous work on hydroelasticity	4
1.4 Objective of the present study	7
CHAPTER 2 STRUCTURAL DYNAMICS OF A FLOATING BODY	10
2.1 Overview	10
2.2 Formulation of structural dynamics	10
2.3 Direct and modal superposition methods	14
CHAPTER 3 THREE-DIMENSIONAL POTENTIAL THEORY	19
3.1 Overview	19

3.2	Governing equation and boundary conditions	21
3.3	Incident wave potential	23
3.4	Body boundary conditions of the radiation and diffraction potentials	24
3.4.1	Body boundary condition for the diffraction potential	24
3.4.2	Body boundary condition for the radiation potential	25
3.5	The Green function method	27
3.5.1	Fredholm integral equation	28
3.5.2	Source distribution method	30
3.6	The constant panel method	31
3.7	Generalized hydrodynamic forces	33
3.8	Generalized hydrostatic force	35
3.9	Utilization of geometric symmetry of the wetted body surface	37
3.9.1	Generalized wave exciting forces and hydrodynamic coefficients	41
3.9.2	Restoring coefficients	43
CHAPTER 4 HYDROELASTIC RESPONSE OF A FLOATING BODY		45
CHAPTER 5 THE MODIFIED MORISON'S EQUATION METHOD		47
5.1	Overview	47
5.2	Structural model in Morison's equation method	48

5.3	Hydrostatic forces	50
5.4	Hydrodynamic forces	51
5.5	The equivalent hydrodynamic coefficients	53
5.5.1	Columns	53
5.5.2	Pontoons	58
5.6	Applications of the modified Morison's equation method to the analysis of semi-submersible systems	61
5.6.1	Single column results	63
5.6.2	The results of semi-submersible systems	64
5.7	Final remarks	66

CHAPTER 6 EFFICIENT HYDROELASTIC ANALYSIS METHOD FOR A		
	MAT-LIKE PLATFORM OF SHALLOW DRAFT	67
6.1	Overview	67
6.2	Structural and hydrodynamic models	68
6.3	The zero-draft Green function	71
6.4	Solution procedure	72
6.5	Verification of the method	74
6.6	Application of the shallow-draft Green function method to a mat-like runway	77
6.6.1	Structural model of the runway	77
6.6.2	Hydroelastic responses of the runway	78

6.7 Final remarks 79

CHAPTER 7 EFFICIENT HYDROELASTIC ANALYSIS METHOD FOR A

FLOATING BODY OF ARBITRARY SHAPE 81

7.1 Overview 81

7.2 Equations of motion 83

7.3 The Green function method for hydrodynamic analysis 84

7.4 Calculation of the three-dimensional Green function and its
derivatives 86

7.5 Iterative sparse solver 89

7.6 Verification of the present method 91

7.7 CPU savings by use of the Green function cut-off criterion and the
iterative sparse solver 91

7.7.1 CPU savings by the use of the cut-off criterion 92

7.7.2 CPU savings by use of the iterative sparse solver 94

7.8 Final remarks 97

CHAPTER 8 COMPARATIVE ANALYSIS OF SEMI-SUBMERSIBLE AND MAT-

LIKE FLOATING STRUCTURES 99

8.1 Overview 99

8.2 Structural model of semi-submersible and mat-like systems 100

8.3 Mode shapes of the dry structures 102

8.4 Numerical results of structural displacement and stress responses	104
8.5 Final remarks	107
CHAPTER 9 CONCLUSIONS AND RECOMMENDATIONS	108
9.1 Conclusions	108
9.2 Recommendations	111
APPENDIX A FRAME AND SHELL ELEMENT	172
APPENDIX B CALCULATION OF PANEL NORMALS	178
APPENDIX C HYDROSTATIC RESTORING COEFFICIENTS OF RIGID BODY MODES	180
REFERENCES	181

LIST OF TABLES

<u>Table</u>	<u>Page</u>
Table 5.1 Main particulars of a single module	62
Table 5.2 Section structural properties	62
Table 6.1 Main particulars of the box	75
Table 6.2 Main particulars of the floating airport	78
Table 6.3 Natural periods of the flexible modes of the floating airport (seconds)	78
Table 7.1 CPU time in the calculation of the Green function and its derivatives (seconds)	92
Table 8.1 Main particulars of the single module mat-like structure	100
Table 8.2 Dry structural natural periods of 5-module semi-submersible and mat-like systems (seconds)	102
Table 8.3 Dry structural natural periods of 20-module semi-submersible and mat-like systems (seconds)	103
Table 8.4 Natural periods of rigid body modes of 5- and 20-module systems	104

LIST OF FIGURES

<u>Figure</u>		<u>Page</u>
Figure 3.1	Schematic sketch of the boundary value problem	113
Figure 3.2	Discretization of the wetted body surface	114
Figure 5.1	Frame element	115
Figure 5.2	Cylindrical coordinate system	115
Figure 5.3	Configuration of a single module (Winkler et al., 1990)	117
Figure 5.4	Schematic of a five module VLFS	118
Figure 5.5	Normalized surge exciting force for a vertical cylinder	119
Figure 5.6	Normalized pitch exciting moment for a vertical cylinder . . .	119
Figure 5.7	Normalized surge added mass coefficients for a vertical cylinder	120
Figure 5.8	Normalized pitch added moment coefficients for a vertical cylinder	120
Figure 5.9	Normalized surge damping coefficients for a vertical cylinder	121
Figure 5.10	Normalized pitch damping coefficients for a vertical cylinder	121
Figure 5.11	Surge transfer functions of a single rigid module in head seas	122
Figure 5.12	Heave transfer functions of a single rigid module in head seas	122
Figure 5.13	Pitch transfer functions of a single rigid module in head seas	123
Figure 5.14	Sway transfer functions of a single rigid module in beam seas	123

Figure 5.15	Heave transfer functions of a single rigid module in beam seas	124
Figure 5.16	Roll transfer functions of a single rigid module in beam seas	124
Figure 5.17	Surge transfer functions of Module 1 in head seas	125
Figure 5.18	Surge transfer functions of Module 8 in head seas	125
Figure 5.19	Heave transfer functions of Module 1 in head seas	126
Figure 5.20	Heave transfer functions of Module 8 in head seas	126
Figure 5.21	Pitch transfer functions of Module 1 in head seas	127
Figure 5.22	Pitch transfer functions of Module 8 in head seas	127
Figure 5.23	Surge transfer functions of Module 1 in quartering seas	128
Figure 5.24	Heave transfer functions of Module 1 in quartering seas	128
Figure 5.25	Pitch transfer functions of Module 1 in quartering seas	129
Figure 5.26	Surge transfer functions of Module 1 for the deck and pontoon connector case	129
Figure 5.27	Heave transfer functions of Module 1 for the deck and pontoon connector case	130
Figure 5.28	Pitch transfer functions of Module 1 for the deck and pontoon connector case	130
Figure 6.1	Heave response of barge model ($3*0.75*0.016m^3$)	131
Figure 6.2	Normal modes of the test box. (A)-rigid mode, (B)-first bending mode, (C)-second bending mode, (D)-third bending mode, T-natural period in seconds	132
Figure 6.3	Normal modes of the equivalent plate. (A)-rigid mode, (B)-first bending mode, (C)-second bending mode, (D)-third bending mode, T-natural period in seconds	133

Figure 6.4	Vertical displacement amplitude transfer function of the box (500*60*20 m ³)	134
Figure 6.5	Vertical displacement amplitude transfer function of the box (500*200*20 m ³)	134
Figure 6.6	Vertical displacement amplitude transfer function of the runway of 300m*300m*25m (d=15m), (a) bow, (b) midship, (c) stern	135
Figure 6.7	Vertical displacement amplitude transfer function of the runway of 300m*300m*25m (d=15m), (a)-real and (b)-imaginary part for a 12 second wave, (c)-real and (d)-imaginary part for a 16 second wave, (e)-real and (f)-imaginary part for a 22 second wave	138
Figure 7.1	(a) the Green function, (b) its normal derivative	139
Figure 7.2	Displacements at bow of the box (80m*10m*10m)	140
Figure 7.3	Responses of the box using different criteria (500m*60m*20m)	142
Figure 7.4	Relative errors of the responses (period=8 sec)	143
Figure 7.5	Number of iterations in solving Eq. (7.7) (Total No. of panel is 936)	143
Figure 7.6	Number of iterations in solving Eq. (7.7) for diffraction source strengths	144
Figure 8.1	Finite element model of 5-module semi-submersible	145
Figure 8.2	Finite element model of 20-module semi-submersible	146
Figure 8.3	Finite element model of 5-module mat-like VLFS	147
Figure 8.4	Finite element model of 20-module mat-like VLFS	148
Figure 8.5	Normal modes of 5-module semi-submersible	152
Figure 8.6	Normal modes of 5-module mat-like VLFS	156
Figure 8.7	Normal modes of 20-module semi-submersible	160

Figure 8.8	Normal modes of 20-module mat-like VLFS	160
Figure 8.9	Heave response of 5-module VLFS	165
Figure 8.10	Pitch response of 5-module VLFS	165
Figure 8.11	Heave response of 20-module VLFS	166
Figure 8.12	Pitch response of 20-module VLFS	166
Figure 8.13	Normal coordinates of 5-module VLFS, (z)-Semi, (b)-Mat . .	167
Figure 8.14	Normal coordinates of 20-module VLFS, (z)-Semi, (b)-Mat . .	168
Figure 8.15	Vertical deflection of 5-module VLFS, (a)-bow, (b)-middle, (c)-stern.	169
Figure 8.16	Vertical deflection of 20-module VLFS, (a)-bow, (b)-middle, (c)-stern.	170
Figure 8.17	Maximum stress of 5-module VLFS	171
Figure 8.18	Maximum stress of 20-module VLFS	171
Figure A.1	Global, local and natural coordinate system for a quadrilateral shell element	177
Figure A.2	Quadrilateral thin shell element	177

LIST OF SYMBOLS

A	= amplitude of the incident wave
A_{ij}	= element of the hydrodynamic added mass matrix
$[B]$	= strain-displacement matrix
$[c]$	= element damping matrix
C_D	= form-drag coefficient in Morison's equation
C_M	= inertia coefficient in Morison's equation
C_{DC}	= equivalent linear drag coefficient in Morison's equation
$[C_s]$	= $ndof \times ndof$ structural damping matrix
$[C_s^*]$	= $q \times q$ modal structural damping matrix
$[C_f^*]$	= $q \times q$ modal hydrodynamic damping matrix
$\{d\}$	= displacement vector at any point
$\{\delta d\}$	= vector of small, arbitrary element nodal virtual displacements
$[E]$	= matrix of elastic material properties of an element
$\{F\}$	= vector of nodal forces
$\{F^*\}$	= vector of modal forces
$\{F_b\}$	= vector of the body forces at the nodes of an element
$\{F_c\}$	= distributed surface force vector in local coordinates
$\{F_D^*\}$	= $q \times 1$ modal diffraction force vector
$\{F_{int}\}$	= vector of element internal forces
$\{F^{ext}\}$	= external force vector for an element
$\{F_H\}$	= $ndof \times 1$ hydrostatic restoring force vector

$\{F_H^*\}$	= $q \times l$ modal hydrostatic restoring force vector
$\{F_R^*\}$	= $q \times l$ modal radiation force vector
$[F_\Psi]$	= modal force matrix
g	= acceleration due to gravity
$G(P,Q)$	= Green function
h	= water depth
H_m	= Hankel function of first kind and m-th order
I_{xx}	= momentum of inertial about x-axis
I_{yy}	= momentum of inertial about y-axis
I_{zz}	= momentum of inertial about z-axis
J_m	= Bessel function of first kind and m-th order
k	= wave number of the incident waves
$[k]$	= element stiffness matrix
$[K_f]$	= $ndof \times ndof$ hydrostatic restoring coefficient matrix
$[K_f^*]$	= $q \times q$ modal hydrostatic restoring coefficient matrix
$[K_s]$	= $ndof \times ndof$ structural stiffness matrix
$[K_s^*]$	= $q \times q$ modal structural stiffness matrix
$[m]$	= element mass matrix
$[M_f^*]$	= $q \times q$ modal hydrodynamic added mass matrix
$[M_s]$	= $ndof \times ndof$ structural mass matrix
$[M_s^*]$	= $q \times q$ modal structural mass matrix
$ndof$	= number of degrees of freedom for the whole structure

$\{n\}$	= normal vector to the body wetted surface, directed into the structure
$\{n^*\}$	= $q \times 1$ generalized normal vector
$[N]$	= matrix of interpolation functions for the structural element
p	= fluid pressure at a point
$\{p\}$	= $q \times 1$ vector of normal coordinates
q	= number of normal modes used in the analysis
$[T]$	= transformation matrix
$\{u\}$	= vector of nodal displacements
$\{\delta u\}$	= vector of small, arbitrary virtual displacements at a point
$\{\dot{u}_j\}$	= structural velocity at any point in mode j
$\{V(x,y,z,t)\}$	= vector of fluid velocities
$V_{n_j}^*$	= modal structural normal velocity in mode j
w	= vertical displacement due to structural deformation
(x,y,z)	= coordinates of a point in the global coordinate system
(x',y',z')	= coordinates of a point in the body fixed coordinate system
$(\bar{x},\bar{y},\bar{z})$	= coordinates of a point in the element local coordinate system
Y_m	= Bessel function of second kind and m -th order
β	= wave heading
$\{\varepsilon\}$	= element strain vector
Φ_T	= total velocity potential
ϕ	= time-independent part of Φ_T

ϕ_D	= diffraction potential
ϕ_I	= incident wave potential
ϕ_j	= radiation potential due to unit displacement in the j-th mode
ϕ_R	= total radiation potential
$[\alpha]$	= potential coefficient matrix
$[\beta]$	= influence coefficient matrix
γ	= Green function cut-off criterion
(ξ, η)	= natural coordinates of a point
λ_i	= amplitude of the motion of the i-th mode
ρ	= mass density of sea-water
$\{\sigma\}$	= element stress vector
$\sigma(Q)$	= source strength at the source point, Q
$[\Sigma_\Psi]$	= modal structural stress matrix
ω	= incident wave frequency
$\{\psi_j\}$	= 3 x 1 vector of the translational displacements at a point in the j-th mode
$\{\psi_w\}$	= $q \times 1$ vector of the vertical components of the displacements at a point due to each normal mode
$\{\psi_j^c\}$	= $\{\psi_j\}$ evaluated at the centroidal location of an element, in the global coordinate system
$\{\Xi_j\}$	= eigenvector containing the structural nodal displacements for the j-th eigenfrequency

$[\Psi]$ = matrix of eigenvectors, with $\{\Xi_j\}$ as the j-th column

$[\Psi_r]$ = 6 x 6 matrix of displacements at a point due to the rigid modes

$[\Psi]$ = 3 x q matrix with $\{\psi_j\}$ as the j-th column

CHAPTER 1

INTRODUCTION

1.1 Background

Very Large Floating Structures (VLFS) have been proposed for many applications. Among them are the floating city concepts (Goo & Yoshida, 1990), floating airports and runways (Lemke, 1987; Takarada, 1984; Webster, 1991; Ertekin et al., 1994), military bases (Bretz, 1988; Brahtz, 1989) and ocean mining platforms (Winkler et al., 1990). A floating runway, which might be 3000m x 300m in plan, represents one of the largest scale VLFS. Because a floating structure of such a scale has never been constructed, some fundamental questions exist regarding its design and construction. A summary of VLFS research and development can be found in Wilkins et al. (1992).

A central aspect of VLFS design is that of hull type. Most proposed designs for VLFS are either of the semi-submersible type (Brahtz, 1989, Winkler et al., 1990, Yoshida and Goo, 1990) or are mat-like (Bretz, 1988; Okamoto et al., 1985). The former is said to be of the deep-draft type (DDT) and the latter, of the shallow-draft type (SDT).

Both types of hulls have advantages and disadvantages. Since as yet little experience is in hand to provide dependable guidance for judgment, it is somewhat difficult to determine the most efficient hull type of VLFS intended to support some

specific activities. The goal of the present research is to provide efficient analytical tools to investigate the applicability of these two types of hulls to specific missions.

To be sure, the type of hull to be employed depends on many factors. However, apart from the economics of its construction, the hull type related to a given mission depends in large part on its qualities of seakindliness and seaworthiness. The last quality is an obvious as well as legal requirement, while seakindliness relates to the system's tolerable motions in anticipated seas states. This research deals with the seaworthiness of the two types of hulls.

To this end, efficient analytical tools are developed to analyze the response of VLFS of shallow-draft and of deep draft in moderate sea states. Hydroelasticity theory is employed for two reasons: the first is that the flexible modes of motion are so important to a VLFS that the interaction between the motion of flexible modes and the waves must be necessarily included in the dynamic response analysis; the other is that difficulties arise in specifying the boundary conditions of the dynamic force if the approach of traditional rigid body hydrodynamics is employed. Hence, it is necessary to introduce simplified static boundary conditions to obtain a static or quasi-static prediction of the structural responses (Reilly et al., 1988). Unlike the approach employed in traditional rigid body hydrodynamics, a unified hydroelasticity theory can be used to predict the behavior as well as the structural response of a VLFS in waves without introducing the approximations discussed above.

1.2 Hydroelasticity Concept

"Hydroelasticity is concerned with the phenomena involving mutual interaction among inertial, hydrodynamic and elastic forces."

Heller and Abramson

The response of a floating system is a problem in fluid-structure interaction. No matter what the action on the structure is, the motion or deformation of the latter will disturb the fluid and, in return, the disturbed fluid will react on the structure to move and deform it. This problem embodies the complexity of the dynamics of fluid and structure considered separately and, also difficulties associated with compatibility at the common boundaries. This mutual compatibility or interaction can be described by the forces, velocities or displacements of the fluid and structure.

In most engineering problems, structures can be treated as linear systems, which implies that the stiffness matrix and the load vector are independent of the displacements and that these latter are small; hence, conventional methods of structural dynamics are employed. It is also assumed that linear potential theory is applicable to the calculation of the fluid action, with the result that the total potential can be decomposed into incident, radiation and diffraction components. Of these, only the radiation potential is coupled with the motions of the structure.

Two methods can be used to solve for the hydroelastic responses: in the first (mode superposition method) a normal coordinate system is employed, whereas in the second (direct method) the coordinate system is a physical one. In the former method, the normal modes of vibration of the structure in air ("dry modes") are employed as the normal coordinates because of their efficiency in reducing the dimensions of the problem. It is assumed that, for an n degrees-of-freedom system, the first q modes, $q \ll n$, which correspond to the lower natural frequencies of the structure, are sufficient to represent the structural response. The total radiation potential is obtained as a linear combination of the radiation potentials for each mode.

The hydroelastic analysis of a floating structure requires much more computational resources than does traditional rigid body hydrodynamic analysis, especially when the structure is a VLFS. Therefore, numerically efficient techniques need to be developed.

1.3 Review of the previous work on hydroelasticity

The concept of hydroelasticity was introduced in the late 50's. Since then a considerable amount of work has been published in this field. During the 60's and 70's, most of the work was concerned with the acoustic radiation and scattering, the underwater free vibration and the underwater shock responses of submerged bodies (Chen and Pierucci, 1977). A significant contribution to the application of hydroelasticity in marine hydrodynamics was made by the research group of Bishop

and Price in the late 70's (Betts et al., 1977, Bishop et al., 1977, Bishop and Price, 1979). It was thus that the well known hydroelasticity theory of ships was established. It is a two-dimensional theory, which embodies strip theory for the fluid hydrodynamics and "beamlike" structural dynamics. Normal coordinates are used in solving for the ship response to the waves. The foundation of this idea was laid by Bishop (1971), Bishop and Taylor (1973) and Bishop and Price (1974). Although "wet modes" were employed before 1974 as normal coordinates in the response analysis, the analysis is simplified by using the ship modes in vacuo i.e., "dry modes", as the normal coordinates because they can be more easily obtained. Hence the "dry modes" are usually employed in hydroelasticity theory.

Two-dimensional hydroelasticity has been used to determine ship responses, distortions in the vertical plane, bending moments and shearing forces at any section of a "beam-like" hull (Bishop et al., 1977). It has also been applied to bridges (Langen and Sigbjornsson, 1980; Georgiadis, 1981; Hartz and Georgiadis, 1982), and to other slender structures (Okamoto et al. 1985; Ertekin et al., 1990; Riggs et al., 1991; Che et al., 1992). However, the assumption of "beam-like" hull shape in two-dimensional hydroelasticity imposes some limitations on the application of the theory.

Two-dimensional hydroelasticity was later modified to include the end plane forces in surge (Riggs and Ertekin, 1993), and to relax the restrictions of the "beam-like" motions or deformations of floating bodies (Wang, 1991; Che et al., 1994).

Wu (1984) developed a general linear hydroelasticity theory in which three-dimensional hydrodynamics are employed for the analysis of the fluid motion and of

the three-dimensional structural dynamics of the responses of a floating body. The source distribution method and the finite element method are used to obtain the potentials and structural responses, respectively. The equations of motion are solved using the normal coordinates represented by the "dry modes".

The three-dimensional hydroelasticity theory is applicable to any arbitrary-shaped structure and is perhaps the most accurate theory to date. However, an analysis by three-dimensional hydroelasticity requires considerable computer resources and its implementation is time consuming. Limited computer resources make the application of three-dimensional hydroelasticity to a floating body, especially a VLFS, very difficult.

To overcome this difficulty, Wu (1984) introduced the composite source distribution method, in which the wetted body port-starboard symmetry is exploited. The method was later extended to a doubly-symmetric body (Wu et al., 1993). The requirements of computational storage and time are reduced by applying these methods. To the same end, Newman (1985) developed an efficient numerical algorithm required for reducing the computational time for calculating the source potential and its derivatives. For a multi-module VLFS, if the fluid coupling, i.e. the effect of the presence of one module on the hydrodynamics of another module, is weak, then the problem may further be simplified by calculating the hydrodynamic coefficients and loads for a single module and then solving the equations of motion in which there is only mechanical coupling due to the presence of connectors (Wang

et al., 1991a; Ertekin et al., 1993). A list of references on efficient methods of hydroelasticity may be found in Ertekin (1994).

Thus it appears that linear three-dimensional hydroelasticity theory has been well developed. The numerically efficient techniques and the developments in computer hardware are the key points in the application of the theory to a VLFS.

1.4 Objective of the present study

The objective of the present study is to evaluate two flexible hull types of VLFS of which one is semi-submersible (or deep-draft), and the other is mat-like (or shallow-draft). The evaluation is based on their structural displacement and stress responses when acted upon by small amplitude (linear) of waves.

To this end, efficient methods of hydroelastic analysis are developed. Obviously, the underwater configuration of the floating body is one of the most important factors for selecting which method is appropriate to the analysis. The common and main feature of VLFS is that of huge size. For a semi-submersible platform, another important feature is the cylindrical components, while for a mat-like platform the important feature is the small ratio of draft to width and length. Three efficient methods of hydroelastic analysis are developed based on the forgoing important distinguishing aspects.

In the first method, the wetted structure is represented by frame elements and the fluid forces are obtained using the modified Morison's equation. The main reason for this choice is the higher efficiency of Morison's equation when compared with a

three-dimensional potential theory (Ertekin et al., 1993; Ertekin et al. 1994). On the other hand, it is well known that the use of constant coefficients in Morison's equation leads to less accurate results especially at the high frequencies at which wave scattering is important. To improve the results, the added mass, damping coefficients and exciting forces/moments entering in the modified Morison's equation are calculated by use of the extended method of MacCamy and Fuchs (1954) (see Garrison, 1984). This method is applicable to a VLFS if the geometry of its wetted body is cylindrical, such as occurs with a semi-submersible.

The second method is developed for the hydroelastic analysis of a mat-like VLFS of shallow draft. The fluid motion is obtained by using a source distribution method in which the zero-draft Green function (Kim, 1963; Maeda and Eguchi, 1976) is employed. Since for such a structure the bending motion is more important than other motions, the structure is modeled as a plate having both a bending stiffness and a total mass equal to those of the mat-like floating body. The use of the zero-draft Green function and of the equivalent plate model results in a highly efficient hydroelastic analysis.

The third method of hydroelastic analysis is efficient for a VLFS of arbitrary shape. Two techniques are introduced to increase the computational efficiency. The first is related to the convergence of the Green function and its derivatives, namely, the introduction of a criterion used to truncate the influence of the Green function and its derivatives. The other involves the use of an iterative sparse solver for the linear system of equations. The principle motivation behind the application of these

two techniques stems from the fact that a source makes a very small contribution to the potential at a point "far away". In this method, the general three-dimensional source distribution is employed for the potentials and three-dimensional finite element method for the structural responses. MIT's FINGREEN subroutine is used in the calculation of the Green function and its derivatives (Newman, 1985).

The three methods are all based on linear structural dynamics and on linear potential theory. It is assumed that the fluid is incompressible and inviscid, the flow is irrotational and the wave amplitude and disturbance are relatively small. The fundamental formulations of structural dynamics and fluid dynamics as well as the interaction between the structure and the fluid at the boundaries are reviewed.

The three methods are first verified by comparison with available experimental data and theoretical predictions and then applied to the analysis of VLFS of semi-submersible and mat-like types. The evaluation of flexible hull types for VLFS is based on the results obtained from the analyses. Some suggestions and recommendations are offered for making a choice of configuration for a VLFS, namely, whether semi-submersible or mat-like.

CHAPTER 2

STRUCTURAL DYNAMICS OF A FLOATING BODY

2.1 Overview

The objective of hydroelastic analysis is to obtain the structural displacements and stresses to provide the necessary information for design purpose. Consider a body floating on free surface: the forces acting on it are gravity, buoyancy and the possible action of waves, current, wind, etc. If all the forces are known, the motion analysis of a floating body is a problem of forced responses. Well developed techniques in structural dynamics dealing with this problem can be applied to obtain the solutions. In this chapter, the linear theory of structural dynamics, finite element method, and modal superposition method are discussed.

2.2 Formulation of structural dynamics

Structural dynamic analysis is based on three relationships: compatibility conditions, i.e. strain-displacement relations; constitutive equations, i.e. strain-stress relations; and equilibrium equations.

When a body is a single, slender hull, the beam theories based on these three relationships may be used to analyze its dynamic vibration characteristics (Bishop and Price, 1979). Such a simple model has been used repeatedly over the years to demonstrate certain fundamental aspects of ship vibration. It is clear continuous models are of little use in vibration analysis of complex structures such as a floating

platform because of the intractability of the solutions. Only discrete models are practical for the analysis of such structures.

The finite element method is widely used in discrete analysis. The basic assumption in the finite element method is that the displacements of the structure at any point can be obtained from the displacements at the nodes of the elements by using an interpolation function, i.e.,

$$\{d\} = [N]\{u\} \quad (2.1)$$

where $\{d\}$ is the displacement vector at any point, $[N]$ is the matrix of interpolation functions and $\{u\}$ is the nodal displacement vector.

The interpolation function is a function of coordinates, not time. Hence,

$$\{\dot{d}\} = [N]\{\dot{u}\} \quad \text{and} \quad \{\ddot{d}\} = [N]\{\ddot{u}\} \quad (2.2)$$

In accord with the basic assumption, the three relationships in structural analysis are expressed as the functions of the nodal values of the element. The strain-displacement relationship is

$$\{\epsilon\} = [B]\{u\} \quad (2.3)$$

where $[B]$ is the strain-displacement matrix. The constitutive relation is

$$\{\sigma\} = [E]\{\epsilon\} \quad (2.4)$$

where $\{\sigma\}$ is the element stress vector, and $[E]$ is the matrix of material stiffness.

The equilibrium equation is obtained by the principle of virtual displacements, which states that the equilibrium of a body requires that for any compatible, small,

virtual displacements $\{\delta \mathbf{u}\}$, imposed onto the body, the total internal virtual work is equal to the total external virtual work (see for example, Bathe and Wilson, 1976).

The forces on a moving body include the general excitation, the inertial and the damping forces. The latter two are related to the mass and to the damping mechanism of the structure. There are six degrees of freedom at each node. The mass distribution matrix is

$$[\bar{\mathbf{m}}] = \begin{bmatrix} \bar{m}_{11} & 0 & 0 & 0 & 0 & 0 \\ 0 & \bar{m}_{22} & 0 & 0 & 0 & 0 \\ 0 & 0 & \bar{m}_{33} & 0 & 0 & 0 \\ 0 & 0 & 0 & \bar{m}_{44} & 0 & 0 \\ 0 & 0 & 0 & 0 & \bar{m}_{55} & 0 \\ 0 & 0 & 0 & 0 & 0 & \bar{m}_{66} \end{bmatrix} \quad (2.5)$$

where \bar{m}_{11} , \bar{m}_{22} , and \bar{m}_{33} are the mass densities (per unit element) subject to translation along the \bar{x} , \bar{y} , and \bar{z} axes respectively, while \bar{m}_{44} , \bar{m}_{55} , and \bar{m}_{66} are the corresponding the moments of inertia about the same axes. The structural damping mechanism is usually approximated by viscous damping.

From D'Alembert's principle, the inertial force is given by

$$\{\mathbf{F}_M\} = -[\bar{\mathbf{m}}]\{\ddot{\mathbf{d}}\} \quad (2.6)$$

If $[\bar{\xi}]$ is used as a material-damping parameter matrix analogous to viscosity, the structural linear damping forces can be written as

$$\{F_c\} = -[\bar{\xi}]\{\dot{d}\} \quad (2.7)$$

The principle of virtual displacements, for a single element, can be expressed as,

$$\int_{V_e} \{\delta u\}^T \{F_b\} dV + \int_{S_e} \{\delta u\}^T \{F_c\} dS + \sum_{i=1}^n \{\delta u_i\}^T \{p_i\} + \{\delta d\}^T \{F_{int}\} - \int_{V_e} (\{\delta u\}^T [\bar{m}]\{\ddot{d}\} + \{\delta u\}^T [\xi]\{\dot{d}\}) dV = \int_{V_e} \{\delta \epsilon\}^T \{\sigma\} dV \quad (2.8)$$

where $\{\delta u\}$, $\{\epsilon\}$ and $\{\delta d\}$ are small, arbitrary and compatible, virtual displacement, strain and nodal displacement vectors, respectively; $\{F_b\}$ is the body force, $\{F_c\}$ is the surface traction, $\{p_i\}$ is a concentrated load, $\{\delta u_i\}$ is a displacement vector, $\{F_{int}\}$ is the internal nodal force vector, T stands for transpose, V_e is the volume of the element, and S_e is the surface of the element.

The substitution of the strain-displacement and constitutive relationships and shape function into Eq.(2.8) yields:

$$[m]\{\ddot{u}\} + [c]\{\dot{u}\} + [k]\{u\} = \{F^{ext}\} + \{F^{int}\} \quad (2.9)$$

where $[m]$, $[c]$, and $[k]$ are the consistent element mass, damping and stiffness matrices, respectively, and

$$[m] = \int_{V_e} [N]^T [\bar{m}] [N] dV \quad (2.10)$$

$$[c] = \int_{V_e} [N]^T [\bar{\xi}] [N] dV \quad (2.11)$$

$$[k] = \int_{V_e} [B]^T [E] [B] dV \quad (2.12)$$

The external load vector is written as

$$\{F^{ext}\} = \int_{V_e} [N]^T \{F_b\} dV + \int_{S_e} [N]^T \{F_c\} dS + \sum_{i=1}^n [n_i]^T \{p_i\} \quad (2.13)$$

The internal force vector $\{F_{int}\}$ will be canceled when the elements are assembled.

Eq.(2.10) is formed based on one element and in its local coordinate system. The equilibrium equation of the body in the global coordinate system can be obtained by assembling the element matrices; i.e.,

$$[M_s]\{\ddot{u}\} + [C_s]\{\dot{u}\} + [K_s]\{u\} = \{F\} \quad (2.14)$$

where

$$[M_s] = \sum_{e=1}^{nelm} [m_e] \quad [C_s] = \sum_{e=1}^{nelm} [c_e] \quad [K_s] = \sum_{e=1}^{nelm} [k_e] \quad \{F\} = \sum_{e=1}^{nelm} \{F_e^{ext}\} \quad (2.15)$$

where "nelm" is the number of elements, $[M_s]$, $[C_s]$ and $[K_s]$ are the structural mass, damping coefficient and stiffness matrices, respectively. The transformation from the local to the global coordinates is included in forming these matrices, i.e.

$$[m_e] = [T]^T [m] [T] \quad [c_e] = [T]^T [c] [T] \quad [k_e] = [T]^T [k] [T] \quad (2.16)$$

where $[T]$ is a transformation matrix.

2.3 Direct and modal superposition methods

The motions of the structure are derived from Eq. (2.16) by an analysis in which the structure is discretized via the employment of the finite element method. It can be solved either directly or by using the modal superposition method.

Direct method. In discrete analysis, a continuous structure is represented by a disposition of finite elements connected at their nodal points. In this analysis, all

forces and displacements are referred to such nodal points. In general, there are six degrees of freedom at each node. Therefore, if there are N nodes in the discretized model, the total degrees of freedom of the model is $\text{ndof} = 6N$. The equilibrium condition hold simultaneously for all of the degrees of freedom. In the direct method, such a system of the ndof coupled equations is solved for the nodal displacements. The displacements at other points are obtained by Eqs. (2.1) and (2.4), in which an interpolation function is employed. The form of an interpolation function depends on the element type and on the number of nodes of the element. Appendix A gives the interpolation functions for a two-node beam element and a 4-node quadrilateral thin shell element.

Modal superposition method. In this method, the displacements are represented by the free-vibration modal shapes. For a ndof -degree-of-freedom system, these shapes constitute ndof independent displacement patterns, the amplitudes of which may serve as normal coordinates to express any possible displacement (Clough and Penzien, 1975).

Lower modes, which correspond to smaller natural frequencies, contribute to the responses much more than higher modes. Hence, there comes a point at which higher modes can be neglected in the analysis. If the responses of the structure can be approximately represented by the first q , mode shapes $q \ll \text{ndof}$, the dimensions of the system will be reduced significantly. This reduction of the dimensions is especially useful in a hydroelastic analysis in which each degree of freedom

corresponds to a radiation potential. Therefore, a lesser number of radiation potentials needs to be solved if the equations of motion are stated in normal coordinates.

The modal shapes are obtained by solving the characteristic equation corresponding to equation (2.14) without damping, i.e.

$$[\mathbf{M}_s]\{\ddot{\mathbf{E}}\} + [\mathbf{K}_s]\{\mathbf{E}\} = 0 \quad (2.17)$$

where $\{\mathbf{E}\}$ is the eigenvector that is the function of time and space and can be expressed as

$$\{\mathbf{E}\} = \{\boldsymbol{\psi}\}e^{i\bar{\omega}t} \quad (2.18)$$

Substitution of Eq. (2.18) to Eq. (2.17) results in

$$([\mathbf{K}] - \bar{\omega}^2[\mathbf{M}])\{\boldsymbol{\psi}\} = 0 \quad (2.19)$$

From Eq. (2.19), the natural frequencies $\bar{\omega}_i$ and corresponding normal vector $\{\boldsymbol{\psi}_i\}$ can be obtained.

If the normal vectors are normalized by mass, then (Clough and Penzien, 1975)

$$\{\boldsymbol{\psi}_i\}^T[\mathbf{M}]\{\boldsymbol{\psi}_j\} = \delta_{ij} \quad (i, j = 1, 2, \dots, q) \quad (2.20)$$

$$\{\boldsymbol{\psi}_i\}^T[\mathbf{K}]\{\boldsymbol{\psi}_j\} = \bar{\omega}^2 \delta_{ij} \quad (i, j = 1, 2, \dots, q) \quad (2.21)$$

where δ_{ij} is the Kronecker delta.

The nodal displacements $\{u\}$ can be obtained by modal superposition, i.e.,

$$\{u\} = [\Psi]\{p\} \quad (2.22)$$

where $[\Psi]$ is the $n \times q$ mode shape matrix with i equal to $\{\psi_i\}$, $\{p\}$ is the $q \times 1$ vector of normal coordinates.

Based on the information of the modal shapes, the modal internal force and moment matrix $[F_\Psi]$ and modal stress matrix $[\Sigma_\Psi]$ can be obtained by stress analysis. By using modal superposition again, the internal forces and stresses within the element can be calculated, respectively, by

$$\{F\} = [F_\Psi]\{p\} \quad (2.23)$$

and

$$\{\sigma\} = [\Sigma_\Psi]\{p\} \quad (2.24)$$

where $\{F\}$ is the vector of internal forces and moments and $\{\sigma\}$ is the vector of stresses at any point within the element.

Eqs. (2.20) and (2.21) indicate the orthogonality relationships for the flexible structural dry modes. Multiplication by the transpose of the corresponding modal shapes and substitution of Eq. (2.22) transform Eq. (2.14) into

$$(-\omega^2[M_s^*] + i\omega[C_s^*] + [K_s^*])\{p\} = \{F^*\} \quad (2.25)$$

where

$$[M_s] = [\Psi]^T [M_s] [\Psi] = [I] \quad (2.26)$$

$$[C_s] = [\Psi]^T [C_s] [\Psi] \quad (2.27)$$

$$[K_s] = [\Psi]^T [K_s] [\Psi] = [\Lambda] \quad (2.28)$$

$$\{F^*\} = [\Psi]^T \{F\} \quad (2.29)$$

where $[I]$ is an identity matrix. Eqs. (2.26) through (2.28) define the generalized structural mass, damping and stiffness matrices, respectively, and Eq. (2.29) defines the generalized force.

The first six vibration modes correspond to the six degrees of freedom of the rigid body motion. In ship motion analysis, these six rigid body modes, namely, surge, sway, heave, roll, pitch and yaw, are usually described by three displacements and three rotations of the center of gravity about the body fixed axes. The rigid body modes have the form of

$$[\Psi_r] = \begin{bmatrix} 1 & 0 & 0 & 0 & (z - z_G) & -(y - y_G) \\ 0 & 1 & 0 & -(z - z_G) & 0 & (x - x_G) \\ 0 & 0 & 1 & (y - y_G) & -(x - x_G) & 0 \\ 0 & 0 & 0 & 1 & 0 & 0 \\ 0 & 0 & 0 & 0 & 1 & 0 \\ 0 & 0 & 0 & 0 & 0 & 1 \end{bmatrix} \quad (2.30)$$

where (x_G, y_G, z_G) are the coordinates of the center of gravity.

Note that although the three translational rigid modes satisfy the orthogonality condition, the three rotational rigid modes do not. Therefore, the modal mass matrix corresponding to the rigid body motion, in general, is not diagonal.

CHAPTER 3

THREE-DIMENSIONAL POTENTIAL THEORY

3.1 Overview

The research work on the motions of a floating body has been carried out for more than a century since Froude (1861) studied the rolling motions of steam ships. The early work also includes Krylov's (1896) study on the pitch motion and the stresses due to this motion. In the early studies (Froude, 1861, and Krylov, 1896), the fluid forces and moments are calculated without considering the interaction between the body and fluid. The fluid forces and moments obtained from the incident waves are now called Froude-Krylov forces. These early works provide the foundation for the later researches.

In the 40's, people began to study the diffraction and radiation problems using the potential theory and try to include these in the motion analysis. One of the great achievements in this field is the strip theory approach (Korvin-Kroukovsky and Jacobs, 1957; Frank, 1967; Smith, 1967; Ogilvie and Tuck, 1969; Salvesen et al., 1970). Its computational simplicity and the generally satisfactory agreement with experiments result in the fast development and widely applications of strip theory. However, that does not mean that people did not know three-dimensional potential theory for a floating body at that period. In fact, the Green function method for the solution of the radiation potential has been known since the early 40's (Havelock, 1942). But, because of the limitations of the then existing computational resources,

the attempt to apply the three-dimensional potential theory was altogether unrewarding.

The development of methods of three-dimensional hydrodynamic analysis date from the 70's (Faltinsen and Michelsen, 1974; Chang, 1977; Eatock-Taylor and Waite, 1977; Garrison, 1978; Inglis and Price, 1982). Of these, Chang (1977) and Inglis and Price (1982) included the body's forward speed in their analyses.

Methods of three-dimensional hydrodynamic analysis are applicable to arbitrarily shaped bodies. Also the solution of the diffraction problem leads to more accurate predictions of the pressure distribution and of the estimate of wave excitation. The advantages of three-dimensional methods over the strip theory approach are quite attractive and the application of these methods has received more attention since then.

In this chapter, the mathematical formulation of the hydrodynamic analysis of a body floating in wave is described. The analysis is based on the assumption that the fluid is incompressible and inviscid, the flow is irrotational and the wave amplitude is relatively small; hence, the problem can be described by a linear potential theory. It is also assumed that waves are regular and long-crested. The extension to irregular and short-crested waves is straight forward.

3.2 Governing equation and boundary conditions

Two sets of coordinate systems are employed to describe the motions of a floating body, see Fig. 3.1.

In the fluid domain, the conservation of mass and momentum are expressed by Euler's equations, i.e.,

$$\frac{\partial v_x}{\partial x} + \frac{\partial v_y}{\partial y} + \frac{\partial v_z}{\partial z} = 0 \quad (3.1)$$

and

$$\left(\frac{\partial}{\partial t} + \{\mathbf{V}\}^T \{\nabla\} \right) \{\mathbf{V}\} = -\nabla \left(\frac{p}{\rho} + g z \right) \quad (3.2)$$

where v_x , v_y , v_z are the three components of fluid velocity, $\{\mathbf{V}\}$ is the fluid velocity vector, p is the fluid pressure, g is the gravitational acceleration, ρ is the water density and $\{\nabla\} = \{\partial/\partial x, \partial/\partial y, \partial/\partial z\}$.

Based on the assumptions stated earlier, the fluid velocity $\{\mathbf{V}\}$ can be described as the gradient of the velocity potential Φ_T , i.e.,

$$\{\mathbf{V}\} = \nabla \Phi_T \quad (3.3)$$

Hence Eqs. (3.1) and (3.2) can be rewritten as the Laplace equation and Euler's integral, respectively, i.e.,

$$\frac{\partial^2 \Phi_T}{\partial x^2} + \frac{\partial^2 \Phi_T}{\partial y^2} + \frac{\partial^2 \Phi_T}{\partial z^2} = 0 \quad (3.4)$$

$$\frac{\partial \Phi_T}{\partial t} + gz + \frac{p}{\rho} = C(t) \quad (3.5)$$

where $C(t)$ can be absorbed in Φ_T thus reducing to zero the right-hand side of Eq. (3.5).

The main task in hydrodynamic analysis is that of solving the boundary value problem that yields the velocity potential.

Consider a three-dimensional floating body partially or wholly immersed in the fluid (see Fig. 3.1) and rewrite the velocity potential as

$$\Phi_T = \phi_T e^{i\omega t} \quad (3.6)$$

where ϕ_T depends on x, y, z only, and decompose it into its three components usual, i.e.,

$$\phi_T = \phi_I + \phi_D + \phi_R \quad (3.7)$$

where ϕ_I , ϕ_D , and ϕ_R are the incident, diffraction and radiation potentials, respectively.

The kinematic and dynamic conditions at the free surface are approximated by reduction to the still water surface, i.e.

$$\frac{\partial \phi}{\partial z} - k\phi = 0 \quad \text{on } z=0 \quad (3.8)$$

where $k = \omega^2/g$ is the wave number in deep water and ϕ denotes either ϕ_I , ϕ_D or ϕ_R . At the wetted body surface, the no-flux condition is

$$\frac{\partial \phi}{\partial \mathbf{n}} = \{\mathbf{V}\}^T \{\mathbf{n}\} \quad (3.9)$$

where $\{\mathbf{n}\}$ is a body normal vector directed into the body.

For an infinite water depth,

$$\lim_{z \rightarrow -\infty} \nabla \phi = 0 \quad (3.10)$$

If the water depth h is finite and it is assumed the bottom is flat, the sea bottom condition is

$$\frac{\partial \phi}{\partial z} = 0 \quad \text{at } z = -h \quad (3.11)$$

The radiation condition, which describes the boundary condition at the infinite horizontal distance, ensures that the energy propagates outward. While this condition is not applicable to the incident potential, for the diffraction and radiation potentials, it is

$$\lim_{R \rightarrow \infty} \left[R^{1/2} \left(\frac{\partial}{\partial R} + i\mathbf{k} \right) \phi \right] = 0 \quad (3.12)$$

where $R = \sqrt{x^2 + y^2}$.

3.3 Incident wave potential

The incident wave potential satisfies the Laplace equation and the linearized free surface and sea-floor boundary conditions, and can be solved by the technique of the separation of variables. The solution for the incident wave potential may be found in many textbooks (Lamb, 1932; Kinsman, 1965; Newman, 1977). The velocity

potential of the plane-progressive wave of constant amplitude and sinusoidal profile is

$$\Phi_I = \frac{igA}{\omega} \frac{\tanh[k(z+h)]}{\tanh(kh)} \exp(-i[k(x \cos \beta + y \sin \beta) - \omega t]) \quad (3.13)$$

where A is the wave amplitude, β the wave heading, positive counter-clockwise, ω the wave frequency, h the water depth and k the wave number.

If the water depth $h \rightarrow \infty$, the potential has the form of

$$\Phi_I = \frac{igA}{\omega} \exp(-i[k(x \cos \beta + y \sin \beta) - \omega t]) \exp(kz) \quad (3.14)$$

3.4 Body boundary conditions of the radiation and diffraction potentials

Although the incident potential is easy to obtain, the solution for the radiation and diffraction potentials is much more complicated because of the presence of the body. In this section, the body boundary conditions of diffraction and radiation potentials are discussed.

3.4.1 Body boundary condition for the diffraction potential

When a fixed body is acted upon by waves, its effect upon them is describable by a diffraction potential and the body boundary condition is expressed by

$$\frac{\partial \phi_D}{\partial \mathbf{n}} + \frac{\partial \phi_I}{\partial \mathbf{n}} = 0 \quad (3.15)$$

3.4.2 Body boundary condition for the radiation potential

The radiation potential ϕ_R , which is the sum of all the potentials arising from the forced oscillations and vibrations of a floating body in an otherwise calm fluid, can be written as

$$\phi_R = \sum_{j=1}^{\text{ndof}} \lambda_j \phi_{Rj} \quad (3.16)$$

where **ndof** is the displacement degrees-of-freedom of the body, ϕ_{Rj} represents the spatial part of the radiation potential corresponding to the motion associated with the j -th degree-of-freedom, and λ_j denotes the amplitude of the motion.

The boundary condition for the radiation potential ϕ_{Rj} is

$$\frac{\partial \phi_{Rj}}{\partial \mathbf{n}} = i \omega \mathbf{d}_n^j \quad (3.17)$$

where \mathbf{d}_n^j is the normal displacement at any point of the mean wetted body surface when the displacement in the j -th degree-of-freedom is a unit.

As discussed in Chapter 2, the motions of the structure can be solved either directly or by using the modal superposition method. If the direct method is used to obtain the structural response, there will be **ndof** corresponding radiation potentials to be solved. The boundary condition for the j -th radiation potential is

$$\frac{\partial \phi_{Rj}}{\partial \mathbf{n}} = i \omega \{N_j\}^T \{\mathbf{n}\} \quad (3.18)$$

where N_j is the shape function corresponding to the j -th degree-of-freedom, and T denotes the transpose.

If the structural response is solved by using the mode superposition method, one of the advantages is that the dimensions of the problem can be reduced. Truncation of the normal modes is possible because the normal coordinates are more efficient than the 'physical' coordinate in representing the structural motion. It is usual to describe the motions of a body by a limited number of normal modes rather than by their totality; thus $q \ll \text{ndof}$. The structural damping is assumed to be Rayleigh with the result that each dry normal mode can be solved independently.

However, when the structure floats in water, the hydrodynamic coefficients, namely added mass and fluid damping, are frequency dependent because of the free surface effect. One consequence of frequency dependent coefficients is that the orthogonality of the normal modes is no longer guaranteed. Also the derivation of the normal modes of the structure in water is complicated and requires an iterative approach. To avoid this complication, in the present work, the normal modes of the dry structure are employed to represent the displacement. The boundary condition for the j -th radiation potential is expressed as

$$\frac{\partial \phi_{Rj}}{\partial \mathbf{n}} = i \omega \{\psi_j\}^T \{\mathbf{n}\} \quad (3.19)$$

where ψ_j is the j -th dry normal mode.

Body boundary condition for rigid body motions. Six degrees-of-freedom of a rigid body are surge, sway, heave, roll, pitch and yaw. The normal modes corresponding to these six motions are given in Eq. (2.31). From Eqs. (3.17) or (3.18), the boundary conditions of the radiation potentials corresponding to the rigid body motions are

$$\frac{\partial \phi_{R1}}{\partial n} = i \omega n_x \quad \text{surge} \quad (3.20)$$

$$\frac{\partial \phi_{R2}}{\partial n} = i \omega n_y \quad \text{sway} \quad (3.21)$$

$$\frac{\partial \phi_{R3}}{\partial n} = i \omega n_z \quad \text{heave} \quad (3.22)$$

$$\frac{\partial \phi_{R4}}{\partial n} = i \omega [(y - y_G)n_z - (z - z_G)n_y] \quad \text{roll} \quad (3.23)$$

$$\frac{\partial \phi_{R4}}{\partial n} = i \omega [(z - z_G)n_x - (x - x_G)n_z] \quad \text{pitch} \quad (3.24)$$

$$\frac{\partial \phi_{R4}}{\partial n} = i \omega [(x - x_G)n_y - (y - y_G)n_x] \quad \text{yaw} \quad (3.25)$$

3.5 The Green function method

The diffraction and radiation potentials can be solved by several methods. The Green function method being a most convenient one has been widely used (Frank, 1967; Yeung, 1973; Faltinsen and Michelsen, 1974; Garrison, 1977). The Green function satisfies the governing equation and the boundary conditions defined above, but not the body boundary condition. Therefore, once the Green function is known, the velocity potential can be obtained from the distribution of singularities on the

body's surface. This distribution guarantees the fulfillment of the body boundary condition.

3.5.1 Fredholm integral equation

The theoretical foundation of the Green function method is Green's second identity, i.e.,

$$\iint_S \left(\phi \frac{\partial G}{\partial n} - G \frac{\partial \phi}{\partial n} \right) dS = \iiint_V (\phi \nabla^2 G - G \nabla^2 \phi) dV \quad (3.26)$$

where V is a three-dimensional fluid domain bounded by a closed surface S ; and where ϕ and G are two scalar functions which are twice differentiable in V and singly differentiable on S ; also $\partial/\partial n$ is the normal derivative, and the normal vector of the surface S points into the body.

Let ϕ be the velocity potential that satisfies the Laplace equation. If a function G can be found that

$$\iiint_V \phi(Q) \nabla^2 G(P,Q) dV = \phi(P) \quad (3.27)$$

where $P = P(x,y,z)$ is any point in the fluid domain, $Q = Q(\xi,\eta,\zeta)$ is the variable point, then the potential ϕ at any point P in the fluid domain can be obtained from

$$\iint_S \left(\phi(Q) \frac{\partial G(P,Q)}{\partial n} - G(P,Q) \frac{\partial \phi(Q)}{\partial n} \right) dS = \phi(P) \quad (3.28)$$

To this end, the function G must satisfy the condition that

$$\nabla^2 G(\mathbf{P}, \mathbf{Q}) = \delta(\mathbf{P} - \mathbf{Q}) \quad (3.29)$$

where $\delta(\mathbf{P} - \mathbf{Q})$ is the Dirac delta function.

Eq. (3.29) is a Poisson equation. The Green function is a solution of Eq. (3.29), which also satisfies the free-surface boundary condition, radiation condition and sea-bottom boundary condition. Functions of such a kind have been found for two- and three-dimensional problems (Weihausen and Laitone, 1960).

Since the Green function satisfies all the boundary conditions except that on the body, the integration in Eq. (3.28) can be applied only to the body's surface S_b only.

To demonstrate this, rewrite Eq. (3.28) as

$$\begin{aligned} \phi(\mathbf{P}) &= \iint_S \left(\phi(\mathbf{Q}) \frac{\partial G(\mathbf{P}, \mathbf{Q})}{\partial \mathbf{n}} - G(\mathbf{P}, \mathbf{Q}) \frac{\partial \phi(\mathbf{Q})}{\partial \mathbf{n}} \right) dS \\ &= \left[\int_{S_b} + \int_{S_f} + \int_{S_w} + \int_{S_s} \right] \left(\phi(\mathbf{Q}) \frac{\partial G(\mathbf{P}, \mathbf{Q})}{\partial \mathbf{n}} - G(\mathbf{P}, \mathbf{Q}) \frac{\partial \phi(\mathbf{Q})}{\partial \mathbf{n}} \right) dS \end{aligned} \quad (3.30)$$

From Eq. (3.8), the integral term on the free-surface can be written as

$$\begin{aligned} &\iint_{S_f} \left(\phi(\mathbf{Q}) \frac{\partial G(\mathbf{P}, \mathbf{Q})}{\partial \mathbf{n}} - G(\mathbf{P}, \mathbf{Q}) \frac{\partial \phi(\mathbf{Q})}{\partial \mathbf{n}} \right) dS \\ &= \iint_{S_f} \phi(\mathbf{Q}) \left[\frac{\partial G(\mathbf{P}, \mathbf{Q})}{\partial z} - k G(\mathbf{P}, \mathbf{Q}) \right] dS = 0 \end{aligned} \quad (3.31)$$

At the sea-bottom, since the both the velocity potential ϕ and the Green function G satisfy the sea-bottom boundary condition, i.e.,

$$\frac{\partial G(\mathbf{P}, \mathbf{Q})}{\partial \mathbf{n}} = 0, \quad \frac{\partial \phi(\mathbf{Q})}{\partial \mathbf{n}} = 0 \quad (3.32)$$

the integral term on the sea-bottom disappears.

The integration term on the control boundary at infinity can be written as

$$\begin{aligned} \iint_{s_{\infty}} \left(\phi \frac{\partial G}{\partial n} - G \frac{\partial \phi}{\partial n} \right) dS &= \iint_{s_{\infty}} \phi \left[\frac{\partial G}{\partial z} - kG \right] dS \\ &= \int \int_{s_{\infty}} \left[\sqrt{R} \phi \cdot \sqrt{R} \left(\frac{\partial G}{\partial R} - ikG \right) - \sqrt{R} G \cdot \sqrt{R} \left(\frac{\partial \phi}{\partial R} - ik\phi \right) \right] d\theta dz \end{aligned} \quad (3.33)$$

From Eq. (3.12), the integration on the control boundary is zero.

If only the potential on the body surface needs to be solved, which is the case in the present study, Eq. (3.28) becomes

$$\phi(\mathbf{p}) = \frac{1}{2\pi} \iint_{s_b} \left(\phi(\mathbf{q}) \frac{\partial G(\mathbf{p}, \mathbf{q})}{\partial n} - G(\mathbf{p}, \mathbf{q}) \frac{\partial \phi(\mathbf{q})}{\partial n} \right) dS \quad (3.34)$$

where \mathbf{p} and \mathbf{q} denote that the points are on the body surface.

3.5.2 Source distribution method

From Eq. (3.34), it can be observed that the Green function $G(\mathbf{P}, \mathbf{Q})$ is akin to a source and its strength is proportional to $\partial \phi / \partial n$. The double integral

$1/(4\pi) \iint_{s_b} (\partial \phi / \partial n) G(\mathbf{P}, \mathbf{Q}) dS$ defines the potential generated by the sources

distributed on the body surface. Similarly, the normal derivative of the Green

function $\partial G / \partial n$ is like a dipole with the strength of ϕ , and $1/(4\pi) \iint_{s_b} \phi (\partial G) / (\partial n) dS$

is the potential generated by the dipole on the body surface. It is known that the solution that satisfies the Laplace equation and the boundary conditions defined

above should be unique. Therefore, once the value of ϕ is given, $\partial\phi/\partial\mathbf{n}$ can be determined, and vice-versa. Therefore, the potential can be obtained using the source or dipole distribution method. In the present study, the source distribution method is used.

In the source distribution method, Eq. (3.34) can be written as

$$\phi(\mathbf{p}) = \frac{1}{4\pi} \iint_{S_b} G(\mathbf{p},\mathbf{q}) \sigma(\mathbf{q}) dS \quad (3.35)$$

where σ is a source strength that can be obtained using the body boundary condition. To do this, it is necessary to obtain the normal derivative of Eq. (3.35), i.e.,

$$\frac{1}{2} \sigma(\mathbf{p}) + \frac{1}{4\pi} \iint_{S_b - \epsilon} G(\mathbf{p},\mathbf{q}) \sigma(\mathbf{q}) dS = \frac{\partial\phi(\mathbf{p})}{\partial\mathbf{n}} \quad (3.36)$$

where the first term results from the integration at the singularity point and ϵ is a small area that includes the singularity point.

3.6 The constant panel method

Eq. (3.36) is usually solved numerically. To this end, the mean wetted body surface needs to be discretized into panels. As in the finite element method, one can choose an interpolation function to describe the variation of the source strength within a panel. The constant panel method implies that the interpolation function is a constant, which means that the source as well as the potential are uniformly distributed within a panel. If a higher order interpolation function is employed (Liu

et al., 1991), the associated method is usually called the higher-order panel method. The higher-order panel method allows a linear or higher-order variation in the source strength and in the potential within a panel. In the present study, the constant panel method is employed.

If the wetted body surface is divided into N panels, N source strengths must be determined. The geometric center of each panel is chosen as a control point at which to satisfy the body boundary condition (Hess and Smith, 1962). Therefore, Eq. (3.36) is an N simultaneous equations, i.e.,

$$\frac{1}{2} \sigma_i(\mathbf{p}_i) + \frac{1}{4\pi} \sum_{j=1}^N \iint_{\Delta S_j - \epsilon} \mathbf{G}(\mathbf{p}_i, \mathbf{q}_j) \sigma(\mathbf{q}_j) dS_j = \frac{\partial \phi(\mathbf{p}_i)}{\partial \mathbf{n}} \quad (3.37)$$

and the velocity potential is expressed as

$$\phi(\mathbf{p}_i) = \frac{1}{4\pi} \sum_{j=1}^N \iint_{\Delta S_j} \mathbf{G}(\mathbf{p}_i, \mathbf{q}_j) \sigma(\mathbf{q}_j) dS_j \quad (3.38)$$

The wetted surface is usually represented by a number of quadrilateral panels (see Fig. 3.2). The four nodes of a space quadrilateral may not be located on the same plane of a generally shaped body. It is convenient to use a plane quadrilateral to simplify the calculation of the integration on the surface. Therefore, a middle plane quadrilateral is employed. This may result in a small gap between adjacent middle plane quadrilaterals and the normal may not be the normal of the body surface but the normal of the middle plane quadrilateral. Also, as mentioned above, the source strength is constant within a panel; hence, it is not continuous at the boundary of

panels. However, it has been shown that when N is large enough, the constant panel method can predict satisfactory results.

Appendix B describes the method for calculating the normal and the center of the geometry of the panel for a generally shaped body surface.

3.7 Generalized hydrodynamic forces

Once the velocity potential is obtained, the hydrodynamic pressure \mathbf{p} is given by the linearized Euler's integral, i.e.,

$$\mathbf{p} = -\rho \frac{\partial \Phi_T}{\partial t} \quad (3.39)$$

By decomposing the total velocity potential Φ_T into incident, diffraction and radiation potentials and taking out the factor of $e^{i\omega t}$, Eq. (3.39) is rewritten as

$$\mathbf{p} = -i\omega\rho\Phi_R - i\omega\rho(\Phi_I + \Phi_D) \quad (3.40)$$

Then the hydrodynamic force is

$$\{\mathbf{F}\} = \iint_{S_b} \mathbf{p}\{\mathbf{n}\}dS \quad (3.41)$$

and the generalized hydrodynamic force is

$$\{\mathbf{F}^*\} = \iint_{S_b} [\Psi]^T \mathbf{p}\{\mathbf{n}\}dS = \iint_{S_b} \mathbf{p}\{\mathbf{n}^*\}dS \quad (3.42)$$

where $[\Psi]$ is the mode shape matrix and $\{\mathbf{n}^*\} = [\Psi]^T\{\mathbf{n}\}$ is called the generalized normal vector.

The generalized hydrodynamic force due to the incident and diffraction potentials along is called the generalized wave exciting force and is calculated by

$$\{F_D^*\} = -i\omega\rho \iint_{S_b} (\phi_I + \phi_D) \{n^*\} dS \quad (3.43)$$

While the generalized hydrodynamic force due to the radiation potential is obtain from

$$\{F_R^*\} = -\sum_{j=1}^q i\omega\rho \iint_{S_b} \phi_{Rj} p_j \{n^*\} dS \quad (3.44)$$

where p_j is the normal coordinate of the j -th modal shape that corresponds to λ_j in Eq. (3.16) and needs to be obtained from the equations of motion.

The radiation potential is related to the motion of the body; therefore, the generalized hydrodynamic force due to the radiation potential is expressed by the added mass, which is related to the acceleration of the body, and by the damping, which is related to the velocity of the body, i.e.,

$$\{F_R^*\} = -\sum_{j=1}^q i\omega\rho \iint_{S_b} \phi_{Rj} p_j \{n^*\} dS = (\omega^2[M_f^*] - i\omega[C_f^*])\{p\} \quad (3.45)$$

where $[M_f^*]$ and $[C_f^*]$ are added mass and damping matrices, respectively. The

element M_{fjk}^* of the added mass matrix is

$$M_{fjk}^* = \frac{\rho}{\omega^2} \text{Re} \left\{ i\omega \iint_{S_b} \phi_{Rk} n_j^* dS \right\} \quad (3.46)$$

and the element C_{fjk}^* of the hydrodynamic damping matrix is

$$C_{fjk}^* = \frac{\rho}{\omega} \text{Im} \left\{ i\omega \iint_{S_b} \phi_{Rk} n_j^* dS \right\} \quad (3.47)$$

where the subscripts j and k represent the j -th normal coordinate and the k -th radiation potential, and where Re and Im denote the real and imaginary parts of the complex functions, respectively.

3.8 Generalized hydrostatic force

The generalized hydrostatic force arises from the static component of the pressure described by the Euler's integral in Eq. (3.5), i.e.,

$$p = -\rho g z \quad (3.48)$$

where z is the vertical coordinate of a point on the wetted surface. The origin of the coordinate system is at the still-water level. In a linear problem, the vertical coordinate of any point can be expressed as the sum of the original vertical coordinate and the displacement due to the modes of motion, i.e.,

$$z = z_0 + \sum_{j=1}^q \psi_{wj} p_j \quad (3.49)$$

where z_0 is the vertical coordinate at any point when the body is in original equilibrium position, ψ_{wj} is the vertical displacement corresponding to the motion of the j -th mode, p_j is the normal coordinates of the j -th mode, $j = 1, 2, \dots, 6$ stands for the rigid body modes of surge, sway, heave, roll, pitch and yaw, respectively, and $j > 7$ for the flexible modes.

Eq. (3.48) can be rewritten as

$$\mathbf{p} = -\rho \mathbf{g} (z_0 + \sum_{j=1}^q \psi_{wj} \mathbf{p}_j) \quad (3.50)$$

The second term of this equation is proportional to the normal coordinates, i.e. to the motion of the body, while the first term is motion independent, which contributes to balance the weight of the body. It is the second term that results in the hydrostatic restoring force \mathbf{F}_H , which can be written as

$$\{\mathbf{F}_H\} = -\rho \mathbf{g} \iint_{S_b} \sum_{j=1}^q \psi_{wj} \mathbf{p}_j \{\mathbf{n}\} dS \quad (3.51)$$

where $\{\mathbf{n}\}$ is the normal vector of the wetted surface. The generalized hydrostatic restoring force is

$$\{\mathbf{F}_H^*\} = -\rho \mathbf{g} \iint_{S_b} \{\psi_w\}^T \{\mathbf{p}\} [\Psi]^T \{\mathbf{n}\} dS - \rho \mathbf{g} \int \int_{S_b} z_0 [\Psi]^T \{\mathbf{n}\} dS \quad (3.52)$$

where $\{\psi_w\} = \{\psi_{w1}, \psi_{w2}, \dots, \psi_{wq}\}$.

The integration of Eq. (3.52) is proportional to the vertical coordinate $z = z_0 + w$, therefore the contribution from the thin strip $0 < z < \zeta$, where ζ is the change of still water level, will be of order ζ^2 . In the linearized analysis, this second-order quantity is neglected, and the wetted surface in the integral can be redefined as the mean body surface below the still-water plane.

It can be seen from Eq. (3.52) that the generalized hydrostatic restoring force is proportional to the displacement of the body, therefore it can be written in the form of hydrostatic restoring coefficients, i.e.,

$$\{F_H^*\} = -\rho g \iint_{S_b} \{\psi_w\}^T \{p\} [\Psi]^T \{n\} dS = -[K_f^*] \{p\} \quad (3.53)$$

where $[K_f^*]$ is the matrix of the generalized hydrostatic restoring coefficient. The

elements of $[K_f^*]$ are

$$K_{fjk}^* = \rho g \iint_{S_b} \psi_{wk} \{\psi_j\}^T \{n\} dS = \rho g \iint_{S_b} n_j \psi_{wk} dS \quad (3.54)$$

Note that in deriving the formulation for the calculation of the hydrostatic restoring coefficient, the weight of the body is not included. Although at the original equilibrium position the forces and moments due to the weight of the body are canceled by the forces and moments due to buoyancy, once the body is moved or deformed, the moments will not cancel each other. Therefore Eq. (3.54) is valid for the case in which the modal shapes are expressed with reference to the center of gravity. A derivation of the hydrostatic restoring coefficients of the rigid body modes for any arbitrary case is given by Newman (1977). In the case of the flexible modes, it is generally assumed that the deformation is so small that the displacements with reference to the original equilibrium system are the same as with reference to the center of gravity. Appendix C gives the hydrostatic restoring coefficients of the rigid body modes.

3.9 Utilization of geometric symmetry of the wetted body surface

If the geometry of the wetted body possesses single symmetry, i.e. port-starboard symmetry, or double symmetry, i.e. port-starboard and fore-aft symmetry, the amount

of work can be reduced in solving for the velocity potentials (Wu, 1984; Seidl, 1990; Wu et al., 1993).

The solution of the potential is a boundary-value problem. If the geometry of the body possesses single or double symmetry, the body boundary condition for the velocity potential, i.e. $\partial\phi/\partial\mathbf{n}$, can always be decomposed into symmetric and anti-symmetric conditions.

Take for example the case of single symmetry. The velocity potential can be written as

$$\phi(x,y,z) = \iint_{S_p} \sigma(\xi,\eta,\zeta) G(x,y,z,\xi,\eta,\zeta) dS + \iint_{S_s} \sigma(\xi,-\eta,\zeta) G(x,y,z,\xi,-\eta,\zeta) dS \quad (3.55)$$

where S_p is the wetted body surface of port side and S_s of starboard side. For the port-starboard symmetric body boundary condition, $\sigma(\xi,\eta,\zeta) = \sigma(\xi,-\eta,\zeta)$, while for the corresponding anti-symmetric condition $\sigma(\xi,\eta,\zeta) = -\sigma(\xi,-\eta,\zeta)$. Hence Eq. (3.39) can be expressed as

$$\phi(x,y,z)^\pm = \iint_{S_p} \sigma(\xi,\eta,\zeta) [G(x,y,z,\xi,\eta,\zeta) \pm G(x,y,z,\xi,-\eta,\zeta)] dS \quad (3.56)$$

where ϕ^+ and ϕ^- denote respectively the potential corresponding to the symmetric and anti-symmetric conditions. Since the Green function G has the property of symmetrization, i.e.,

$$G(+,+) = G(-,-) \quad (3.57)$$

$$G(+,-) = G(-,+) \quad (3.58)$$

ϕ^+ can be written as

$$\phi^{\pm} = \phi(x,y,z) \pm \phi(x,-y,z) \quad (3.59)$$

Therefore, if the geometry of the wetted body possesses symmetry, the potentials ϕ^{\pm} are solved first by using only one half of the body boundary condition, i.e., one half of the wetted body surface is discretized and entered in the calculation. When the potentials ϕ^{\pm} are obtained, the potential at any point can be easily solved by Eq. (3.43).

The boundary conditions for the radiation potentials of a symmetric body are expressed as

$$\frac{\partial \phi_{Rk}^+}{\partial \mathbf{n}} = 2i\omega\{\psi_k\}^T\{\mathbf{n}\} \quad (3.60)$$

Similarly, the boundary conditions of an anti-symmetric body are

$$\frac{\partial \phi_{Rk}^-}{\partial \mathbf{n}} = 2i\omega\{\psi_k\}^T\{\mathbf{n}\} \quad (3.61)$$

The body boundary conditions for the diffraction potentials corresponding to the symmetric and anti-symmetric conditions are

$$\frac{\partial \phi_D^+}{\partial \mathbf{n}} = - \left[\frac{\partial \phi_I(x,y,z)}{\partial \mathbf{n}} + \frac{\partial \phi_I(x,-y,z)}{\partial \mathbf{n}} \right] \quad (3.62)$$

$$\frac{\partial \phi_D^-}{\partial \mathbf{n}} = - \left[\frac{\partial \phi_I(x,y,z)}{\partial \mathbf{n}} - \frac{\partial \phi_I(x,-y,z)}{\partial \mathbf{n}} \right] \quad (3.63)$$

Similarly, if the geometry of the wetted body is port-starboard and fore-aft symmetric, then

$$\phi_{\pm}^{\pm} = \iint_{S_{pf}} \sigma(\xi, \eta, \zeta) G_{\pm}^{\pm}(x, y, z, \xi, \eta, \zeta) dS \quad (3.64)$$

where S_{pf} is one quarter of the wetted body surface and the superscript indices + and - correspond to port-starboard symmetry and anti-symmetry, respectively; and also the subscript indices + and - correspond to fore-aft symmetry and anti-symmetry, respectively, and

$$G_{+}^{+}(x, y, z, \xi, \eta, \zeta) = G(x, y, z, \xi, \eta, \zeta) + G(x, y, z, \xi, -\eta, \zeta) \\ + G(x, y, z, -\xi, -\eta, \zeta) + G(x, y, z, -\xi, \eta, \zeta) \quad (3.65)$$

$$G_{-}^{+}(x, y, z, \xi, \eta, \zeta) = G(x, y, z, \xi, \eta, \zeta) + G(x, y, z, \xi, -\eta, \zeta) \\ - G(x, y, z, -\xi, -\eta, \zeta) - G(x, y, z, -\xi, \eta, \zeta) \quad (3.66)$$

$$G_{+}^{-}(x, y, z, \xi, \eta, \zeta) = G(x, y, z, \xi, \eta, \zeta) - G(x, y, z, \xi, -\eta, \zeta) \\ - G(x, y, z, -\xi, -\eta, \zeta) + G(x, y, z, -\xi, \eta, \zeta) \quad (3.67)$$

$$G_{-}^{-}(x, y, z, \xi, \eta, \zeta) = G(x, y, z, \xi, \eta, \zeta) - G(x, y, z, \xi, -\eta, \zeta) \\ + G(x, y, z, -\xi, -\eta, \zeta) - G(x, y, z, -\xi, \eta, \zeta) \quad (3.68)$$

and

$$\phi_{+}^{+} = \phi(x, y, z) + \phi(x, -y, z) + \phi(x, -y, -z) + \phi(-x, y, z) \quad (3.69)$$

$$\phi_{-}^{+} = \phi(x, y, z) + \phi(x, -y, z) - \phi(-x, -y, z) - \phi(-x, y, z) \quad (3.70)$$

$$\phi_{+}^{-} = \phi(x, y, z) - \phi(x, -y, z) - \phi(-x, -y, z) + \phi(-x, y, z) \quad (3.71)$$

$$\phi_{-}^{-} = \phi(x, y, z) - \phi(x, -y, z) + \phi(-x, -y, z) - \phi(-x, y, z) \quad (3.72)$$

The body boundary conditions for the radiation potentials are

$$\partial \phi_{R\pm}^{\pm} = 4i \omega \{ \psi \}^T \{ \mathbf{n} \} \quad (3.73)$$

and the body boundary conditions for the diffraction potentials are

where $P_D = -\partial \phi_I / \partial \mathbf{n}$ and

$$\frac{\partial \phi_{D\pm}^{\pm}}{\partial \mathbf{n}} = P_{D\pm}^{\pm} \quad (3.74)$$

$$P_{D+}^+ = P_D(x,y,z) + P_D(x,-y,z) + P_D(x,-y,-z) + P_D(-x,y,z) \quad (3.75)$$

$$P_{D-}^+ = P_D(x,y,z) + P_D(x,-y,z) - P_D(-x,-y,z) - P_D(-x,y,z) \quad (3.76)$$

$$P_{D+}^- = P_D(x,y,z) - P_D(x,-y,z) - P_D(-x,-y,z) + P_D(-x,y,z) \quad (3.77)$$

$$P_{D-}^- = P_D(x,y,z) - P_D(x,-y,z) + P_D(-x,-y,z) - P_D(-x,y,z) \quad (3.78)$$

3.9.1 Generalized wave exciting forces and hydrodynamic coefficients

The generalized wave exciting forces and the hydrodynamic coefficients can be obtained from the potentials corresponding to the symmetric and anti-symmetric body boundary conditions.

For the single symmetry case, the generalized wave exciting forces are expressed by

$$F_j = -i\omega\rho \iint_{S_p} (\phi_I^+ + \phi_D^+) \mathbf{n}_j^* dS \quad (3.79)$$

where \mathbf{n}_j^* is defined as before and j corresponds to the mode whose shape is port-starboard symmetric and

$$F_j = -i\omega\rho \iint_{S_p} (\phi_I^- + \phi_D^-) \mathbf{n}_j^* dS \quad (3.80)$$

where j corresponds to the mode whose shape is port-starboard anti-symmetric.

The generalized radiation forces are expressed by means of hydrodynamic coefficients defined by Eq. (4.45) and can be calculated by

$$F_{Rjk} = -2i\omega\rho \iint_{S_p} \phi_k^+ n_j^* dS \quad (3.81)$$

where k, j correspond to port-starboard symmetric modes, and

$$F_{Rjk} = -2i\omega\rho \iint_{S_p} \phi_k^- n_j^* dS \quad (3.82)$$

where k, j correspond to a port-starboard anti-symmetric modes.

Similarly, for the doubly symmetric case, i.e. of port-starboard and fore-aft symmetry, the generalized wave exciting forces are

$$F_j = -i\omega\rho \iint_{S_p} (\phi_{I+}^+ + \phi_{D+}^+) n_j^* dS \quad (3.83)$$

where j corresponds to a port-starboard symmetric and fore-aft symmetric modal shape,

$$F_j = -i\omega\rho \iint_{S_p} (\phi_{I-}^+ + \phi_{D-}^+) n_j^* dS \quad (3.84)$$

where j corresponds to a port-starboard symmetric and fore-aft anti-symmetric modal shape,

$$F_j = -i\omega\rho \iint_{S_p} (\phi_{I+}^- + \phi_{D+}^-) n_j^* dS \quad (3.85)$$

where j corresponds to a port-starboard anti-symmetric and fore-aft symmetric modal shape,

$$F_j = -i\omega\rho \iint_{S_p} (\phi_{I-}^- + \phi_{D-}^-) n_j^* dS \quad (3.86)$$

where j corresponds to a port-starboard anti-symmetric and fore-aft anti-symmetric modal shape.

The generalized radiation forces are

$$F_{RjK} = -4i\omega\rho \iint_{S_{pf}} \phi_k^+ \cdot n_j^* dS \quad (3.87)$$

where k, j correspond to port-starboard symmetric and fore-aft symmetric modes,

$$F_{RjK} = -4i\omega\rho \iint_{S_{pf}} \phi_k^+ \cdot n_j^* dS \quad (3.88)$$

where k, j correspond to port-starboard symmetric and fore-aft anti-symmetric modes,

$$F_{RjK} = -4i\omega\rho \iint_{S_{pf}} \phi_k^- \cdot n_j^* dS \quad (3.89)$$

where k, j correspond to port-starboard anti-symmetric and fore-aft symmetric modes,

$$F_{RjK} = -4i\omega\rho \iint_{S_{pf}} \phi_k^- \cdot n_j^* dS \quad (3.90)$$

where k, j correspond to port-starboard anti-symmetric and fore-aft anti-symmetric modes.

3.9.2 Restoring coefficients

For the singly symmetric case, the elements of the restoring coefficient matrix are calculated from

$$C_{jk} = -2\rho g \iint_{S_p} w_k n_j^* dS \quad (3.91)$$

where w_k is the vertical displacement at any point due to the motion in the k -th mode and k, j correspond to two symmetric modes or anti-symmetric modes.

Similarly, for the doubly symmetric case, the elements of the restoring coefficient matrix are

$$C_{jk} = -4\rho g \iint_{S_{\text{pt}}} w_k n_j^* dS \quad (3.92)$$

where k, j correspond to the two modal shapes that are of the same symmetric and anti-symmetric characteristics.

CHAPTER 4

HYDROELASTIC RESPONSE OF A FLOATING BODY

As discussed in Chapter 2, once the forces acting on a floating body are known, the motions of the body can be obtained without difficulty. Although there are several kinds of external forces acting on a floating body, only the fluid forces are considered in this study. According to Chapter 3, the generalized fluid force F^* can be written as

$$\{F^*\} = \{F_H^*\} + \{F_R^*\} + \{F_W^*\} \quad (4.1)$$

where F_H^* , F_R^* and F_W^* are the generalized hydrostatic force, radiation force and wave exciting force, respectively. By using Eqs. (3.45), (3.53), the modal equations of motion (2.25) can be written as

$$\left[-\omega^2 ([M_s^*] + [M_f^*]) + i\omega ([C_s^*] + [C_f^*]) + ([K_s^*] + [K_f^*]) \right] \{p\} = \{F_W^*\} \quad (4.2)$$

where $[M_s^*]$, $[C_s^*]$ and $[K_s^*]$ are the generalized structural mass, damping coefficient and stiffness matrices, respectively; $[M_f^*]$, $[C_f^*]$ and $[K_f^*]$ are the generalized added mass, fluid damping coefficient and hydrostatic stiffness matrices, respectively; and $\{F_W^*\}$ is the generalized wave exciting force.

Note that matrices with subscript f in Eq. (4.2) are not diagonal. The present method of solution is not a standard mode superposition method that relies on the uncoupling of the equations of motion in normal coordinates. Rather, in

hydroelasticity, a truncated set of normal coordinates is used to reduce the dimensions of the system of equations of motion. The truncation is possible because the normal coordinates are more efficient in representing the structural motion than are the 'physical' coordinates.

Eq. (4.2) represents q modal equations that are coupled with each other. The solution of Eq. (4.2) for the normal coordinates $\{p\}$ permits the calculation of the structural responses such as displacements and stresses required by engineering design. The nodal displacement can be obtained from Eq. (2.22) and the structural internal forces and stresses from Eqs. (2.23) and (2.24).

CHAPTER 5

THE MODIFIED MORISON'S EQUATION METHOD

5.1 Overview

Chapters 2 and 3 present an overview of the theories involved in three-dimensional hydroelastic analysis of a floating body. Although the linear three-dimensional hydroelasticity theory has been well developed, its application to a VLFS at the present time is difficult because of the limitations of computer resources. Consequently, various more efficient approaches have been developed (see Ertekin, 1994 for a review). The Morison's equation method is one of them.

Morison's equation (Morison et al., 1950) has been successfully used in the offshore industry to determine, especially during the preliminary design stage, the motion response of floating structures. This equation includes the effects of fluid acceleration and viscous form drag in terms of empirically determined coefficients. The equation was developed as an ad hoc approach to a limited set of experimental data and was introduced originally to calculate the wave exciting forces and moments on fixed vertical piles of circular cross section. This approach has been later extended to fixed tubular structures and semi-submersibles (Burke, 1969; Paulling, 1970; Paulling and Tyagi, 1991; Chitrapu et al., 1993; Chitrapu and Ertekin, 1995). Recently Morison's equation has been applied in the hydroelastic analysis of very large floating structures (Ertekin et al., 1993; Hirayama et al., 1994).

The main reason for introducing the Morison's equation method to the hydroelastic analysis of a VLFS is due to its high efficiency and the considerable computational cost of using three-dimensional hydroelasticity. To be sure, Morison's equation is applicable only to the structures that have tubular components below the still-water surface, such as semi-submersibles.

However, it is well known that use of constant coefficients in Morison's equation leads to less accurate results, especially at the high frequencies at which wave scattering is important. In the attempt to improve the prediction of the fluid loading at high frequencies, the added mass, damping coefficient and excitation in this study are calculated by potential theories. The extended MacCamy & Fuchs' method is used to solve for the fluid action on vertical cylinders and strip theory is employed for horizontal pontoons. The total fluid force is expressed in the form of Morison's equation by introducing the equivalent hydrodynamic coefficients based on the results obtained from potential theories.

In this chapter, the formulation used in the modified Morison's equation method is introduced and then applied to a semi-submersible system. The derived numerical results are presented.

5.2 Structural model in Morison's equation method

The structure is discretized by the finite element method. Since the submerged members of a VLFS of semi-submersible type are columns and pontoons, it is convenient to employ frame elements to model the structure.

The formulation of the finite element method has been described in Chapter 2. A frame element is defined by two end nodes (see Fig. 5.1), each of which has three translational and three rotational degrees-of-freedom. The displacements of an element at any point can be obtained from the displacements of the nodes by the use of interpolation functions:

$$\{d\} = [N]\{u\} \quad (5.1)$$

where $\{d\}$ is a 6×1 vector of translational and rotational displacements at a point of an element defined in the local coordinate, $\{u\}$ is the 12×1 vector of nodal displacements at the two end nodes of the element, $[N]$ is a 6×12 matrix of interpolation functions that are given in Appendix A.

The forces distributed along an element obtained from Morison's equation are replaced by equivalent nodal forces given by

$$\{F^a\} = \int_{L_e} [N]^T \{f\} dL \quad (5.2)$$

where $\{F^a\}$ is the vector of the equivalent nodal forces in the element's local coordinate system, $\{f\}$ is the vector of distributed force calculated from Morison's equation, and L_e is the length of the element.

The consistent structural mass $[M_s]$ and stiffness matrices $[K_s]$ for an element in the local coordinate system are given in Appendix A. To obtain the global matrices for the equations of motion (2.15), the quantities need to be transformed from local to global coordinate systems and assembled at the common nodes.

5.3 Hydrostatic forces

The hydrostatic forces require special attention within the framework of the three-dimensional structural frame model, since the sectional restoring forces must be considered rather than the restoring forces for the whole structure, as is the case in rigid-body motion analysis (Che, 1993). The major difference between the hydrostatic restoring force of a unit section and that of the whole body is that the displacement of a unit section beam may not be equal to its weight.

It is convenient to write the restoring forces $\{F_H\}$ in terms of the hydrostatic stiffness matrix, i.e.

$$\{F_H\} = -[K_f]\{u\} \quad (5.3)$$

This stiffness matrix has both a stabilizing component, due to the water plane area of the surface-piercing structural members, and a destabilizing component, due to the shift of the application point of the net buoyancy forces of columns and pontoons.

The stabilizing component of the hydrostatic stiffness is modeled by locating a node at each intersection of the still-water plane and column, and attaching discrete vertical and rotational springs to these nodes. The only non-zero components of the hydrostatic stiffness are given by

$$k_{\bar{z}\bar{z}} = \rho g A_c, \quad k_{\bar{x}\bar{x}} = \rho g I_{\bar{x}\bar{x}}, \quad k_{\bar{y}\bar{y}} = \rho g I_{\bar{y}\bar{y}} \quad (5.4)$$

where A_c is the water-plane area of a column, $I_{\bar{x}\bar{x}}$ and $I_{\bar{y}\bar{y}}$ are the second moments of water plane area of the column about the axes of \bar{x} and \bar{y} , respectively, also in the local coordinate system (see Fig. 5.1), .

A shift in the center of buoyancy such that it is no longer vertically aligned with the center of gravity causes an overturning moment on the deck. This destabilizing effect of buoyancy is caused by the pitching/rolling motion. This overturning moment is transmitted to the deck by the columns. To incorporate this into the structural model, the geometric stiffness of the column frame elements is used. This is equivalent to subjecting the column to an axial force. This additional term in the hydrostatic stiffness matrix in the local coordinates can be written as

$$[k_g] = \int_{L_e} f_a [N']^T [N'] d\bar{x} \quad (5.5)$$

where f_a is the axial force and primes indicate differentiation of interpolation functions.

The consistent hydrostatic stiffness matrix of an element is then assembled by adding the stabilizing and destabilizing components and then transforming them into the global coordinates.

5.4 Hydrodynamic forces

Since Morison's equation is used in the hydrodynamic analysis, the structural components below the still-water plane are modeled as circular cylinders. The displaced volumes of the circular cylinders are the same as the original structural components.

The hydrodynamic force due to waves includes the structural displacement force, namely the inertial force that is proportional to the acceleration and the damping

force that is proportional to the velocity, as well as the exciting force due to the incident and scattered waves. In terms of Morison's equation, the sectional hydrodynamic force $\{F_{cp}\}$ can be written as

$$\begin{aligned} \{F_{cp}\} = & \frac{1}{2} \rho C_D D |\{\dot{u}_{fn}\} - \{\dot{u}_n\}| (\{\dot{u}_{fn}\} - \{\dot{u}_n\}) \\ & + \frac{1}{4} \rho \pi D^2 (C_M \{\ddot{u}_{fn}\} - (C_M - 1) \{\ddot{u}_n\}) \end{aligned} \quad (5.6)$$

where C_D is the form-drag coefficient; C_M the inertia coefficient; $\{u_{fn}\}$ the water particle displacement vector normal to the element; $\{u_n\}$ the displacement vector of a point on the element in the normal direction; D the diameter of the tubular member of the structure. The nonlinear drag force can be written in terms of the equivalent linear drag coefficient (Blagoveshchensky, 1962)

$$\{F_{cpD}\} = \frac{1}{2} \rho C_{DL} D (\{\dot{u}_{fn}\} - \{\dot{u}_n\}) \quad (5.7)$$

where C_{DL} is the equivalent linear drag coefficient and can be obtained by

$$C_{DL} = \frac{8}{3} \pi C_D (\dot{u}_{fn0} - \dot{u}_{n0}) \quad (5.8)$$

where \dot{u}_{fn0} is the amplitude of the water particle velocity and \dot{u}_{n0} is the amplitude of velocity of a point on the element in the normal direction. Note that C_{DL} is a dimensional coefficient.

5.5 The equivalent hydrodynamic coefficients

As mentioned before, the use of the constant form-drag coefficient C_D and inertia coefficient C_M in Morison's equation may lead to less accurate results. Hence, potential theory is used in this study to calculate the hydrodynamic forces of radiation and wave excitation. The hydrodynamic force so obtained is expressed in the form of Morison's equation. By doing so, the equivalent linear drag coefficient C_{DL} and the inertia coefficient C_M can be obtained. To obtain the hydrodynamic force for columns, the extended MacCamy & Fuchs' (1954) method proposed by Garrison (1984) is used, and for pontoons Frank's (1967) close-fit method based on the strip theory is employed. Obviously, the use of such methods imply that any hydrodynamic interference effects between members are negligible. Moreover, such approximations cannot predict the three-dimensional flow structure at the end of a column or pontoon.

5.5.1 Columns

It is assumed that columns of a module are hydrodynamically isolated. If this assumption proves to lead to great inaccuracies in certain cases, it is possible to consider the mutual interaction between neighboring columns by using the interaction theory for a matrix of columns (see for example, Kagemoto and Yue 1993).

In the extended MacCamy-Fuchs approach, the total potential is decomposed into incident ϕ_I , diffraction ϕ_D and radiation ϕ_R potentials, i.e.

$$\phi_T = \phi_I + \phi_D + \phi_R \quad (5.9)$$

If the vertical column is circular, it is convenient to solve the velocity potentials in cylindrical coordinates. A right-handed cylindrical coordinate system is used (see Fig. 5.2). The governing equation and boundary conditions in the cylindrical system are

$$\frac{\partial^2 \phi_T}{\partial r^2} + \frac{1}{r} \frac{\partial \phi_T}{\partial r} + \frac{1}{r^2} \frac{\partial^2 \phi_T}{\partial \theta^2} + \frac{\partial^2 \phi_T}{\partial z^2} = 0 \quad (5.10)$$

$$\omega^2 \phi_T + g \frac{\partial \phi_T}{\partial z} = 0 \quad \text{at } z = 0 \quad (5.11)$$

$$\frac{\partial \phi_T}{\partial z} = 0 \quad \text{at } z = -h \quad (5.12)$$

where h is the water depth.

The incoming wave potential is written as

$$\phi_I = \frac{igA}{\omega} \frac{\cosh[k(z+h)]}{\cosh(kh)} e^{-ikr\cos\theta} e^{i\omega t} \quad (5.13)$$

where A is wave amplitude, ω the angular wave frequency, g the gravitational acceleration and k the wave number.

According to the theory of Bessel functions (Abramowitz and Stegun, 1964), the exponential term can be written as

$$e^{ikr\cos\theta} = \sum_{m=-\infty}^{\infty} i^m J_m(kr) e^{im\theta} \quad (5.14)$$

The diffraction potential should have a form similar to the incident wave potential. Given the body boundary condition, the radiation condition that must be satisfied by

the diffraction potential, and the properties of the Bessel function, the diffraction potential may be expressed as

$$\phi_D = \sum_{m=-\infty}^{\infty} A_m \frac{\cosh[k(z+h)]}{\cosh(kh)} H_m(kr) e^{im\theta} e^{i\omega t} \quad (5.15)$$

where A_m is a coefficient that can be determined by the body boundary condition.

In (Garrison, 1982), this coefficient is expressed as

$$A_m = \frac{iAg}{\omega} i^m \frac{J'_m(ka)}{H'_m(ka)} \quad (5.16)$$

where a is the cylinder radius, J'_1 is the derivative of the Bessel function of the first

kind and of order one, and Y'_1 is the derivative of the Bessel function of the second

kind and of order one.

Hence the diffraction potential is written as

$$\phi_D = \frac{iAg}{\omega} \sum_{m=-\infty}^{\infty} i^m \frac{\cosh[k(z+h)]}{\cosh(kh)} \frac{J'_m(ka)}{H'_m(ka)} H_m(kr) e^{im\theta} e^{i\omega t} \quad (5.17)$$

The pressure due to the incident and scattered waves can then be calculated by Euler's integral, and the sectional force can be obtained by integration of the pressure. The sectional force is obtained as

$$\delta F(z,t) = \frac{4\rho g A}{k} \frac{\cosh k(z+h)}{\cosh(kh)} R(ka) \cos(\omega t + \alpha) \quad (5.18)$$

where

$$R(ka) = [J_1'(ka)^2 + Y_1'(ka)^2]^{-1/2}, \quad \alpha(ka) = \tan^{-1}(Y_1'/J_1') \quad (5.19)$$

If this force is made equal to the force obtained by the linearized Morison's equation, the following coefficients are obtained

$$C_M = C \cos \delta, \quad C_{DL} = \pi \omega a C \sin \delta \quad (5.20)$$

where

$$C = \left(\frac{2L}{\pi D} \right)^2 \frac{1}{\pi \sqrt{J_1'(ka)^2 + Y_1'(ka)^2}} \quad (5.21)$$

$$\delta = \tan^{-1}[J_1'(ka)/Y_1'(ka)]$$

in which L is the wave length. These coefficients provide approximations to the exciting forces that could have been obtained by potential theory when used in Morison's equation. Note that these coefficients are depth independent. Once the sectional forces are calculated, they are used only from the still-water plane down to the bottom of a column. This is equivalent to using a shape function for the exciting forces, for which $\psi(z)=0$ if $z < -d$ (d = draft of the column).

The radiation potential must satisfy the same conditions as that of the diffraction potential except the body boundary condition. At the body's boundary, the normal velocity of the fluid particles is equal to the normal velocity of the body. That is

$$\frac{\partial \phi_R}{\partial \mathbf{r}} = i \omega \psi(z) \cos \theta \quad (5.22)$$

where $\psi(z)$ is the displacement of the cylinder in the x direction.

The radiation potential can be written as

$$\phi_R = A_0 \cosh[k(h+z)] H_1(kr) \cos \theta + \sum_{i=1}^{\infty} A_i \cos[\mu_i(h+z)] K_1(\mu_i r) \cos \theta \quad (5.23)$$

where A_0 and A_i can be determined by applying the kinematic boundary conditions on the body surface and μ is the root of $\omega^2 = -g\mu \tan(\mu h)$.

Since the radiation potential ϕ_R is proportional to the motion of the structure, it is expressed by

$$\phi_R = \sum_j \lambda_j \phi_{Rj} \quad (5.24)$$

where λ_j is the displacement amplitude of j -th mode. The displacement d at any point can be expressed as $d = \sum_j \psi_j(z) \lambda_j$, where $\psi(z)$ denotes the shape function.

The shape functions for surge are

$$\psi(z) = 1 \quad 0 < z < -d, \quad \psi(z) = 0 \quad z < -d \quad (5.25)$$

and for pitch they are

$$\psi(z) = z/d \quad 0 < z < -d, \quad \psi(z) = 0 \quad z < -d \quad (5.26)$$

By imposing the body boundary condition, the radiation potential can be obtained explicitly (see Garrison, 1984), and the pressure and the force can be calculated.

The hydrodynamic coefficients related to the sectional radiation forces are:

$$\begin{aligned} C_{d1} &= \text{Re}(\phi'_{Rj})/a\psi_j(z) \\ C_m &= \text{Im}(\phi'_{Rj})/a\psi_j(z) \end{aligned} \quad (5.27)$$

where primes indicate differentiation with respect to r . If needed, the overall hydrodynamic inertia and damping coefficients can be obtained by integration over the length of the column to determine A_{ij} and B_{ij} , $i,j=1$ (surge), $=5$ (pitch), as the hydrodynamic inertia and damping coefficients, respectively.

5.5.2 Pontoons

The pontoons of a semi-submersible are relatively slender and, therefore, it appears suitable to use Frank's close-fit method to calculate the hydrodynamic coefficients. To do this, the two-dimensional problem of a submerged cylinder is solved to obtain the radiation potentials for surge and heave (see also Ogilvie, 1963). The wave exciting forces are calculated using the Haskind-Hanaoka relationship.

Frank's close-fit method is based on strip theory. In this theory, the velocity potential is solved for each section. Each section has three rigid body modes: sway, heave and roll. The radiation potential ϕ_j for the j -th mode, satisfies the following boundary conditions,

$$\frac{\partial^2 \phi_j}{\partial y^2} + \frac{\partial^2 \phi_j}{\partial z^2} = 0 \quad \text{in } \Omega \quad (5.28)$$

$$\frac{\partial \phi_j}{\partial z} + \frac{\omega^2}{g} \phi_j = 0 \quad \text{on } z=0 \quad (5.29)$$

$$\frac{\partial \phi_j}{\partial n} = i \omega n_j \quad \text{on body} \quad (5.30)$$

$$\frac{\partial \phi_j}{\partial z} = 0 \quad \text{on the sea bottom} \quad (5.31)$$

$$\lim_{y \rightarrow \pm \infty} \left[\frac{\partial \phi_j}{\partial y} \mp ik \phi_j \right] = 0 \quad (5.32)$$

where Ω is the two-dimensional fluid domain and k is the wave number.

Frank's "Close-Fit" method considers not only the interior and exterior problems but also the upper imaginary part that is mirrored from the strip contour line above the still water line. The Green function that is used in this method is given by Wehausen and Laitone (1960) as

$$G(P,Q) = \ln(r) - \ln(r_1) + 2P.V. \int_0^{\infty} e^{z+\eta} \frac{\cos[m(y-\xi)]}{m-k} dm - e^{k(z+\eta)} \cos k(y-\xi) \quad (5.33)$$

where k is the wave number, $r = \sqrt{(y-\xi)^2 + (z-\eta)^2}$, $r_1 = \sqrt{(y-\xi)^2 + (z+\eta)^2}$ and P.V.

denotes the Cauchy principal value integral.

The velocity potential at any point P in the two-dimensional domain can be written as

$$\phi(P) = \frac{1}{2\pi} \int_{C_b} G(P,Q) \sigma(Q) dC \quad (5.34)$$

where C_b is the wetted contour of the cross section and σ is the source strength.

By taking the derivative of Eq. (5.34), it obtains that

$$\frac{1}{2} \sigma(\mathbf{P}) + \frac{1}{2\pi} \int_{c_b - \epsilon} \sigma(\mathbf{Q}) \frac{\partial(\mathbf{P}, \mathbf{Q})}{\partial \mathbf{n}} d\mathbf{C} = \frac{\partial \phi_j(\mathbf{P})}{\partial \mathbf{n}} \quad (5.35)$$

where ϵ is a small segment of line that includes the singularity point. Eq. (5.35) can be solved numerically by applying the body boundary condition to obtain the source strength. Then the potential can be determined from Eq. (5.34).

The hydrodynamic forces due to the radiation potential is expressed as

$$\mathbf{f}_{ij} = i\omega\rho \int_{c_b} \phi_j \mathbf{n}_i d\mathbf{C} = i\omega\rho \int_{c_b} \phi_j \frac{\partial \phi_i}{\partial \mathbf{n}} d\mathbf{C} \quad (5.36)$$

where \mathbf{n}_i is the component in the i -th direction of the unit normal vector of the body surface, the index j denotes the mode of motion, \mathbf{f}_{ij} is the radiation force in the i -th direction due to a unit displacement in the j -th direction. \mathbf{f}_{ij} includes two terms: one is proportional to the unit acceleration of the body while the other is proportional to the unit velocity of the body. The inertial and damping coefficients are expressed by

$$\mu_{ij} + \frac{i}{\omega} \lambda_{ij} = \rho \int_{c_b} \phi_j \frac{\partial \phi_i}{\partial \mathbf{n}} d\mathbf{C} \quad (5.37)$$

where μ_{ij} and λ_{ij} are the sectional inertial and damping coefficients, respectively.

By using the Haskind-Hanaoka relationship (Ertekin et al., 1995), the force related to wave diffraction can be obtained from the incident and radiation potentials, i.e.,

$$f_{Dj} = \rho \int_{C_b} \phi_j \frac{\partial \phi_I}{\partial n} dC \quad (5.38)$$

where f_{Dj} denotes the scattering force or moment in the j -th direction, ϕ_I is the incident wave potential and ϕ_j is the radiation potential due to the motion in the j -th direction.

5.6 Applications of the modified Morison's equation method to the analysis of semi-submersible systems

The modified Morison's equation method is applied to the analysis of the hydroelastic response of a single module and a 16-module semi-submersible floating systems. The single module floating structure used here was designed by Winkler et al. (1990) and the 16-module floating structure is assembled from 16 identical single modules connected at the deck level or at both the deck and pontoon levels. The overall geometry of a single module is shown in Fig. 5.3 and a schematic layout of multi-modules appears in Fig. 5.4. The main particulars of a single module are given in Table 5.1. and the section structural properties are given in Table 5.2. More details of the module design can be found in Winkler et al. (1990).

The obtained results by the present method are compared with those predicted by Morison's equation method. Also, in order to determine the accuracy of the approximate theory based on the extended MacCamy & Fuchs' approach, the hydrodynamic coefficients of and the wave excitation on a single column are computed and compared with the results obtained from a three-dimensional panel

method. To this end, a vertical cylinder of 15.8m diameter and 14.7m draft is employed. This cylinder is of the draft and volume equivalent to the draft and volume of a column (which has a rectangular cross section) of the semi-submersible used.

Table 5.1 Main particulars of a single module

Length x width x height, m	100x100x59
Column (width x depth x height), m	12x17x35
Pontoon (width x height x length), m	18x10x96
Operating draft, m	25
Displacement (mass) ,kg	46440x 10 ³
I _{x1} , kg-m ²	7.91x 10 ¹⁰
I _{x2} , kg-m ²	6.49x 10 ¹⁰
I _{x3} , kg-m ²	9.35x 10 ¹⁰
KG, KB, m	30.67, 8.25
GM _L , GM _T , m	5.01, 4.13

Table 5.2 Section structural properties

Modulus of Elasticity: 2.07*10 ¹¹ (N/m ²) Shear Modulus: 8.0*10 ¹⁰ (N/m ²)					
Member	Steel area (m ²)	I _{yy} (m ⁴)	I _{zz} (m ⁴)	J (m ⁴)	\bar{m} (kg/m)
Pontoon	2.8	40	90	60	57290
Column	2.21	70	40	70	39230
Deck					
Longitudinal	0.80	25	25	50	23400
Transverse	0.25	20	40	50	23400

5.6.1 Single column results

Fig. 5.5 through Fig. 5.10 present the added inertial and damping coefficients and wave excitations of a truncated vertical cylinder. These results are obtained by Morison's equation method (labeled as Morison), the modified Morison's equation method (labeled as M-Morison) and the three-dimensional panel method (labeled as GFM). In Morison's equation method, the constant coefficients $C_M = 2.0$ and $C_D = 0.0$ are used.

Fig. 5.5 shows the normalized wave exciting force in surge. As expected, Morison's equation predicts inaccurate results at high frequencies. The calculations using the Modified Morison's equation are quite satisfactory with results obtained in comparison with the three-dimensional panel method. The normalized wave exciting moment in pitch shown in Fig. 5.6 also follows the same trend.

The normalized added mass and damping coefficient in surge are shown in Figs. 5.7 and 5.9, and the added moment and damping coefficient in pitch are shown in Figs. 5.8 and 5.10. Note that the added mass in surge A_{11} in the Morison's equation method is given by $A_{11} = \rho \pi D^2 (C_m - 1) d / 4$ and the damping coefficient B_{11} is given by $B_{11} = \rho C_{DL} D d / 2$ where d is the submerged length (or draft) of the column. In Figs. 5.9 and 5.10, two constant damping lines are shown since the damping coefficient in Morison's equation depends on the amplitude of motion. Morison-1

refers to displacement over cylinder radius ratio of 0.033 and Morison-2 refers to 0.05.

Of all the results presented, those obtained from the modified Morison's equation method are very close to the results predicted by the three-dimensional panel method, while those obtained from Morison's equation are unsatisfactory.

5.6.2 The results of semi-submersible systems

The modified Morison's equation method is applied to a single module and a VLFS that is composed of 16 modules connected at the deck level or both at the deck and pontoon levels. For simplicity, in the hydrodynamic analysis, only four columns and two pontoons are used to model the semi-submersible. Some results for head, quartering and beam seas are shown in Figs. 5.11 through 5.26. In the Morison's equation results, constant inertia and drag coefficients ($C_M = 2.0$ and $C_D = 1.0$) are employed.

The entire structure is modeled by frame elements; a total of 171 elements per module is used. There are 2464 nodes for the entire VLFS. Module 1 is at the bow, Module 16 is at the stern and Module 8 is near the origin at the center. The results presented in the figures. are the motions of the center of gravity of the modules. Figs. 5.11 through 5.13 show the motions of a single module, in the absence of all others, to check the accuracy of the predictions based on the modified Morison's equation. It is seen from these figures, which are for head seas, that there is some

improvement of the results in the high frequency range over those obtained from the Morison's equation.

Figs. 5.14 through 5.16 show the single rigid module results for beam seas. It is clear that in the results where Morison's equation method does not predict results close to the three-dimensional panel method results, the three-dimensional flow structure must be important.

As to the 16 module system, the motion responses of the center of gravity of Modules 1 and 8 are presented, predicted by the Morison's equation method and the modified Morison equation's method, respectively. Figs. 5.17 through 5.22 show the surge, heave and pitch motion comparisons for the head-sea case. Note that Figs. 5.17 through 5.25 correspond to the deck connector (at $x_3 = 26.5$ m above SWL) only case. These results consistently indicate that when wave scattering and radiation are included, the motions become less at most frequencies. A similar conclusion was reached in Ertekin et al. (1993) when Morison's equation results are compared with the Green function results.

Figs. 5.23 through 5.25 show the quartering sea cases for Module 1, again for connectors located at the deck level only. Except at low frequencies, Morison's equation with constant coefficients predicts large motion amplitudes as before.

Figs. 5.26 through 5.28 show the motion responses for the case when there are connectors at the pontoon level in addition to those at the deck connectors. The connectors' structural properties were assumed to be the same as the deck

connectors'. Comparison of this case with earlier ones for deck-connector only shows that the motions are damped significantly.

5.7 Final remarks

The extended MacCamy-Fuchs approach is used to determine the frequency dependent hydrodynamic inertia, damping coefficients and wave excitation to be used in Morison's equation to supply the fluid loading in the Morison's equation's method. This is done for the columns, and Frank's close-fit method is used to do the same for the pontoons.

When these frequency-dependent hydrodynamic coefficients are used in the Morison's method, the predicted motions are significantly suppressed at most wave frequencies. This comparison leads to the same conclusion reached in earlier works, namely that the Morison's equation with constant coefficients over- predicts the hydroelastic response.

On the other hand, the assumption that there is negligible interaction between neighboring members may prove to lead to rather inaccurate results that are seen when motions of a module of VLFS obtained by the modified Morison's equation method and by the Green function method are compared. This then suggests that in a hydroelasticity problem where there are many modules, it is necessary to further extend the present approach to: (i) multiple vertical cylinders, and (ii) endplane forces.

CHAPTER 6

AN EFFICIENT HYDROELASTIC ANALYSIS METHOD FOR A MAT-LIKE PLATFORM OF SHALLOW DRAFT

6.1 Overview

A mat-like platform is characterized by a small ratio of depth to length and beam; hence it is more flexible when compared with a three-dimensional floating structure of normal dimensions and these elastic deformations are important and cannot be neglected in the dynamic response analysis. A mat-like platform can be approximated by a two-dimensional plate with the consequence that it is possible to employ plate theory in the structural analysis (Webster, 1991; Mamidipudi and Webster, 1994). Because the draft is small, it should also be possible to use the zero-draft Green-function method to solve the hydrodynamic problem (Kim, 1963; Maeda and Eguchi, 1976; Wu and Price, 1986). The computational advantage of using plate theory and the zero-draft Green function should be significant in the hydroelastic response analysis of such a structure. Masuda et al. (1987) employed the zero-draft Green function and combined it with simple beam theory to analyze the hydroelastic response of a ship. The computational time is considerably reduced compared with that of using the three-dimensional Green function. However, the simple beam theory is suitable only for slender bodies, and the structure is limited to have only beam motions and deformations.

In this chapter, the mat-like platform is modeled as a plate for the purpose of structural analysis and the zero-draft Green function is employed in the hydrodynamic analysis. Since bending motion is more important than other motions for a mat-like structure, the plate model is proportioned so that its bending stiffness and mass are the same as those of the mat-like floating body. The finite element method is used to obtain the structural deformations and the equations of motion are solved in normal coordinates. The velocity potentials are obtained numerically using the source-distribution method. The predicted results are compared with the available data to verify the accuracy of the present method (Wang et al., 1995a).

6.2 Structural and hydrodynamic models

By introducing the zero-draft assumption, the governing equations and boundary conditions discussed in Chapters 2 and 3 for a general three-dimensional hydroelasticity problem are modified accordingly.

In the structural domain, the governing equation is the same as Eq. (2.16) employed in the finite-element model. It is written as

$$(-\omega^2[\mathbf{M}_s^*] + i\omega[\mathbf{C}_s^*] + [\mathbf{K}_s^*])\{\mathbf{p}\} = \{\mathbf{F}^*\} \quad (6.1)$$

where $[\mathbf{M}_s^*]$, $[\mathbf{C}_s^*]$ and $[\mathbf{K}_s^*]$ are the generalized structural mass, damping and stiffness matrices, respectively, and $\{\mathbf{F}^*\}$ is the generalized fluid force vector.

In the fluid domain, the governing equation and boundary conditions of the velocity potential are expressed as

$$\frac{\partial^2 \phi}{\partial x^2} + \frac{\partial^2 \phi}{\partial y^2} + \frac{\partial^2 \phi}{\partial z^2} = 0 \quad \text{in } \Omega \quad (6.2)$$

$$\omega^2 \phi - g \frac{\partial \phi}{\partial z} = 0 \quad \text{at } z = 0, \notin S_B \quad (6.3)$$

$$\frac{\partial \phi}{\partial z} = V_n \quad \text{at } z = 0, \in S_B \quad (6.4)$$

$$\frac{\partial \phi}{\partial n} = 0 \quad \text{at sea bottom} \quad (6.5)$$

$$\lim_{R \rightarrow \pm\infty} \{R^{1/2} \left(\frac{\partial}{\partial R} \mp ik \right) \phi\} = 0 \quad (6.6)$$

where ϕ is the velocity potential, Ω is the fluid domain, S_B is the wetted surface, V_n is the normal velocity of the body boundary, ω is the wave frequency, k is the wave number, and $R = \sqrt{x^2 + y^2}$.

The Green function method is used to solve for the diffraction and radiation potentials and Eq. (3.35) is repeated here again for convenience,

$$\phi(\mathbf{p}) = \frac{1}{4\pi} \int_{S_b} G(\mathbf{p}, \mathbf{q}) \sigma(\mathbf{q}) ds \quad (6.7)$$

Note that the Green function satisfies the free-surface boundary condition given by

$$\frac{\partial G(\mathbf{p}, \mathbf{q})}{\partial n} = \frac{\partial G(\mathbf{p}, \mathbf{q})}{\partial z} = kG(\mathbf{p}, \mathbf{q}) \quad (6.8)$$

in which $k = \omega^2/g$ is the deep water wave number, and $\partial\phi/\partial n = \partial\phi/\partial z$; hence

$$\frac{\partial \phi(\mathbf{p})}{\partial z} = \frac{k}{4\pi} \int_{S_B} G(\mathbf{p}, \mathbf{q}) \sigma(\mathbf{q}) ds \quad (6.9)$$

The source strength is obtained by solving Eq. (6.9). By substituting Eq. (6.9) into Eq. (6.7), the potential is obtained as

$$\phi(\mathbf{p}) = \frac{1}{\mathbf{k}} \left(\frac{\partial \phi(\mathbf{p})}{\partial \mathbf{n}} - \sigma(\mathbf{p}) \right) \quad (6.10)$$

As usual, the hydrodynamic pressure \mathbf{p} is calculated using Euler's integral, i.e.

$$\mathbf{p} = -\rho \mathbf{g} \mathbf{w} - i \rho \omega \phi \quad (6.11)$$

where \mathbf{w} is the vertical displacement.

The generalized fluid force is decomposed into the generalized restoring, wave exciting and radiation forces, i.e.

$$\{\mathbf{F}^*\} = \{\mathbf{F}_H^*\} + \{\mathbf{F}_D^*\} + \{\mathbf{F}_R^*\} \quad (6.12)$$

The generalized restoring force is due to the hydrostatic pressure and is calculated as

$$\mathbf{F}_{Hj}^* = -\sum_N \int_{\Delta S} \rho \mathbf{g} \mathbf{w}_j \mathbf{n}_j^* \, ds \quad (6.13)$$

where j denotes the j -th mode, \mathbf{n}_j^* is the generalized normal defined in Chapter 3 and \mathbf{w}_j is the vertical displacement due to the motion of the j -th mode.

The generalized wave exciting force, which is due to the incident and diffraction potentials, is expressed as

$$\mathbf{F}_{Dj}^* = \sum_N \int_{\Delta S} -i \omega \rho (\phi_I + \phi_D) \mathbf{n}_j^* \, ds \quad (6.14)$$

The generalized radiation forces are due to the radiation potentials and related to the motion of the structure. Hence, they are represented in terms of the added mass and damping coefficients as

$$F_{Rjk}^* = \omega^2 M_{fjk}^* p_k - i\omega C_{fjk}^* p_k \quad (6.15)$$

where F_{Rjk} is the generalized j -th modal force due to the motion in the k -th mode,

p_k is the amplitude of the k -th normal coordinate, and the generalized added mass M_{fjk}^*

and damping coefficient C_{fjk}^* are calculated by

$$M_{fjk}^* - \frac{i}{\omega} C_{fjk}^* = \frac{1}{\omega^2} \sum_N \int_{\Delta S} i\omega \rho \phi_{Rk} n_j^* ds \quad (6.16)$$

Substitution of the generalized fluid forces, Eqs. (6.13), (6.14) and (6.15) into Eq. (6.1) results in

$$[-\omega^2([M_s^*] + [M_f^*]) + i\omega([C_s^*] + [C_f^*]) + ([K_s^*] + [K_f^*])]\{p\} = \{F_D^*\} \quad (6.17)$$

where p is the normal coordinate, $[M_f^*]$ and $[C_f^*]$ are the generalized added mass

and damping coefficient matrices with the elements of M_{fjk}^* and C_{fjk}^* , respectively;

and $\{F_H^*\}$ is written as $-[K_f^*]\{p\}$, in which $[K_f^*]$ is the generalized hydrostatic

restoring matrix.

The normal coordinates can be obtained by solving Eq. (6.17) and the structural displacements and stresses are calculated by using Eqs. (2.22) and (2.24), respectively.

6.3 The zero-draft Green function

As discussed in Chapter 3, the Green function must satisfy the Laplace equation, the free-surface boundary condition, radiation condition and sea-bottom condition.

The Green function for a three dimensional problem is given by

$$\begin{aligned}
G = & i2\pi \frac{k^2 - v^2}{k^2 h - v^2 h + v} \cosh[k(z+h)] \cosh[k(\zeta + h)] H_0^{(1)}(kR) \\
& + 4 \sum_{n=1}^{\infty} \frac{k_n^2 + v^2}{h(k_n^2 + v^2) - v} \cos[k_n(z+h)] \cos[k_n(\zeta + h)] K_0(k_n R)
\end{aligned} \tag{6.18}$$

where h is water depth, k is the wave number, k_n is the positive root of equation of $k_n \tan(k_n h) + v = 0$, $R = \sqrt{x^2 + y^2}$, $H_0^{(1)}$ is the Hankel function of the first kind and order zero and K_0 is the modified Bessel function of the second kind of order zero.

If the draft is assumed to be zero, the vertical coordinates of the source and field points vanish, i.e. $z = 0$ and $\zeta = 0$. By rewriting $k^2 - v^2$ as

$$k^2 - v^2 = k^2(1 - \tanh^2(kh)) = \frac{k^2}{\cosh^2(kh)} \tag{6.19}$$

the Green function (Eq. 6.1) becomes

$$\begin{aligned}
G = & i2\pi \frac{k^2}{k^2 h - v^2 h + v} H_0^{(1)}(kR) \\
& + 4 \sum_{n=1}^{\infty} \frac{k_n^2 + v^2}{h(k_n^2 + v^2) - v} \cos^2(k_n h) K_0(k_n R)
\end{aligned} \tag{6.20}$$

6.4 Solution procedure

The solution process can be divided into three stages. The first is the solution of the structural dry mode shapes to provide the body boundary conditions for the radiation potentials. The second is the solution of the hydrodynamic problem to obtain the generalized wave exciting forces and the generalized added mass and damping coefficients. The last is the solution to the coupled equations of motion to

obtain the normal coordinates. The structural displacements and stresses can then be easily calculated using Eqs. (2.22) and (2.24), respectively, once the normal coordinates and the mode shapes are in hand.

The finite element code COSMOS/M is employed to obtain for the structural dry mode shapes. The floating mat-like platform is modeled as an equivalent plate that has the same cross sectional bending stiffness and the same mass as those of the platform, i.e.,

$$EI_M = EI_P, \quad M_M = M_P \quad (6.21)$$

where E is the modulus of elasticity, I is the moment of inertia of the cross section, M is the total mass of the body and the sub-index M and P stand for the mat-like and the equivalent plate platforms, respectively. The equivalent floating plate is represented by a number of plate elements in the analysis.

The hydrodynamic problem is solved numerically by using the constant panel method. The main task is to obtain the source strengths by solving Eq. (6.9). To this end, the wetted body surface is discretized into N panels with the consequence that Eq. (6.9) is converted into N linear equations, i.e.,

$$\{V_n\} = [\beta]_{N \times N} \{\sigma\}_{N \times 1} \quad (6.22)$$

where

$$\beta_{ij} = \frac{k}{4\pi} \int_{\Delta s} G(p_i, q_j) ds_j \quad (6.23)$$

in which Δs is the panel area.

When the size of the body is very large, the solving of the linear system of equation, Eq. (6.23) could be time consuming. However, if the under-water geometry of the body is symmetric, the number of equations can be reduced by using the composite source distribution method (Wu et al., 1993). In the case of single symmetry, the linear system of N equations is replaced by two linear systems of $N/2$ equations, and by four linear systems of $N/4$ equations in the case of double symmetry. The replacement of a large linear system of equations by two or four smaller linear system of equations results in computational savings in CPU time and required storage. The details of the composite source distribution method can be found in Wu et al. (1993) and Chapter 3 presents the key formulations of this technique.

Once the generalized wave exciting force, added mass and damping coefficients are obtained, the final step is the solution of the coupled equations of motion, Eq. (6.17) for the normal coordinates and hence to calculate the structural displacements and stresses.

6.5 Verification of the method

First, as usual, the results predicted by the method developed in this Chapter are compared with the available data to verify the applicability or correctness of the method. Two floating bodies are chosen for the comparisons. One is the experimental model of a barge whose dimensions are 3.006m in length, 0.75m in width and 0.0150m in draft. The details of the barge can be found in Wu and Price

(1986), and the other is a floating box (Tangirala, 1995) with the particulars listed in Table 6.1.

Table 6.1 Main particulars of the box

Length, width, depth (m)	500 * 60 * 20
Draft (m)	10
Displacement (kg)	$3.075 * 10^8$
Mass moment of inertia I_{xx} (kg-m ²)	$1.025 * 10^{11}$
I_{yy} (kg-m ²)	$6.416 * 10^{12}$
I_{zz} (kg-m ²)	$6.498 * 10^{12}$
Modulus of elasticity E (N/m ²)	$2.11 * 10^{11}$
Cross sectional rigidity EI (N-m ²)	$2.954 * 10^{14}$

Fig. 6.1 shows the transfer function of heave obtained by the present zero-draft Green function method (S-draft), by the three-dimensional Green function method (Nojiri, 1981) and from experimental data (Nojiri, 1981) for the 3-meter long barge model. The present results agree with the three-dimensional predictions and they reasonably reflect the trends and magnitudes of the experimental data.

For the box of Table 6.1, the displacement response of five modal shapes obtained by the present and three-dimensional hydroelasticity methods (Wang et al., 1995b) are compared. The structural damping is neglected in the calculation. The first two modes are heave and pitch, respectively, and the last three are the flexible bending modes.

The present shallow-draft hydroelasticity method involves mainly two assumptions. One is on the use of the zero-draft Green function and the other is the equivalent plate mode. Figs. 6.2 and 6.3 show the first three flexible bending modal shapes of the actual box and the equivalent plate model. The number of the structural elements for the box is 1785 and for the plate is 375. The natural frequencies and the modal shapes of the two structural models show good agreement. Fig. 6.4 presents the displacement amplitudes in the vertical (z) direction at the bow of the box for the heave, pitch, first-bending, second-bending and third-bending modes, respectively. The results are for a unit wave amplitude. The wave heading is zero degrees. In Fig. 6.4, 3-D stands for three-dimensional hydroelasticity theory, and S-G-P stands for the shallow-draft Green function combined with the plate theory, i.e. the present method. It can be seen that the results from the two methods are close to each other. It seems that the displacements obtained by the equivalent plate structural model are slightly over-estimated.

Fig. 6.5 shows the results for a box whose dimensions are 500m*200m*20m and whose draft is 10m. It is the box of Table 6.1 but with a wider beam. It appears that the larger the ratio of width to draft, the more the results agree with each other. Matsuoka (1994) did a study on the validity of the simplified zero-draft Green function method. His study concludes that, for a box shaped body, the zero-draft Green function method can predict the wave action and body motions quite accurately when the ratio of width to draft is larger than 10. However, it appears,

as expected, that the wave period is also an important parameter in the evaluation of the applicability of the zero-draft Green function method.

6.6 Application of the shallow-draft Green function method to a mat-like runway

6.6.1 Structural model of the floating runway

The box-like floating airport whose dimensions are 3000m in length, 300m in width and 25m in depth and whose draft is 15m is studied next. The main particulars of the airport are given in Table 6.2. The airport has continuous longitudinal and transverse buckheads at intervals of 10m, of 2.5cm thick. The mass distribution is assumed to be uniform. The equivalent plate whose bending stiffness and mass are the same as those of the box-like airport of Table 6.2 is used for the structural deformation analysis. The total number of panels used in the hydrodynamic analysis is the same as that of the structural elements. Since the geometry of the airport is of double symmetry, the double-composite source distribution method is employed in the hydrodynamic analysis. The number of panels is 525 per quarter of the structure.

The equations of motion are solved in normal coordinates. The first 22 modal shapes are chosen to represent the motion of the airport. The first six modes are those of the rigid body. The natural periods of the first 12 flexible modes are listed in Table 6.3. The rigid body modes of surge, sway and yaw are lacking in the calculations because of the use of zero-draft Green function.

Table. 6.2 Main particulars of the floating airport

Dimensions (m)	3000*300*25
Draft (m)	15
Mass moment of inertia I_{xx} (kg-m ⁴)	$1.04 * 10^{14}$
I_{yy} (kg-m ⁴)	$1.035 * 10^{16}$
I_{zz} (kg-m ⁴)	$1.045 * 10^{16}$
Displacement (kg)	1.38^{10}
Modulus of elasticity E (N/m ²)	$2.11 * 10^{11}$
Cross sectional rigidity per length EI/m (N-m)	$7.368 * 10^{12}$

Table. 6.3 Natural periods of the flexible modes of the floating airport (seconds)

mode	7	8	9	10	11	12
T_n	115.5	41.82	21.28	19.20	12.84	9.53
mode	13	14	15	16	17	18
T_n	8.58	6.28	6.12	4.63	4.59	3.63

6.6.2 Hydroelastic response of the runway

Fig. 6.6 shows the vertical displacements at the centerline and bow, midship and stern, respectively. It can be seen, as expected, that small-period waves do not generate large motions for a large floating body. Under the action of a zero-degree heading wave, the displacements at the bow are the largest among those three points and the responses at amidship are the smallest. Note that responses peak at three points. These points correspond approximately to the natural periods of some of the flexible dry-modes, i.e. $T_{n9} = 21.28$, $T_{n10} = 19.2$ and $T_{n11} = 12.84$ seconds. The

displacements are mainly due to flexible modes of motion. The rigid body motions are small. For example, the displacement amplitude at the bow due to pitch and heave for a 22-second wave of 1m amplitude is about 2m and 0.026m, respectively.

The displacements of the body are given in Fig. 6.7 which shows the real and imaginary parts of the displacement response for 12, 16 and 22 second incoming waves.

6.7 Final remarks

There are two simplifying assumptions introduced in the present hydroelasticity method that are not used in the three-dimensional hydroelasticity theory. One is the use of the simplified zero-draft Green function and the other is the equivalent plate model used here in the structural analysis. By comparison with the results obtained by other methods, it appears that these assumptions used in analyzing a VLFS are acceptable for practical purposes. Therefore, the present approach is a convenient and promising method for employment in preliminary design.

The two simplifications mentioned above result in a highly efficient hydroelasticity method. By using the equivalent plate model, the number of the structural elements is reduced significantly. The application of the zero-draft Green function to the potential analysis produces a large reduction in the computational time in hydrodynamic analysis for two reasons: the first is that the panels on the side walls are eliminated; the second is that the zero-draft Green function has a much simpler form and also there is no need to compute the derivatives of the Green function.

Once the source strengths are obtained, the potentials can easily be calculated by using Eq. (6.10).

Since, in the zero-draft Green function method, the sources are distributed on the still-water surface where the body is located, the irregular-frequency problem disappears. In the hydrodynamic analysis of a mat-like structure, this gives a big advantage over the use of the three-dimensional Green function method because there may exist a number of irregular frequencies at which points dynamic responses cannot be obtained.

The maximum vertical displacement responses of the floating airport occur at about the 22 second wave period that corresponds to the natural period of the flexible dry modes. The flexible motions are thus the main contributors to the displacement. The maximum vertical displacement amplitude is about 8m, which is quite large. The reason for this high response is likely related to panel size used in this study. The effect of panel length to wave length ratio is being studied currently and will be reported elsewhere (Wang et al., 1995a, IJOPE).

The oblique sea case, which may be important in the study of sway and lateral bending deflection of the floating body, is not included here because of lack of lateral forces in the calculations, i.e. surge and sway forces and yaw moment. However, one can use the Froude-Krylov part of the exciting forces to calculate these lateral forces as it was done by Wu and Price (1986).

CHAPTER 7
EFFICIENT HYDROELASTIC ANALYSIS METHOD FOR
A FLOATING BODY OF ARBITRARY SHAPE

7.1 Overview

Two efficient hydroelastic analysis methods are presented in Chapters 5 and 6, respectively. They are the modified Morison's equation method and the shallow-draft Green function method. The former is applicable to floating bodies whose underwater structural components are cylindrical, and the latter to floating bodies of shallow draft and relatively flat bottom. In this Chapter, an efficient hydroelastic analysis method for floating bodies of arbitrary shape is presented.

As discussed above, limited computer resources make the application of three-dimensional hydroelasticity theory to a VLFS very difficult, if not impossible. This difficulty is mainly related to the hydrodynamic analysis. In such an analysis, the wetted surface of the body is represented by a large number of discrete panel elements. The velocity potentials at the panels are described by a corresponding linear system of equations. This linear system of equations is characterized by a square matrix of complex coefficients of dimensions equal to the number of panels. The coefficients are related to the source potential and its derivatives. The difficulty stems from two numerical problems: one is the evaluation of very large number of complex coefficients and the other is the solution of also very large linear system of equations.

To overcome the difficulty, Newman (1985) has developed an efficient numerical algorithm by which to calculate the source potential and its derivatives in reduced computational time. Wu (1984) has introduced a composite source distribution method that increases the computational efficiency in solving the linear system of equations if the body is of single symmetry. The method has since been extended to apply to a double symmetric body (Wu et al., 1993). However, the hydroelastic analysis of a VLFS still remains untractable if the structure size is on the order of that of an airport. To this end, an efficient approach that is applicable to any size and kind of structural geometry is developed. The approach includes not only the very efficient double-composite source distribution technique mentioned above, but also two new techniques introduced for the first time in a hydroelastic analysis by Wang et al. (1995b).

The first technique is related to the computation of the potential coefficients, which relate the velocity potential to source strengths, and to that of the influence coefficients, which relate the normal derivatives of the velocity potential to source strengths. Since the potential and the influence coefficients are very small when source and the field points are far away from each other, it may be reasonable to establish a criterion by which to determine under what conditions they can justifiably be assumed to vanish altogether. This criterion is then used to calculate only the large, significant, coefficients, thereby reducing the CPU time.

The second technique applies to the solution of the system of equations that relates the known boundary conditions (normal derivatives of the potential) to the

calculated influence coefficients and the unknown source strengths. Once the influence (and the potential) coefficient matrix is calculated by using the criterion mentioned above, many elements of this matrix will have zero entries, i.e. it will be a sparse matrix which is diagonally dominant. Such a matrix can be solved efficiently by an iterative sparse solver. An algorithm that is based on the diagonal-preconditioned conjugate gradient method (Hackbusch, 1994) is developed to solve these complex equations.

The new techniques developed here will be applied to the solution of a hydroelasticity problem that involves a VLFS. The computational efficiency achieved by using these techniques will be illustrated by examples, and special attention will be given to the reduction in CPU time. Of course, the inaccuracies caused by the implementation of the criterion for zero entries of the coefficient matrices will also be discussed.

7.2 Equations of motion

The structural and hydrodynamic models for the hydroelastic response analysis of a three-dimensional floating body of arbitrary shape are presented in Chapters 2 and 3, respectively. The equations of motion are repeated here for convenience. In this Chapter, the motions of the body and the fluid are described with reference to a Cartesian, right-handed coordinate system $Oxyz$, with Oz axis pointing upward. The generalized linear equations of motion of a floating body in waves is then expressed by (see Chapter 4)

$$[-\omega^2([\mathbf{M}_s^*] + [\mathbf{M}_f^*]) + i\omega([\mathbf{C}_s^*] + [\mathbf{C}_f^*]) + ([\mathbf{K}_s^*] + [\mathbf{K}_f^*])]\{\mathbf{p}\} = \{\mathbf{F}_D^*\}, \quad (7.1)$$

where $\{\mathbf{p}\}$ is the vector of the normal coordinates, $[\mathbf{M}_s^*]$, $[\mathbf{C}_s^*]$ and $[\mathbf{K}_s^*]$ are the diagonal matrices of modal mass, damping and stiffness of the structure, respectively; $[\mathbf{M}_f^*]$ and $[\mathbf{C}_f^*]$ are the generalized added mass and damping coefficient matrices, respectively; $[\mathbf{K}_f^*]$ is the generalized hydrostatic restoring matrix; and $\{\mathbf{F}_D^*\}$ is the vector of the generalized wave exciting forces. The generalized added mass and damping coefficient matrices and the wave exciting forces are obtained from the hydrodynamic analysis.

7.3 The Green function method for hydrodynamic analysis

The velocity potentials are usually solved by the Green function method. The velocity potential $\phi(x, y, z)$ at any point is expressed by:

$$\phi(x, y, z) = \int_{S_b} G(x, y, z, \xi, \eta, \zeta) \sigma(\xi, \eta, \zeta) ds, \quad (7.2)$$

where $G(x, y, z, \xi, \eta, \zeta)$ is the Green function, $\sigma(\xi, \eta, \zeta)$ is the source strength, (x, y, z) and (ξ, η, ζ) are the coordinates of the field and source points, respectively, and S_b is the wetted body surface. To determine the source strength σ , it is necessary to take the derivative of Eq. (7.2) in the direction normal to the body surface and then apply the body boundary condition. This results in the following integral equation from which σ is to be determined, i.e.

$$\frac{\partial \phi}{\partial \mathbf{n}} = \int_{s_b} \frac{\partial G(\mathbf{x}, y, z, \xi, \eta, \zeta)}{\partial \mathbf{n}} \sigma(\xi, \eta, \zeta) ds. \quad (7.3)$$

Eqs. (7.2) and (7.3) are solved numerically. To this end, the wetted body surface is discretized into N panels and the source strength on each panel is assumed to be constant. These equations can be rewritten in matrix form as

$$\{\phi\}_{N \times 1} = [\alpha]_{N \times N} \{\sigma\}_{N \times 1}, \quad (7.4)$$

$$\{\mathbf{V}_n\}_{N \times 1} = [\beta]_{N \times N} \{\sigma\}_{N \times 1}, \quad (7.5)$$

where

$$\alpha_{ij} = \int_{\Delta s_j} G(\mathbf{x}_i, y_i, z_i, \xi, \eta, \zeta) ds, \quad (7.6)$$

$$\beta_{ij} = \int_{\Delta s_j} \frac{\partial}{\partial \mathbf{n}} G(\mathbf{x}_i, y_i, z_i, \xi, \eta, \zeta) ds. \quad (7.7)$$

It can be seen that two distinct numerical problems are involved in solving for the source strengths and velocity potentials, i.e. Eqs. (7.4) and (7.5), for a very large floating body. The first problem is the evaluation of the matrix of the source potentials $[\alpha]$, and of the derivatives of such source potentials $[\beta]$. These are complicated mathematical functions and need to be evaluated for each combination of panels. The second problem is that of solving the linear system of equations, i.e. Eq. (7.5) for the source strengths. The solution of these two numerical problems is the main computational difficulty in performing the three-dimensional hydroelastic analysis of a VLFS. To overcome these difficulties, two techniques are introduced

in this study. One is related to the evaluation of the matrices and the other to the solution of the linear systems of equations.

7.4 Calculation of the three-dimensional Green function and its derivatives

The calculation of the Green function and its derivatives, i.e. the coefficient matrices in Eqs. (7.6) and (7.7), is very demanding in computer time. However, it is possible to find a way to reduce this time without losing the required accuracy.

For the case of infinite water depth, the conventional form (Wehausen and Laitone, 1960) of the Green function is defined by the expression

$$G = \frac{1}{r} + \text{PV} \int_0^{\infty} \frac{m+k}{m-k} e^{m(z+\zeta)} J_0(mR) dm - 2\pi i k e^{k(z+\zeta)} J_0(kR) \quad (7.8)$$

where $r = \sqrt{(x-\xi)^2 + (y-\eta)^2 + (z-\zeta)^2}$, $R = \sqrt{(x-\xi)^2 + (y-\eta)^2}$, k is the wave number, PV indicates the principal value of the integral, J_0 denotes the Bessel function of the first kind of order zero, and the contour of the integration passes above the pole to satisfy the radiation condition of outgoing waves at infinity. Fig. 7.1 shows the Green function and its normal derivatives.

When the field point is far away from the source point, then

$$\frac{1}{r} \sim O\left(\frac{1}{R}\right) \quad (7.9)$$

and

$$J_0(mR) \sim \sqrt{\frac{2}{\pi R m}} \cos\left(mR - \frac{\pi}{4}\right) + O\left(\frac{1}{R}\right) \quad (7.10)$$

Note that

$$\cos(mR - \frac{\pi}{4}) = \cos(kR - \frac{\pi}{4})\cos[R(m-k)] - \sin(kR - \frac{\pi}{4})\sin[R(m-k)] \quad (7.11)$$

If $f(x)$ is a differentiable function in $[a, \infty)$, if $f''(x_0)$, $x_0 > a$, exists, and if $f(x)/x$ and $f'(x)/x$ are both absolutely integrable in $[a, \infty]$, then, as $R \rightarrow \infty$,

$$PV \int_a^{\infty} f(x) \frac{\cos[R(x-x_0)]}{x-x_0} dx = O\left(\frac{1}{R}\right) \quad (7.12)$$

The asymptotic form ($R \rightarrow \infty$) of the Green function can then be expressed (Wehausen and Laitone, 1960) as

$$G \sim 2\pi i k e^{k(z+\zeta)} \sqrt{\frac{2}{\pi k R}} e^{i(kR - \pi/4)} + O\left(\frac{1}{R}\right) \quad (7.13)$$

Note that

$$e^{k(z+\zeta)} < \frac{1}{1-k(z+\zeta)} = \frac{1}{1+k(|z+\zeta|)}, \quad (z+\zeta) < 0 \quad (7.14)$$

Then

$$\begin{aligned} G &< 2\pi i k \left(\frac{1}{1+k(|z+\zeta|)} \right) \sqrt{\frac{2}{\pi k R}} e^{i(kR - \pi/4)} + O\left(\frac{1}{R}\right) \\ &< 2\pi i k \sqrt{\frac{2}{\pi k R}} e^{i(kR - \pi/4)} + O\left(\frac{1}{R}\right) \\ &= 2\sqrt{2}\sqrt{\pi} i \sqrt{\frac{k}{R}} e^{i(kR - \pi/4)} + O\left(\frac{1}{R}\right) \end{aligned} \quad (7.15)$$

It can be seen that the asymptotic form of the Green function is an outgoing sinusoidal wave, and the amplitude of the wave is proportional to $1/\sqrt{R}$ for a specific wave number. For a specific R , the amplitude is proportional to $\sqrt{k} = \sqrt{(2\pi)^2/gT^2}$, in which T is the wave period. Therefore, at any field point the potential due to a source will be very small if the distance between them is large, especially when the wave period is also large. These properties of the Green function can be used in the hydroelastic analysis of a VLFS to reduce the required computational time and storage. There are two reasons for this: the first is that many source and field points are far away when a floating body is large; the second is that the wave periods of interest in the analysis are large because the short-period waves do not induce any appreciable response in a VLFS.

Based on these properties of the Green function, many of the coefficients, α_{ij} and β_{ij} , will be sufficiently small that they can be omitted. Therefore, a critical value, say γ , can be introduced and chosen to determine when the coefficients can be assumed to be zero. Specifically, in this study, when $kr > \gamma$, where r is the distance between the source and field points and k is the wave number, the coefficients are set to zero. For a VLFS, many coefficients can be set to zero by using this criterion, hence significant savings in CPU time spent on the calculation of the coefficients can be achieved.

7.5 Iterative sparse solver

CPU time spent on the calculation of the Green function is proportional to N^2 and to N^3 for the solution of the linear system of equations, in which N is the number of panels. Hence when N is large, the solving for the source strength will be the major time-consuming part in the hydroelastic response analysis. However, if the matrices $[\alpha]$ and $[\beta]$ are obtained by using the criterion mentioned above, they will be large, sparse matrices. The use of a direct solver in such problems is wasteful because of the unnecessary time spent on zero elements, and CPU and storage savings can be achieved by using an iterative sparse solver. To this end, a sparse solver based on the diagonal preconditioned conjugate gradient method (Hackbusch, 1994) is developed. The algorithm includes two parts: one is the sparse storage and the other is the iterative complex solver.

The matrices are stored in a row-indexed sparse storage mode (William et al., 1992). The row-indexed sparse storage method sets up two one-dimensional arrays. The first of these stores the values of non-zero matrix elements and the second stores the indices of the non-zero matrix elements. This method requires storage of about twice the number of nonzero matrix elements. For the analysis of a VLFS, the required storage will be reduced considerably by using the row-indexed sparse storage mode.

The conjugate gradient method minimizes the residual $\{\varepsilon\} = \{b\} - [A]\{x\}$ by searching for the direction of the steepest descent of the residual at each iteration.

The diagonal preconditioner is a scaling matrix which improves the conditioning of the original matrix $[A]$ so that the convergence of iterations for $[P]^{-1}[A]\{x\} = [P]^{-1}\{b\}$ is faster than that of $[A]\{x\} = \{b\}$, in which $[P]$ is the preconditioner. The best preconditioner is, of course, $[A]$. In this work, the diagonal preconditioner is used since it is easy to construct and is a good approximation to the matrix $[A]$ in our problem because it is diagonally dominant. There are three advantages of this solver to obtain the solution of Eq. (7.3). The first is that the operations related to the matrix $[\beta]$ are only the multiplication of the latter by a vector and the multiplication of its transpose by a vector. These operations can be very efficient for a sparse matrix stored by row-index. The second advantage is that the initial guess for the solution can be well predicted, because the matrix $[\beta]$ is diagonally dominant and the analysis is carried out for multiple wave periods. The third advantage is the fast convergence to the solution because of the use of the diagonal preconditioner.

Although the convergence of the conjugate gradient method for symmetric matrices has been proved, the corresponding result for asymmetric complex matrices has not been known yet. To this end, some numerical experiments have been carried out to find the applicability of the iterative solver to the boundary value problems in which the linear system of equations is characterized by an asymmetric complex matrix. In this feasibility study, the iterative solver is applied to the problems that correspond to three types of floating bodies: a semi-submersible system, a mat-like

body and a SWATH ship. The geometric configuration of the semi-submersible and mat-like floating systems can be found in Chapters 5 and 6, respectively, and the information about the SWATH ship is given in Che (1993). The numerical experiments indicate that the linear systems involved in these three problems are quite amendable to the iterative solver. The required number of iterations for a tolerance of 10^{-5} is usually less than 20.

7.6 Verification of the present method

Before the discussion of the details of CPU savings by use of the present method, the results predicted by such method are compared with published data to verify its correctness. The results, obtained by Newman (1994), for a box with dimensions of 80m*10m*10m floating at a draft of 5m are chosen for the comparison. In the present analysis, the criterion of $\gamma = 15$ is used and the results agree well with Newman's predictions (see Fig.7.2). Note that Mode 7 in Fig. 7.2 refers to the first flexible bending mode.

7.7 CPU savings by use of the Green function cut-off criterion and the iterative sparse solver

Both techniques discussed above, namely, the use of a cut-off criterion for the Green function and its derivatives, and the sparse solver, contribute to CPU savings, and the sparse solver also contributes to the savings of storage space.

7.7.1 CPU savings by the use of the cut-off criterion

In this section, the Green function cut-off criterion is applied in the hydrodynamic analysis of a box. The box is the one used in Chapter 6. The particulars of the box are given in Table 6.2. The half of the wetted surface is discretized into 936 panels.

Table 7.1 lists the CPU time required for the calculation of the Green function and its derivatives by using different criteria. As expected, Table 7.1 shows that the smaller the influence distance determined from $\gamma = kR$, the more CPU savings can be achieved.

Table 7.1. CPU time in the calculation of the Green function and its derivatives (seconds).

T (sec)	$\gamma = kR$								
	15	12	10	8	6	4	2	1	0.6
8	146	126	111	98	78	58	36	28	24
12	193	191	183	166	138	103	62	37	29
16	202	192	190	185	176	143	91	55	40

Fig. 7.3 shows the results of the response to wave periods ranging from 8 to 26 seconds when different criteria are used. The responses are the heave and pitch and the normal coordinates of the first and second bending modes. The wave heading is zero degree. It appears that the predicted responses are close when $\gamma \geq 4$.

Fig. 7.4 shows the relative errors in the responses corresponding to each criterion when the wave period is 8 seconds. The "exact" responses are obtained when using $\gamma = 35$

so that all the elements in the matrices $[\alpha]$ and $[\beta]$ are included in the calculations. The general trend of the relative errors decreases as γ increases, although the errors oscillate within a certain range. The oscillation of the errors may be due to the oscillation of the Green function itself and error cancellation for a specific γ . Note that, in strip theory, the interference of the source and field points are considered only within one cross section. In the present method, if γ is chosen so that the interference distance is larger than the maximum distance within any cross section, the results obtained are at least better than those obtained by strip theory.

If $\gamma = 4$ is chosen as critical criterion in the calculation of the Green function and its derivatives, namely the responses obtained using that criterion are reasonable, then for an 8-second wave, the CPU time used for the calculation of the Green function and its derivatives is reduced from about 200 seconds to 58 seconds, that is about 1/4 of the original CPU time. This CPU savings correspond to the case of the given box, which has a number of 936 panels on the half wetted surface. For a larger floating body, more panels will be required, and, therefore, the CPU time will be reduced even more if the above criterion is applied. Thus, the larger the floating body, the more CPU time savings will be achieved by using the criterion proposed here.

7.7.2 CPU savings by use of the iterative sparse solver

Eq. (7.3) is usually solved by a direct method that terminates after many operations with an exact solution (excluding the round-off errors). For a general asymmetric matrix, for example, the coefficient matrix in Eq. (7.3), direct solution of a system of N equations, $[A]\{x\} = \{b\}$, requires the following number of operations when the Gaussian elimination method is used

$$\text{NOP} = 2N^3/3 + O(N^2), \quad (7.16)$$

where N is the total number of equations and NOP is the total number of operations, in which each addition, subtraction, multiplication or division is counted as one operation.

For the iterative solution of a system of equations, one starts with an arbitrary initial vector $\{x_0\}$ and computes a sequence of iterates $\{x_m\}$ for $m=1,2,\dots$. Any iteration requires at least the computation of $[A]\{x_m\} - \{b\}$. For a general $N \times N$ -matrix $[A]$, the multiplication $[A]\{x_m\}$ would require $2N^2$ operations.

The diagonal preconditioned conjugate gradient method for the solution of the system of equations requires the following number of operations:

$$\text{NOP} = \text{MT} * [2N^2 + O(N)], \quad (7.17)$$

in which MT is the number of iterations required for convergence. If the matrix $[A]$ is sparse, the number of operations can be reduced by using an iterative sparse

solver. For example, if the number of nonzero elements of matrix $[A]$ is NS , the number of operations required to solve the equations is

$$NOP = MT * [2NS + O(N)]. \quad (7.18)$$

If NS is much smaller than $N \times N$, the CPU time in solving Eq. (7.3) can be reduced considerably.

The box defined above is used again as a model to study the CPU savings when solving Eq. (7.3). The single composite source distribution method (Wu, 1984) is employed for the solution of the potentials. In the single composite source distribution method, two source strengths are calculated. Therefore, Eq. (7.3) is replaced by two linear systems of equations, each one involving $N/2$ equations. In other words, in the single source distribution method two linear systems of $N/2$ equations are solved to obtain the composite source strengths. The CPU savings in solving the linear system of equations is studied from the view point of the convergence of the method and the sparsity of the matrix.

Three discretizations for the box are used. The number of panels (N) are 262, 549 and 936, respectively. The results of the motion responses obtained by use of these three discretizations are found to be close to each other. Fig. 7.5 shows the number of iterations required for various wave periods and the motion responses for the case of 936 panels. The tolerance used is 10^{-5} . It can be seen that the number of iterations required to converge to the results is much smaller than the number of panels. Comparison of Eqs. (7.16) and (7.17) shows, therefore, that the number of

operations required reduces significantly if the iterative method is used. Fig. 7.5 also shows that the number of iterations required decreases as the wave period lengthens. This is because a better initial guess can be made based on the results for the previous period.

Fig. 7.6 presents the number of iterations required to solve for the diffraction source strengths for three discretizations. The same tolerance is used. It can be seen that the number of iterations increases slightly for the larger panel case. According to Eqs. (7.16) and (7.17), the iterative method can provide a big CPU savings compared with the direct method, especially for the analysis of a VLFS.

An estimation is made of the CPU time required to solve Eq. (7.7) by use of the Gaussian elimination and the iterative method for the case of 936 panels. The dimension of the linear system is 936. If Eq. (7.7) is solved for the diffraction source strengths of an 8-second wave, the approximate number of operations required is about $5.47 \cdot 10^8$ when using the Gaussian elimination method, and $5.43 \cdot 10^7$ when using the iterative method. Therefore, the CPU time required when using the iterative method is about 1/10 of the CPU time when using the Gaussian elimination method.

More CPU time can be saved by using the iterative sparse solver. If the criterion $\gamma = 4$ is used in the calculation of the matrix $[\beta]$, the influence distance determined from the criterion is about 64m for an 8-second wave. For the box, about 78% of the matrix elements are zero. It can be seen from Eqs. (7.17) and (7.18) that the CPU time required to solve the equations is much less when using the iterative sparse

solver than when using the iterative method. A comparison of the CPU time required when using the iterative solver as against the iterative sparse solver is made for the case when $\gamma = 4$ and the wave period is 8 seconds. From Eqs. (7.17) and (7.18), the ratio of the number of operations when using the iterative solver to that when using the iterative sparse solver is about N^2/NS . The CPU time in the latter case is, therefore, about 22% of the CPU time required using the iterative solver.

7.8 Final remarks

Two techniques are proposed for increasing the computational efficiency of the hydroelastic analysis of a VLFS. By using a cut-off criterion for the Green function and its derivatives, the CPU time for the calculation of the potential and influence coefficients is reduced, and sparse matrices instead of full matrices result. An iterative sparse solver is developed that when applied to the linear system of equations reduces the CPU time.

A comparison of the results obtained by the use of different cut-off criteria suggests that an appropriate criterion can be found for any practical purposes. The CPU time can be reduced significantly by applying a proper criterion and using the iterative sparse solver. For the 500m long box used, a reasonable criterion would be about 6, i.e. $\gamma = 6$. It is also shown that relative errors related to the use of the criterion differ with wave period. That is because the amplitude of the Green function oscillation.

In this study, the same cut-off criterion is used in the calculation of the Green function and its derivatives. Fig. 7.1 indicates that the derivatives of the Green function decrease faster than the Green function itself. A greater error is caused by the truncation of the Green function than by that of its derivatives when the same criterion is used. It may be more reasonable to use separate criteria for the Green function and its derivatives.

There is a disadvantage in using $\gamma = kR$ as a cut-off criterion, because, as mentioned above, the potential amplitude is not proportional to kR . It may be better to use $\gamma = R$, in which case, for a given γ , the error at the longer wave periods should be smaller than that at the shorter wave periods because of the asymptotic form of the Green function. But still an oscillatory error will be present because of the term containing $\exp[i(kR - \pi/4)]$.

The use of an iterative sparse solver reduces the computational storage required, since only non-zero elements need to be stored. Therefore, the analysis of the problems associated with large number of panels can be carried out within present available computational resources.

These two techniques should be especially useful in the hydroelastic analysis of a VLFS, which is usually accompanied by computational difficulties.

CHAPTER 8
COMPARATIVE ANALYSIS OF SEMI-SUBMERSIBLE AND MAT-LIKE
FLOATING STRUCTURES

8.1 Overview

A central aspect of a VLFS design is that of configuration. At the present state of the art, it is difficult to determine either a priori or empirically the most efficient configuration of a VLFS for a given mission, because little experience is in hand as yet to provide dependable guidance for judgment.

The usually proposed hull types are semi-submersible and mat-like. The essential difference between these types lies in the distribution of the buoyancy; hence, of the action thereon of the surface waves. In the case of a mat-like hull, the resultant action may diminish with increase in platform area because of wave force cancellation effects; in the case of a semi-submersible, the wave action diminishes with increase in the draft of the buoyant elements and with increase in the narrowness of the surface-piercing columns.

Of the many qualities that a sea-going system must possess, the most important one is that of seaworthiness. In this Chapter, this quality is studied for both types of VLFS in terms of hull motion and stress responses. Two floating bodies, i.e. a five-module and a 20-module system, of each hull type are studied. The displacement and the deck area are the same for semi-submersible and mat-like systems in the comparative analysis.

8.2 Structural model of semi-submersible and mat-like systems

Both 5-module and 20-module semi-submersible systems are assembled from the single VLFS module designed by Winkler et al. (1990). The main particulars of the single VLFS module are given in Chapter 5 and the details on the module design may be found in Winkler et al. (1990).

The mat-like single module floating structure is designed by the author for the purpose of this comparative analysis. The dimensions of the mat-like floating body are based on an equality of displacement and deck area when compared with those of the semi-submersible single module. The same steel weight is used. The total steel weight of a single module is about 27,100 tons (Winkler et al., 1990). The main particulars of the single mat-like floating body are given in Table 8.1. The body has continuous longitudinal and transverse bulkheads at intervals of 10m, of thickness 2.5 cm. The main hull plating is 13.3 cm thick. The mass is assumed to be uniform.

Table 8.1 Main particulars of the single module mat-like structure

Length, width, depth (m)	100 * 100 * 10
Draft (m)	4.53
Displacement (kg)	46,440 * 10 ³
Mass moment of inertia I_{xx} (kg-m ²)	3.8 * 10 ¹⁰
I_{yy} (kg-m ²)	3.8 * 10 ¹⁰
I_{zz} (kg-m ²)	7.55 * 10 ¹⁰
Modulus of elasticity E (N/m ²)	2.11 * 10 ¹¹
Cross sectional rigidity EI (N-m ²)	1.446 * 10 ¹⁴

In this study, the multi-module systems are constructed by connecting single modules in the longitudinal direction. The structural strength of the cross section of the connectors is assumed to be the same as that of any other cross sections in the case of mat-like VLFS. For the semi-submersible module, one can identify at least two sections with different properties: a column-pontoon section and a pontoon-deck section. The structural strength of the cross section of the latter is the same as that of the connector section.

The finite element models of the 5-module and 20-module semi-submersible systems are shown in Figs 8.1 and 8.2. Beam elements are used to represent the structural models. The total number of elements are 1218 and 4878 respectively for the 5-module and 20-module semi-submersible systems, and the total number of nodes is 1015 for the 5-module system and 4045 for the 20-module system. There are six- degrees-of-freedom at each node; three translational and three rotational displacements.

The finite-element models of the 5-module and 20 module mat-like systems are given in Figs. 8.3 and 8.4. The equivalent plate model discussed in Chapter 6 is employed to represent the mat-like floating bodies. The plates are discretized into 4 node elements. The total number of elements for the 5-module and 20-module systems are 500 and 2000, respectively, and the total number of nodes is 561 for the 5-module system and 2211 for the 20 module system.

8.3 Mode shapes of the dry structure

The dry structural modal shapes are used as a set of space vectors to represent the displacements of the body; hence, these shapes are used in the hydrodynamic analysis for the body boundary conditions. The interaction between the structural deformation and fluid motion is linked through these modal shapes.

The dry modal shapes of the four floating bodies discussed above are obtained by using the finite element code COSMOS/M. The mass of all nonstructural components has been incorporated in the mass densities of the elements.

The first 16 modes are considered in the calculation for the 5-module systems. The first 6 modes are the rigid body motions, namely surge, sway, heave, roll, pitch and yaw, and the remaining are the flexible modes. Fig. 8.5 presents selected flexible modes of the 5-module semi-submersible system and Fig 8.6 shows selected modes of the 5-module mat-like system. The natural periods of the dry structure of the 5-module semi-submersible and mat-like systems are given in Table 8.2.

Table 8.2 Dry structural natural periods of 5-module semi-submersible and mat-like systems (seconds)

T_n	7	8	9	10	11	12	13	14	15
Semi	2.10	1.97	1.57	0.93	0.86	0.70	0.60	0.58	0.56
Mat	3.97	1.44	1.34	0.73	0.65	0.44	0.42	0.30	0.29

Similarly, for the 20-module system, the first 20 modes are considered. The first 6 modes are the rigid body motions as above. Figs. 8.7 through 8.8 show some of the

flexible modes of the 20-module semi-submersible and mat-like systems, respectively.

Table 8.3 gives the dry structural natural periods of the 20-module systems.

Table 8.3 Dry structural natural periods of 20-module semi-submersible and mat-like systems (seconds)

T_n	7	8	9	10	11	12	13
Semi	42.3	25.8	15.7	9.9	8.8	8.3	5.36
Mat	63.6	23.08	11.76	7.11	5.39	4.76	3.4
T_n	14	15	16	17	18	19	20
Semi	5.25	4.38	3.69	3.50	3.47	2.89	2.78
Mat	2.69	2.64	2.55	1.98	1.79	1.59	

It can be seen from the dry structural natural periods of the VLFS given above that the mat-like VLFS are more flexible than the semi-submersible one. The modal stresses are also calculated by using COSMOS/M. The structural stresses are obtained by the superposition of the modal stresses as discussed in Chapter 2.

The natural period of the rigid body modes of the 'dry' structure are theoretically infinite. However, for the 'wet' structure, they are not, and vary with the wave period, because the hydrodynamic inertias vary with the wave period. Table. 8.4 gives the approximate natural periods of heave, roll and pitch of the 5-module and 20-module systems of both hull types.

Table. 8.4 Natural periods of rigid body modes of 5- and 20-module systems (seconds)

5-module systems			
T_n	Heave	Roll	Pitch
Semi	23.9	62	21.7
Mat	10.5	9.1	11.4
20-module systems			
T_n	Heave	Roll	Pitch
Semi	24.3	65.7	23.4
Mat	12.4	9.2	12.3

8.4 Numerical results of structural displacement and stress responses

The efficient hydroelastic analysis method presented in Chapter 7 is applied to the response analysis of the VLFS given above. The Green function cut-off criterion is chosen so that the maximum influence distance between the two points is 200m by considering the factors of accuracy and the available computational resources. The structural damping is assumed to be zero. The response is calculated for wave periods ranging from 6 to 64 seconds (a wave period of 64 seconds may be an unreal, but its purpose is to obtain the asymptotic trend of the response at very long wave periods. The wave heading is zero degree, i.e. the sea is following. This may be the worse case for the longitudinal bending.

A comparison is made of the rigid body motions of heave and pitch of the two types of VLFS. Figs. 8.9 and 8.10 are the heave and pitch responses of the 5-module systems, and Figs. 8.11 and 8.12 are the same responses of the 20-module systems.

It can be seen that the responses of the 5-module systems mat-like VLFS are larger than those of the 5-module semi-submersible VLFS at most of the calculated wave periods. However, the responses of the two types of the 20-module VLFS are quite close, although the responses of the mat-like VLFS are still slightly larger than those of semi-submersible VLFS.

The normal coordinates of the flexible modes of the 5-module and 20-module systems are given in Figs. 8.13 and 8.14, respectively. The normal coordinates of the 5-module mat-like system are larger than those of the 5-module semi-submersible system. There may be two reasons for this: one is that the mat-like VLFS is subjected to more wave excitation than the semi-submersible is, the other is that the mat-like VLFS is more flexible and has larger deformations.

In the case of the 20-module mat-like VLFS the normal coordinates are slightly larger than those of semi-submersible VLFS at most wave periods. However, two response peaks in the normal coordinate of the 20-module semi-submersible VLFS are much larger than the corresponding ones for the 20-module mat-like VLFS. These two peaks correspond to the natural periods of the 20-module semi-submersible VLFS. In comparison to the mat-like VLFS, the damping force of the semi-submersible VLFS is smaller. At the resonant periods, the damping force plays an important role, although it is not important to the response at other periods.

Once the normal coordinates are obtained, the deflection and stresses can be easily calculated using the superposition method. Figure 8.15 gives the total deflections in the vertical direction at the bow, center and stern of the 5-module

VLFS of two types ("Semi" stands for semi-submersible VLFS and "Mat" for mat-like VLFS). As expected, the deflections in the vertical direction of semi-submersible VLFS are much smaller than those of mat-like VLFS.

However, for the 20-module VLFS, the total deflections in the vertical direction at the bow, center and stern of the two types of VLFS are of the same order. These deflections are shown in Fig. 8.16. As discussed above, two peak responses of the semi-submersible VLFS are much larger than those of the mat-like VLFS.

By comparing the normal coordinates and the total deflections of the two types of VLFS, it can be seen that the contribution of the lower modes dominate.

In this study, the stresses are calculated and the maximum normal stress is used for the comparison. For the 5-module VLFS, the maximum normal stresses occurs at the center sections of both VLFS and they are plotted in Fig. 8.17. It can be seen that the lower mode stresses also dominate the total stresses. The maximum normal stress of the 5-module mat-like VLFS is larger than that of 5-module semi-submersible VLFS.

Fig. 8.18 gives the maximum normal stresses of the 20-module semi-submersible and mat-like VLFS. They also occur at the middle section of the VLFS. The maximum stresses of the semi-submersible VLFS are larger than those of mat-like VLFS.

The rigid body motions of 20-module VLFS are much smaller than those of the 5-module VLFS, while the flexible deformations are the opposite. It is necessary to apply a hydroelasticity method to the analysis of the response.

8.5 Final remarks

Two types of VLFS of 5-module and 20-module systems have been analyzed by using the hydroelasticity theory. Based on the structural displacement and stress responses to regular waves, the semi-submersible type is recommended for a relatively small size of VLFS, because of its small response to waves. However, if the size of a floating body should be very large, like a 20-module VLFS, the mat-like hull type could be a better choice. Although the response of the mat-like system is generally larger than that of the semi-submersible one, the difference is small and the response at the resonant periods may not be very serious, since the damping of the mat-like VLFS is relatively larger.

However, for a firm conclusion, one needs to study the response of the systems of both hull-types to irregular seas to obtain the spectrum of the response. To this end, one needs to employ a wave spectrum. The wave spectrum varies from place to place. Therefore, at some locations, the peak responses, for example, of semi-submersible may not be the serious because the wave energy at the corresponding periods may be small.

There are many other factors that will affect the decision of choosing the hull type for a VLFS, such as the difficulties related to their construction. Cost is obviously a major factor in making such decision. Such factors are not studied in this work.

CHAPTER 9

CONCLUSIONS AND RECOMMENDATIONS

9.1 Conclusions

Three hydroelastic analysis methods have been developed and applied to the response analysis of VLFS of two types, i.e. semi-submersible and mat-like. These methods are: that of the modified Morison's equation, that of the zero-draft Green function and that of the three-dimensional Green function.

The development of the first employs linear structural dynamics. The hydrodynamic coefficients in Morison's equation are obtained from the extended method of MacCamy & Fuchs and from strip theory. Frame elements are used to represent the structural model. This method is applicable to a VLFS whose underwater geometry is a system of cylindrical components and the mutual interactions of which are assumed to be negligible. When compared with the method employing Morison's equation with constant hydrodynamic coefficients, this method predicts more accurate results at all wave periods.

The method that makes use of the zero-draft Green function is applicable to a VLFS of shallow draft. Two simplifying techniques are introduced in this method that are not used in three-dimensional hydroelasticity theory: the use of the zero-draft Green function, and the equivalent plate model used in the structural analysis. The results obtained have shown that such techniques are acceptable for all practical

purposes. These two simplifications result in a highly efficient hydroelasticity method for the analysis of a shallow draft floating body.

The general three-dimensional hydroelasticity method developed here is applicable to the analysis of a floating body of arbitrary geometry. This method is especially efficient in terms of CPU time and required computational storage when the size of a floating body is large. In this method, two efficient techniques are introduced for the first time. One is the Green function cut-off criterion and the other is the iterative sparse solver. The selection of the Green function cut-off criterion is based on the asymptotic property of the Green function. By using this criterion, the full asymmetric influence and potential matrices are replaced by two sparse matrices. An iterative sparse solver is developed to efficiently solve the large sparse linear system of equations and this solver has been tested on three types of floating bodies, i.e. a semi-submersible, a mat-like hull and a SWATH ship. In all three cases the iterative solver proved useful. The results obtained using different criteria are compared mutually and an appropriate criterion can be found for all practical purposes.

The development of these three methods is for the purpose of analyzing the two types of VLFS with the computational resources available, and hence to make an evaluation of the two types of hulls based on the obtained results and provide some suggestions and recommendations for making a choice between the configurations. The main features of each method are the computational efficiency. All three methods have been verified by comparing the results with the available data.

In the comparative analysis of semi-submersible and mat-like VLFS, two structural models of each type are selected: a 5-module system and a 20-module system. Both have the same displacement, deck area and steel weight. The calculations are carried out for wave periods from 6 to 64 seconds. The results show that the structural displacements and the stress responses of the 5-module semi-submersible VLFS are smaller than those of the 5-module mat-like VLFS, although the stress differences are smaller than the differences in displacement. In the case of the 20-module VLFS, the rigid body motions of both types are close; however, the deflections of the 20-module semi-submersible VLFS are smaller than those of 20-module mat-like VLFS. But at the resonant periods of 16 and 10 seconds the vertical deflections of semi-submersible VLFS are larger than those of mat-like VLFS. Also, the structural stress of 20-module semi-submersible VLFS at mid section is larger than that of the mat-like VLFS. One reason for the large responses of the 20-module semi-submersible VLFS at the resonant periods is that the damping force is small when compared with that of the mat-like VLFS, and the damping force plays an important role in the response at resonant periods.

Based on structural displacements and stress responses, a semi-submersible hull type is preferable for VLFS of relatively small size, such as the 5-module type, whereas mat-like hull type is a better choice for the large size VLFS, such as the 20-module. In the case of the semi-submersible VLFS, one needs to pay special attention to the response at the resonant periods because of its small damping force.

The maximum stress interests of the both type VLFS are less than the allowable (that is $2.05 \times 10^8 \text{ N/m}^2$).

9.2 Recommendations

In hydroelastic analysis, a high-order panel method is recommended. There are two reasons for this: the first is that less panels are required and more accurate results can be obtained by using a high-order rather than a constant panel method; the second is that in a hydroelastic analysis, the high-order panel method is more consistent with the finite-element method than is the constant panel method. In the high-order panel method, the body boundary condition can be applied at the nodes of the panels. In the finite-element analysis of the structural dynamics, the nodal displacements are employed to represent the modal shapes. If these nodes are made to correspond to those of the panels, the nodal displacements obtained from the finite-element analysis can be directly used in the calculation of the body boundaries in the hydrodynamic analysis. However, in the constant panel method, the nodal displacement needs be transferred to the center of the panels by using an interpolation function.

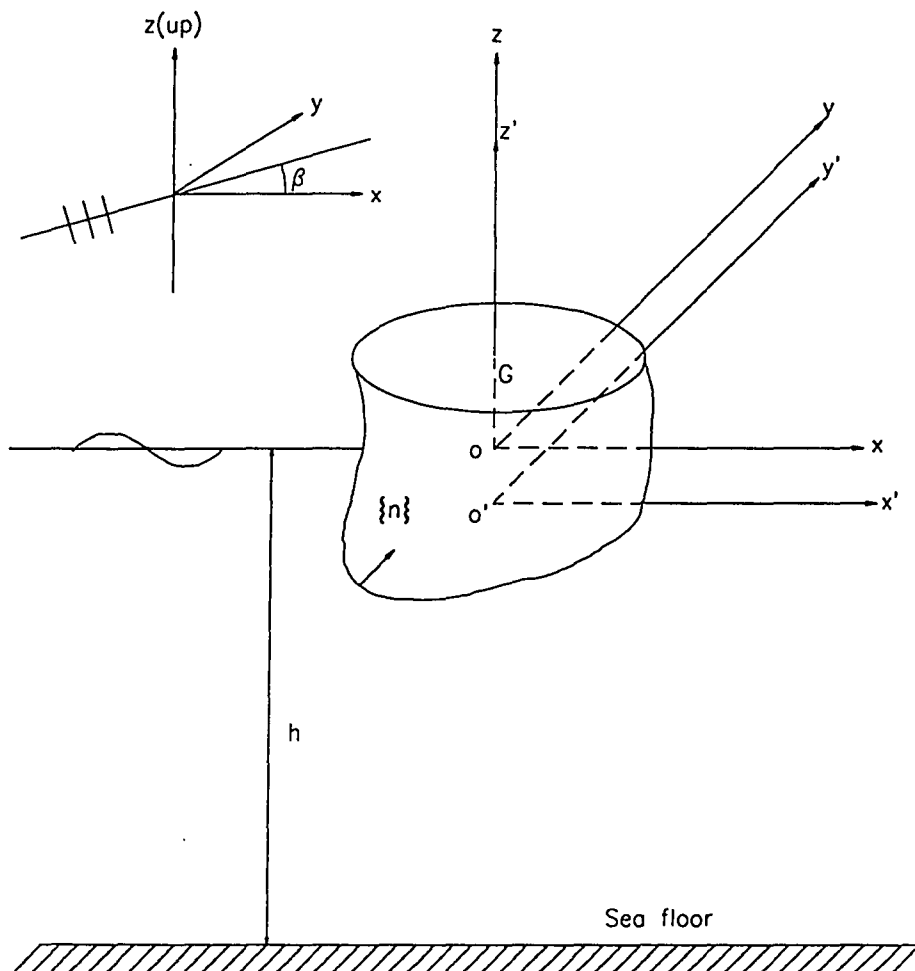
In the zero-draft Green function method, it may be necessary to include the calculation of lateral wave excitation, i.e. surge and sway forces and yaw moment, which are important in the study of sway and lateral bending deflection when the sea is oblique.

An efficient algorithm for the calculation of the zero-draft Green function needs to be developed.

Non-linearities may have to be considered in the analysis, since VLFS are so flexible that the deformations may be very large.

More comparative studies of the two types of VLFS are needed. These may include connectors of different design, different bases of comparison instead of displacement, deck area and steel weight, as used here.

There is also a need for conducting systematic experimental studies on the comparative behavior of the two types of VLFS herein discussed.



$x y z$ = inertial axes

h = water depth

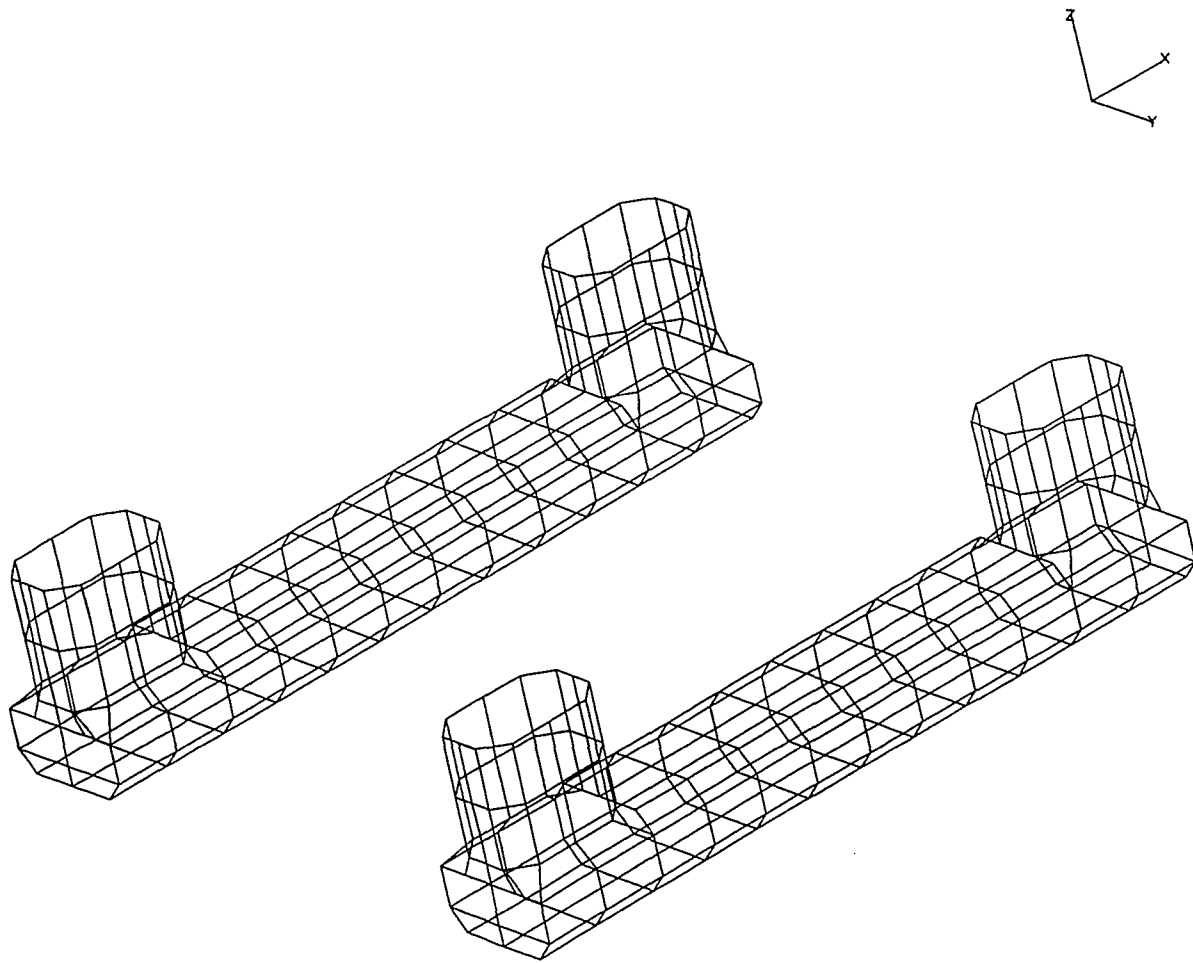
$x' y' z'$ = body fixed axes

$\{n\}$ = body normal vector

G = center of gravity

β = wave heading

Fig. 3.1 Schematic sketch of the boundary value problem



x: 30 y: 30 z: 30

Fig. 3.2 Discretization of the wetted body surface

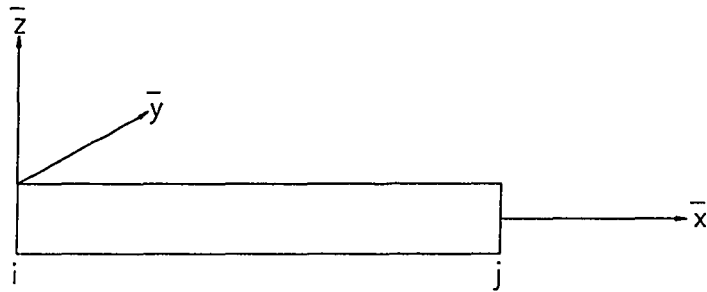


Fig. 5.1 Frame element

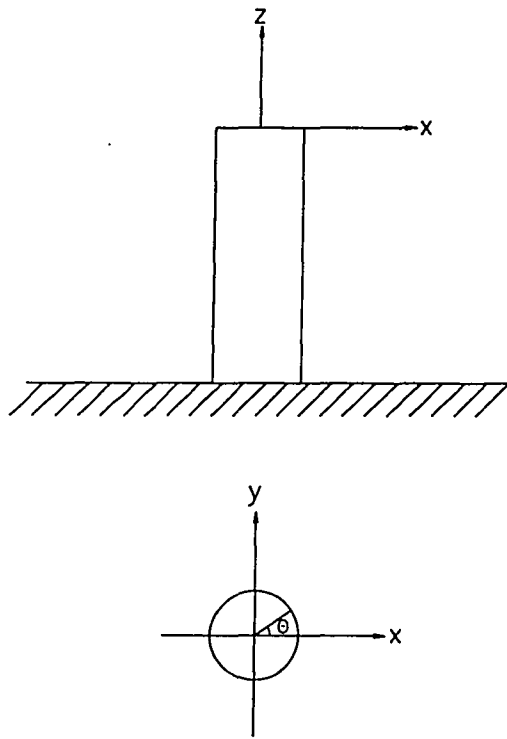
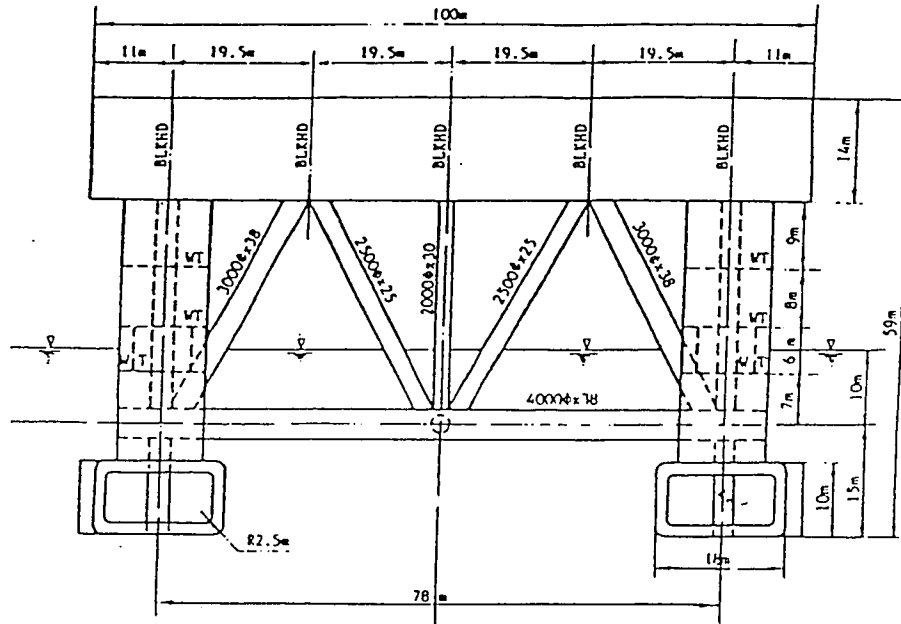
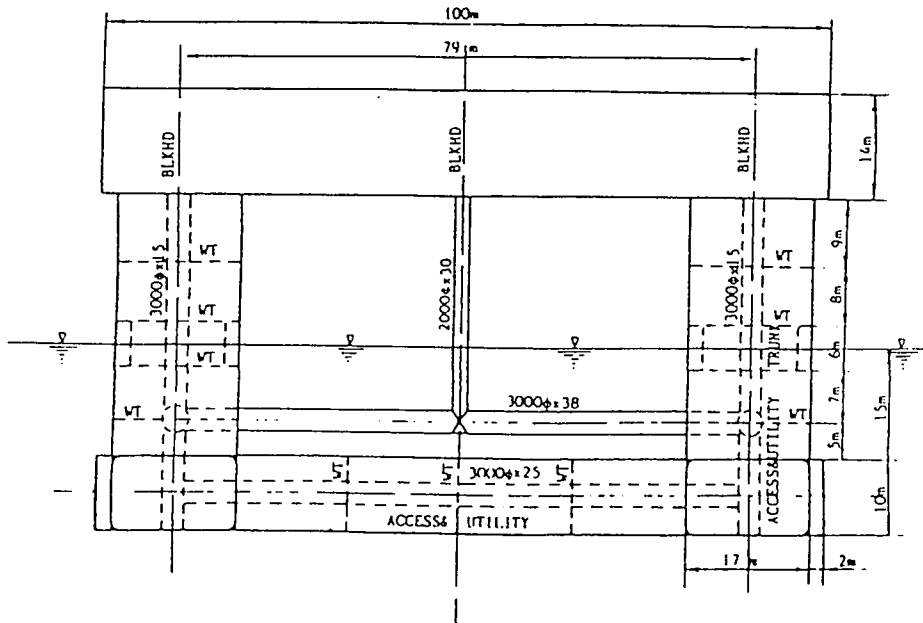


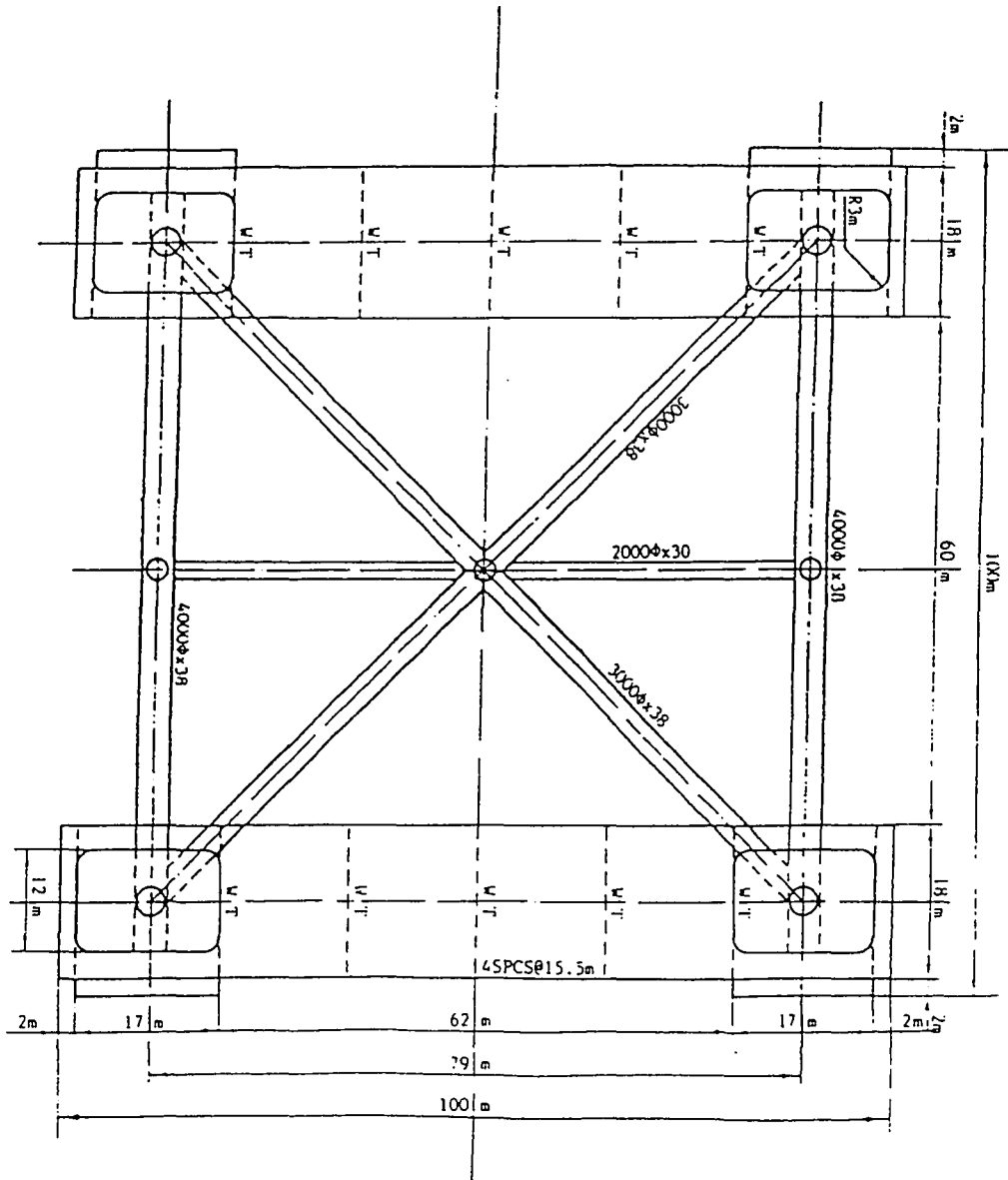
Fig. 5.2 Cylindrical coordinate system



(a) Forward elevation of the single module



(b) Starboard elevation of the single module



(c) Plan view of the single module

Fig. 5.3 Configuration of a single module (Winkler et al., 1990)

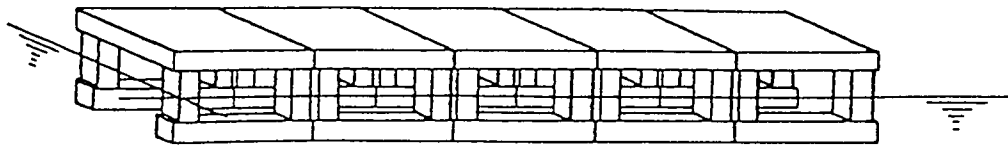


Fig. 5.4 Schematic of a five module VLFS

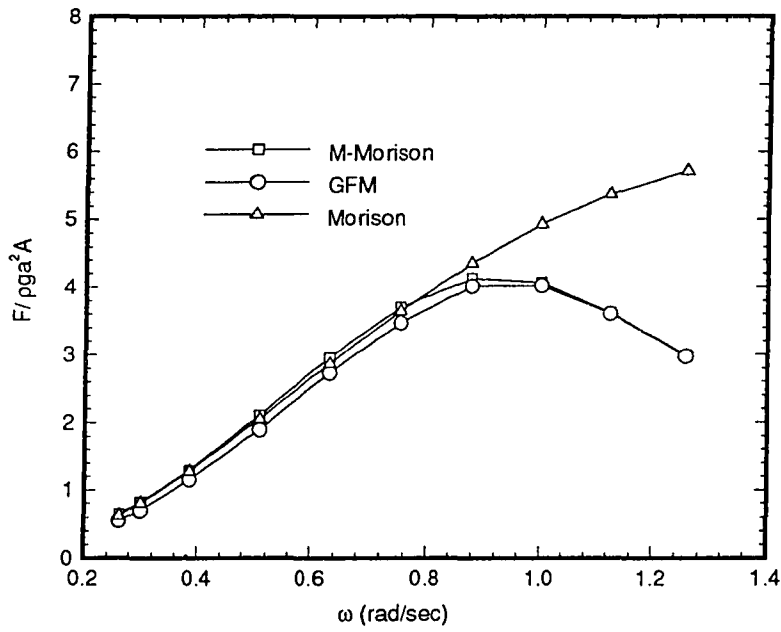


Fig. 5.5 Normalized surge exciting force for a vertical cylinder

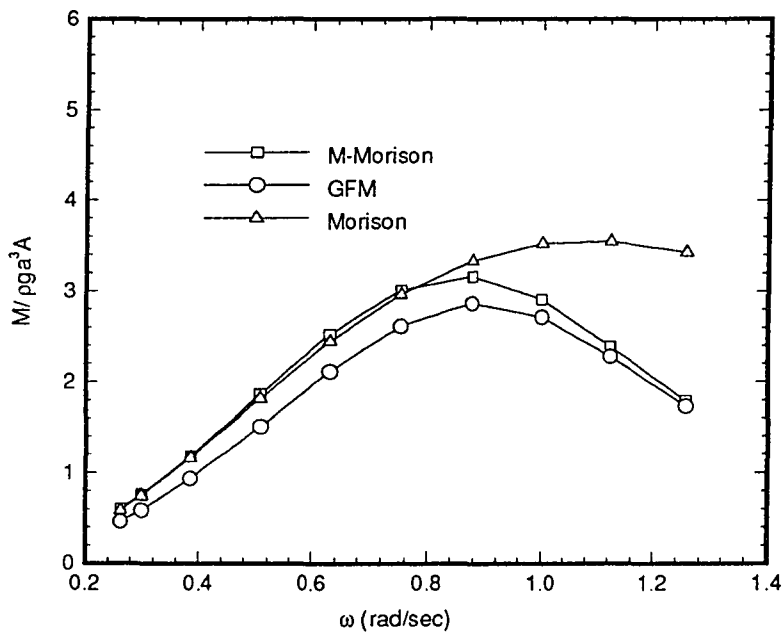


Fig. 5.6 Normalized pitch exciting moment for a vertical cylinder

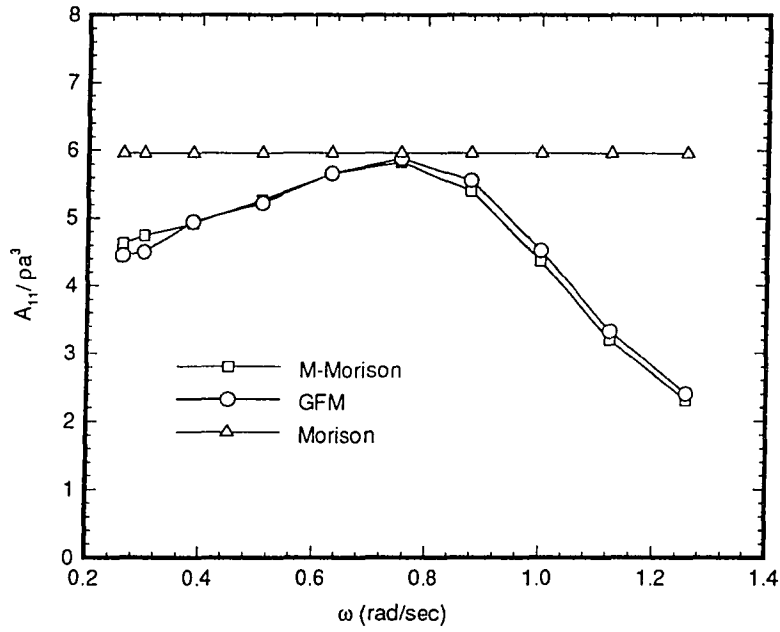


Fig. 5.7 Normalized surge added mass coefficients for a vertical cylinder

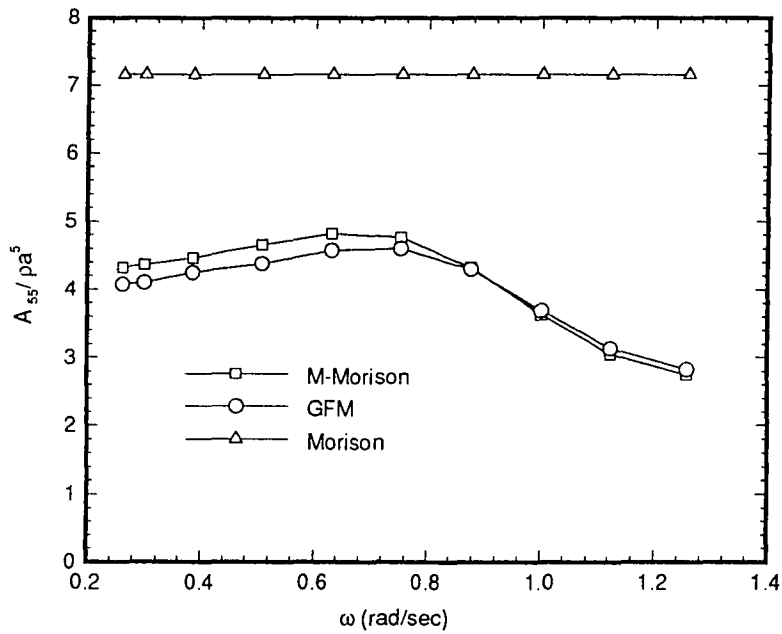


Fig. 5.8 Normalized pitch added moment coefficients for a vertical cylinder

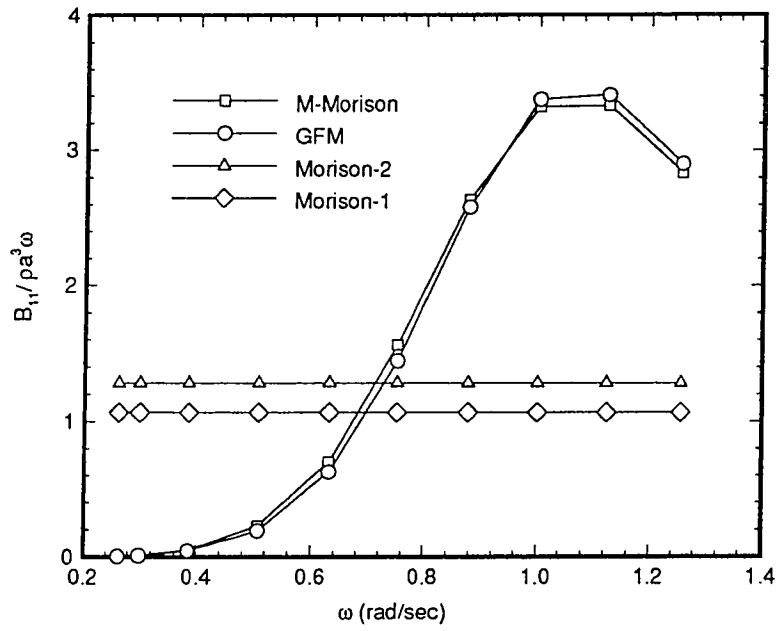


Fig. 5.9 Normalized surge damping coefficients for a vertical cylinder

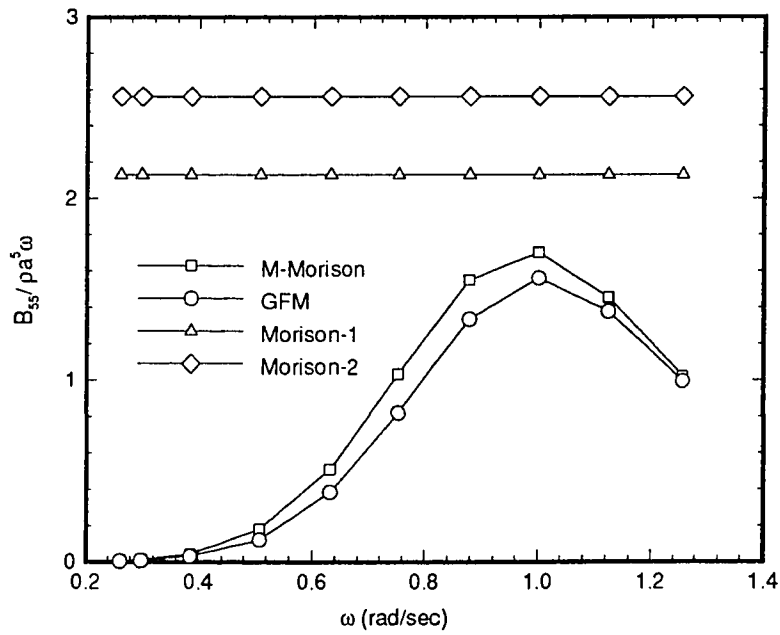


Fig. 5.10 Normalized pitch damping coefficients for a vertical cylinder

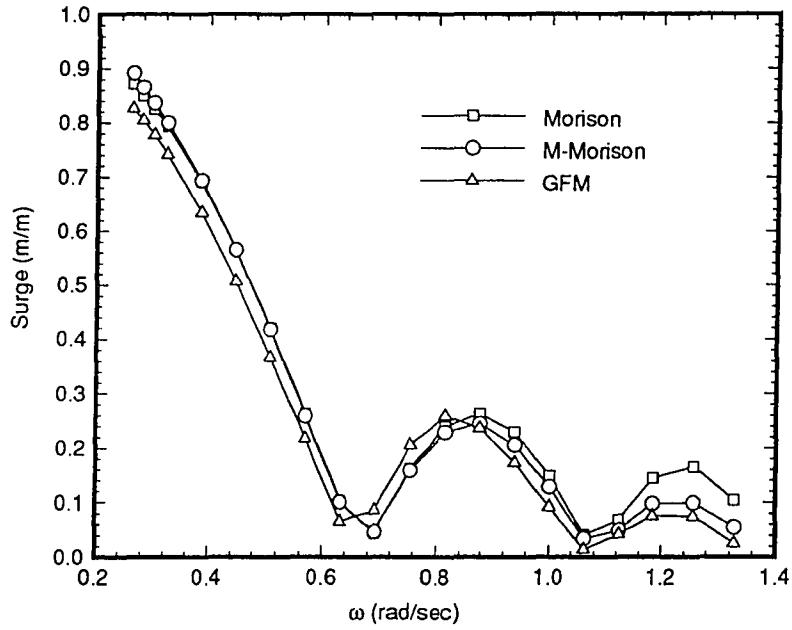


Fig. 5.11 Surge transfer functions of a single rigid module in head seas

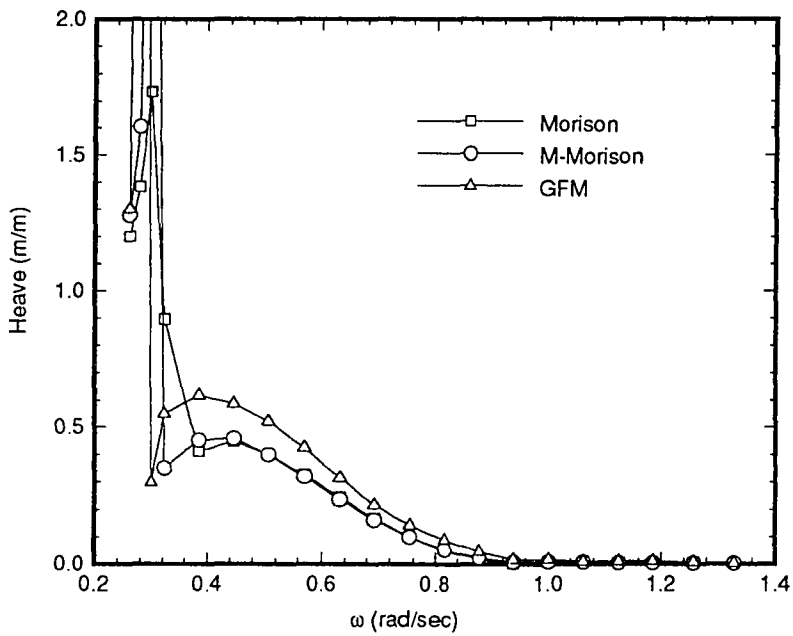


Fig. 5.12 Heave transfer functions of a single rigid module in head seas

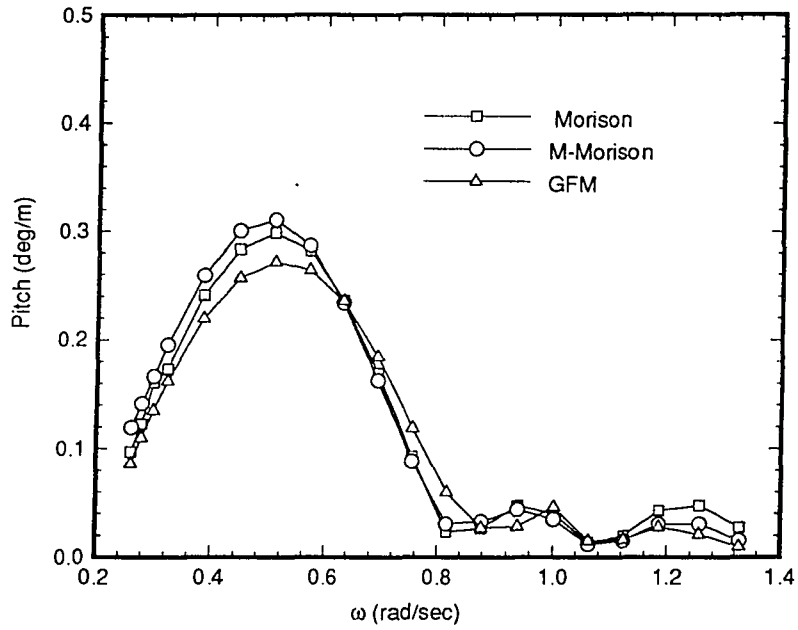


Fig. 5.13 Pitch transfer functions of a single rigid module in head seas

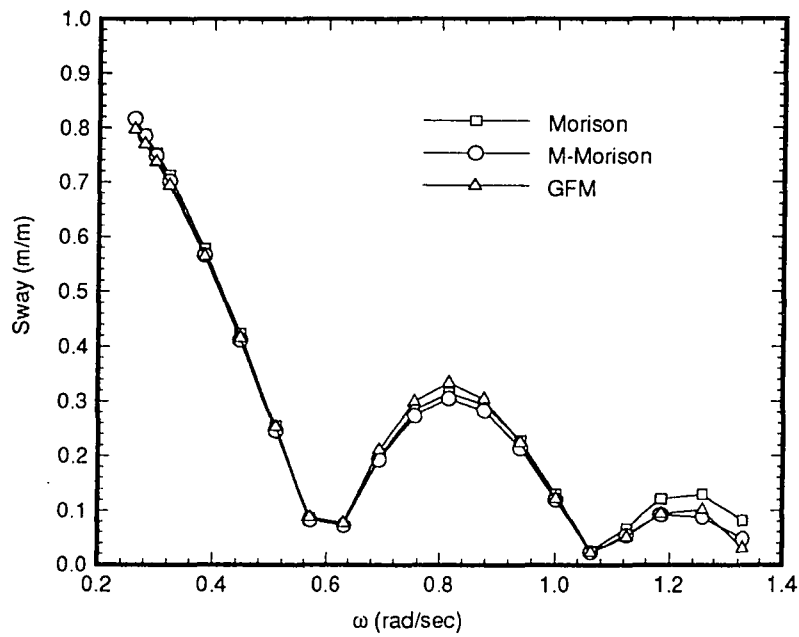


Fig. 5.14 Sway transfer functions of a single rigid module in beam seas

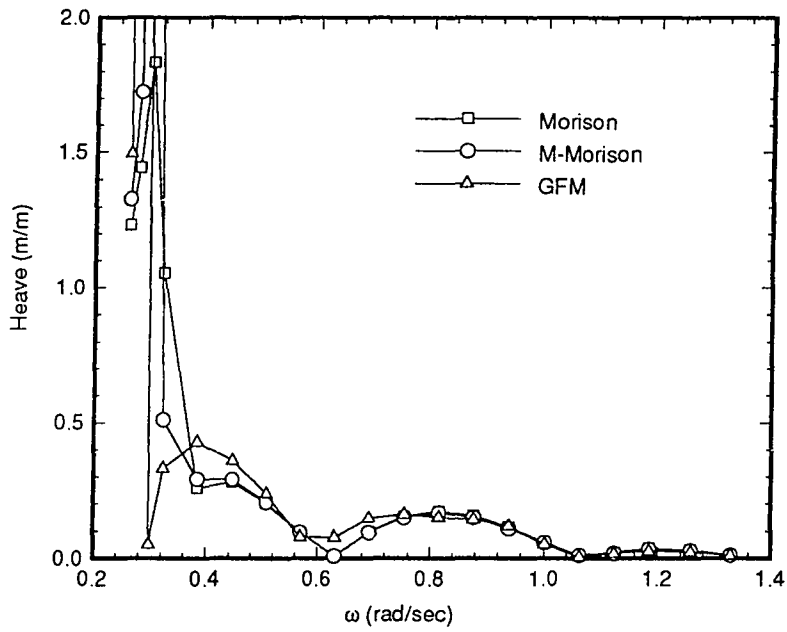


Fig. 5.15 Heave transfer functions of a single rigid module in beam seas

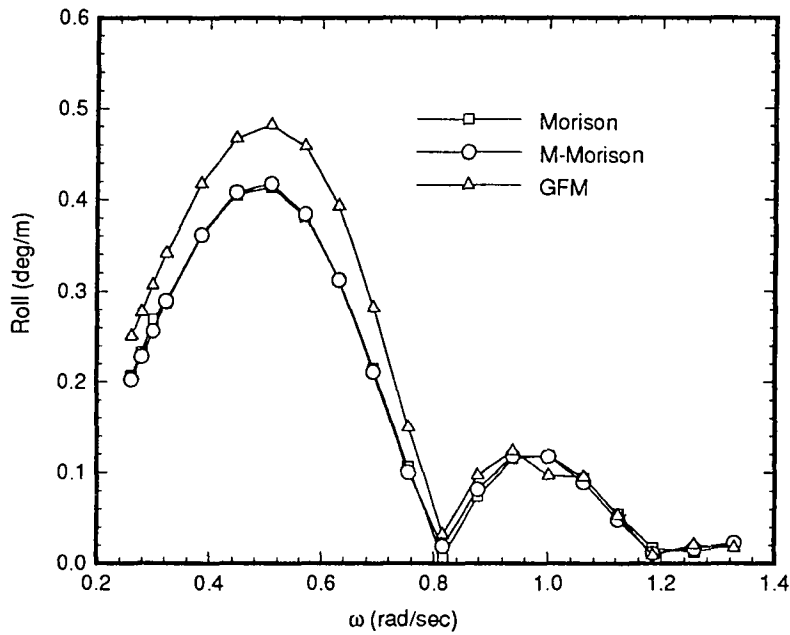


Fig. 5.16 Roll transfer functions of a single rigid module in beam seas

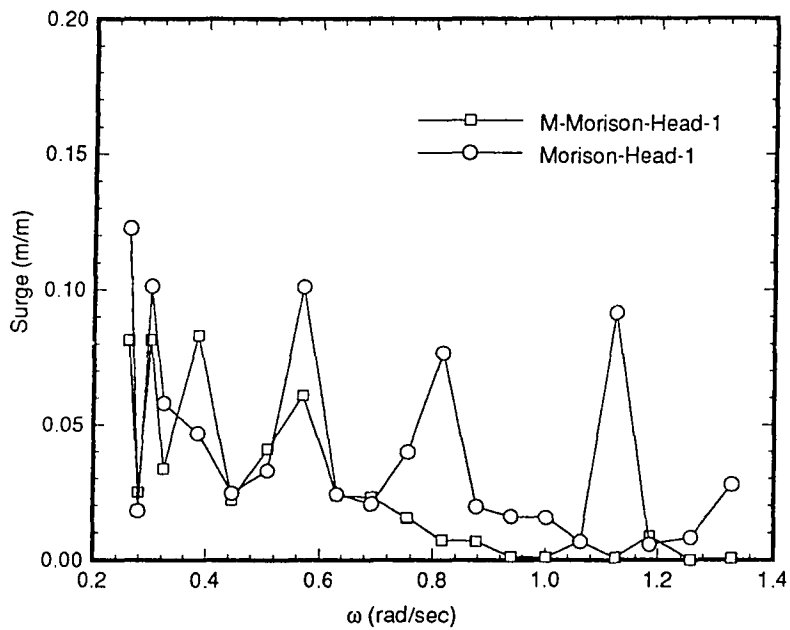


Fig. 5.17 Surge transfer functions of a Module 1 in head seas

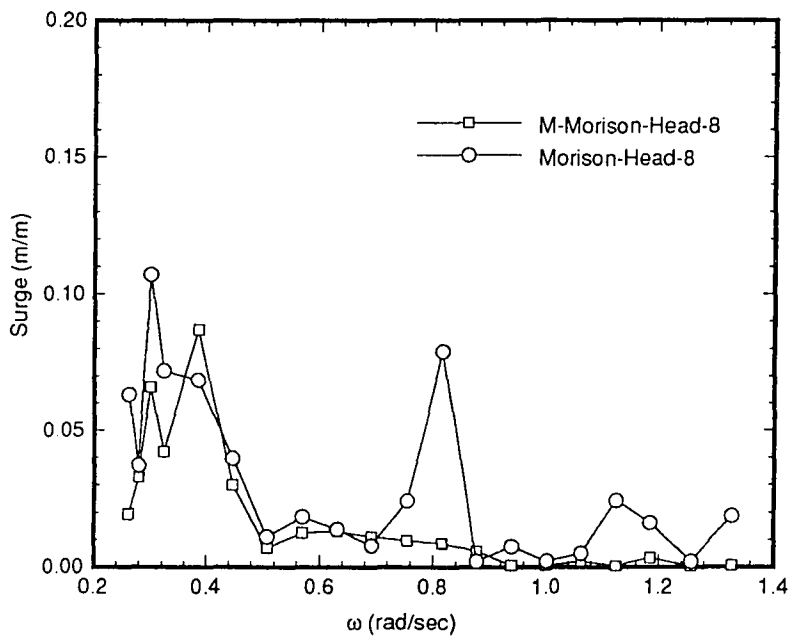


Fig. 5.18 Surge transfer functions of Module 8 in head seas

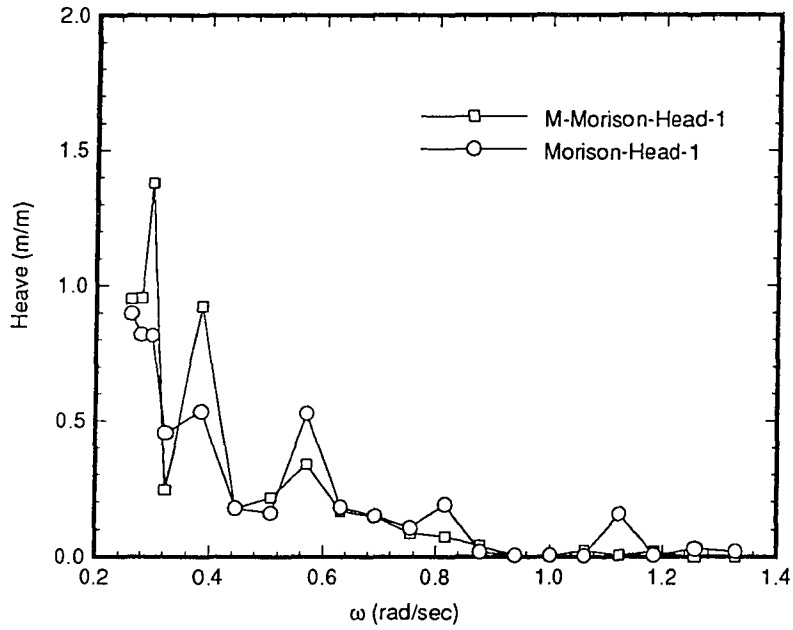


Fig. 5.19 Heave transfer functions of Module in head seas

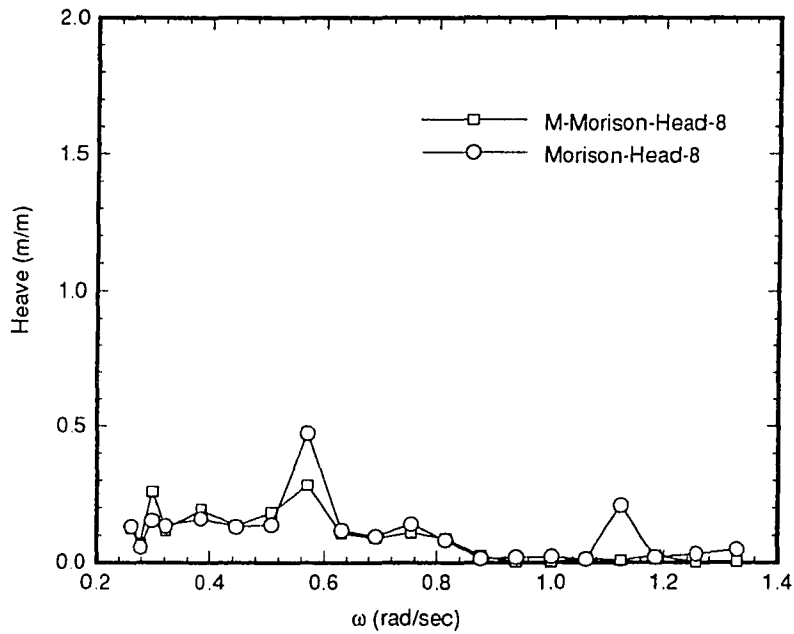


Fig. 5.20 Heave transfer functions of Module 8 in head seas

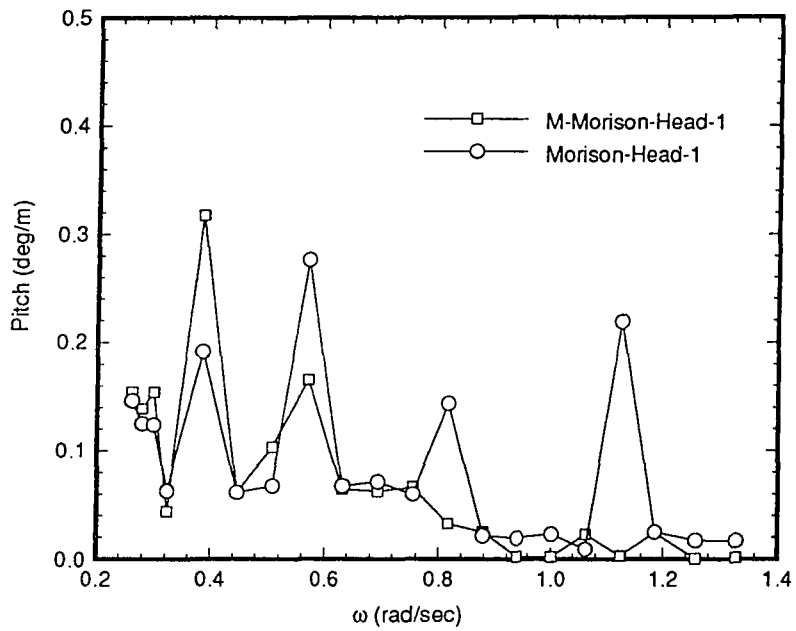


Fig. 5.21 Pitch transfer functions of Module 1 in head seas

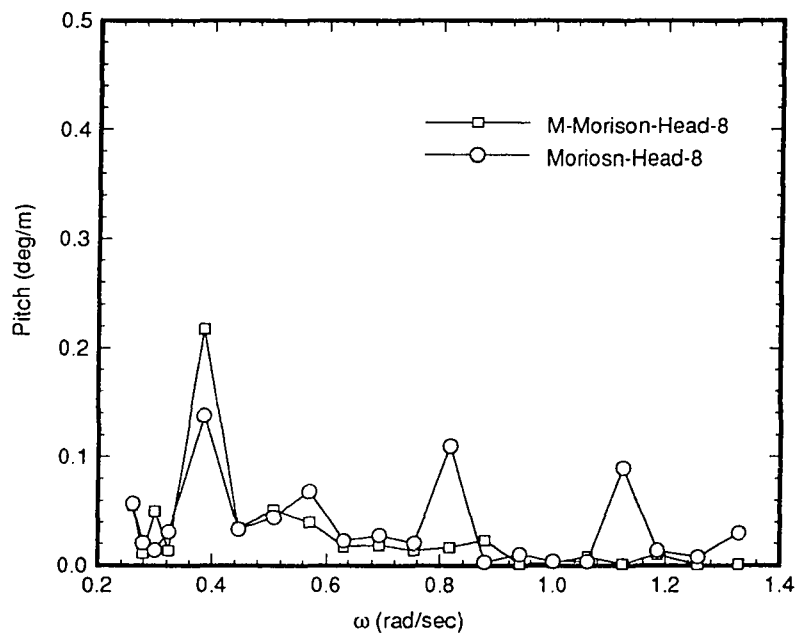


Fig. 5.22 Pitch transfer functions of Module 8 in head seas

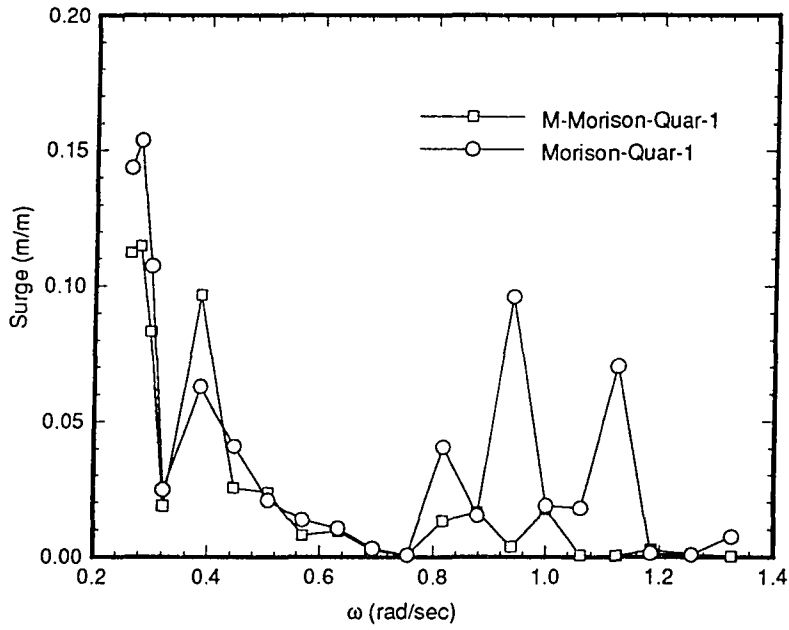


Fig. 5.23 Surge transfer functions of Module 1 in quartering seas

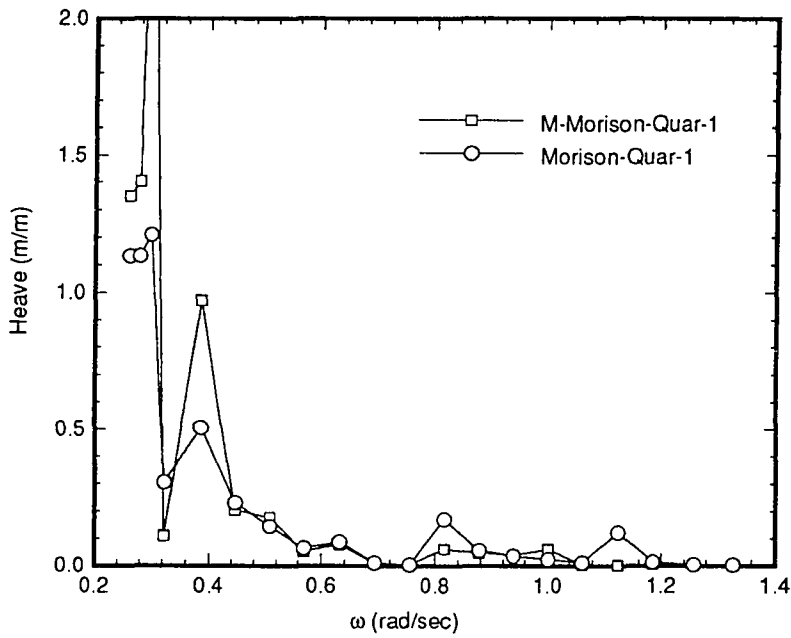


Fig. 5.24 Heave transfer functions of Module 1 in quartering seas

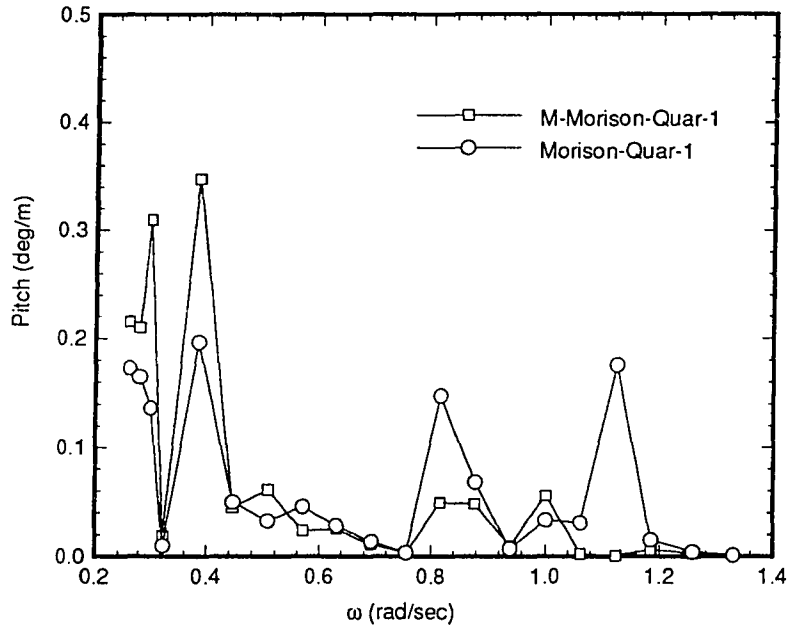


Fig. 5.25 Pitch transfer functions of Module 1 in quartering seas

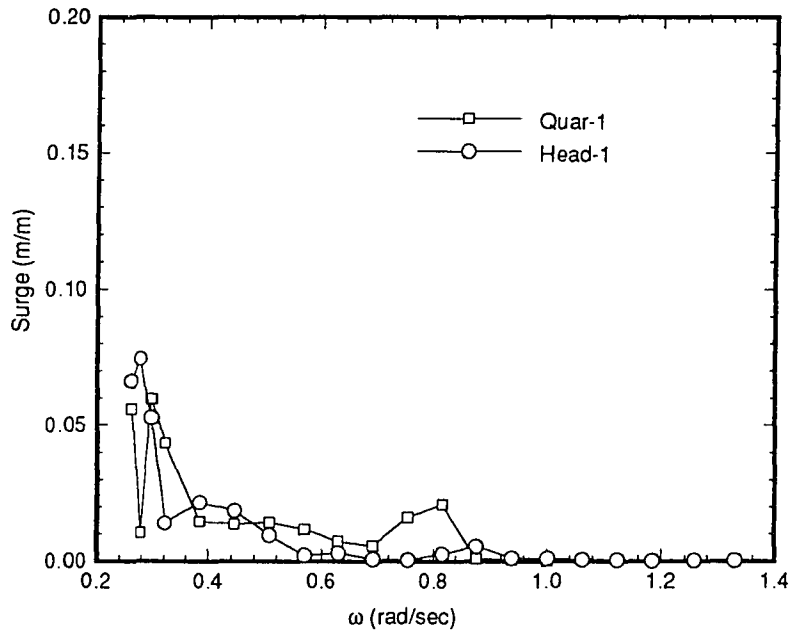


Fig. 5.26 Surge transfer functions of Module 1 for the deck and pontoon connector case

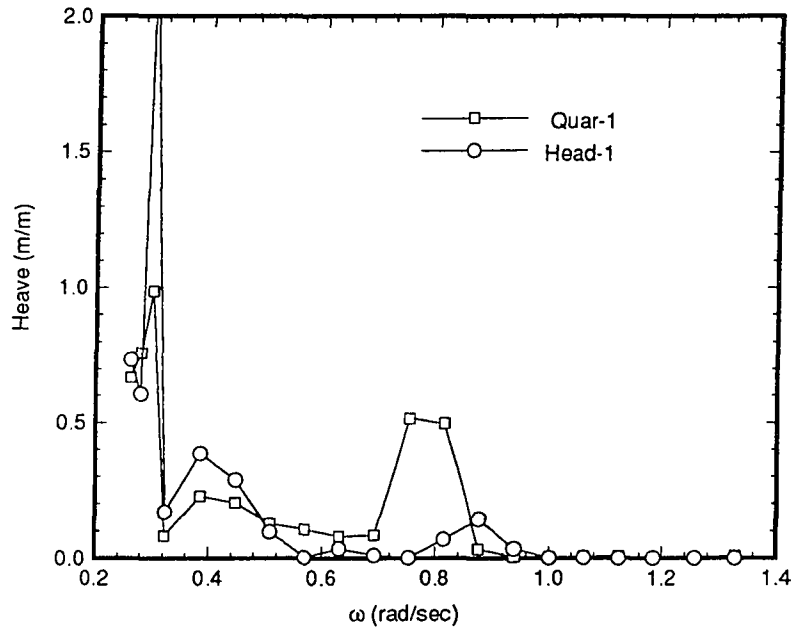


Fig. 5.27 Heave transfer functions of Module 1 for the deck and pontoon connector case

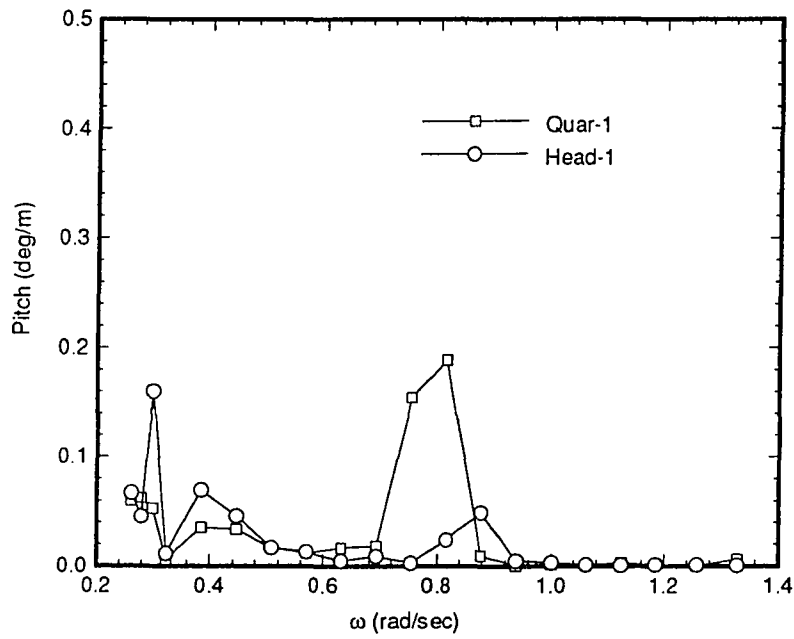


Fig. 5.28 Pitch transfer functions of Module 1 for the deck and pontoon connector case

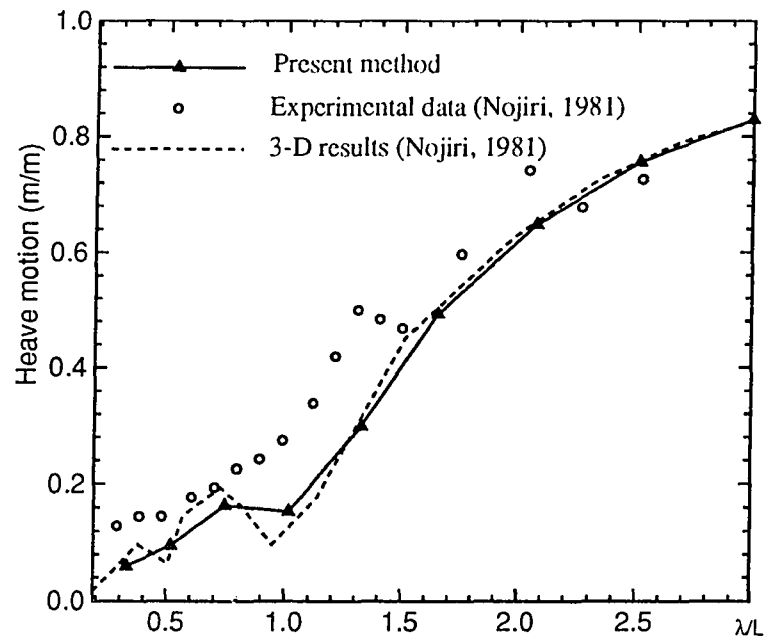


Fig. 6.1 Heave response of barge model ($3 \times 0.75 \times 0.016 \text{ m}^3$)

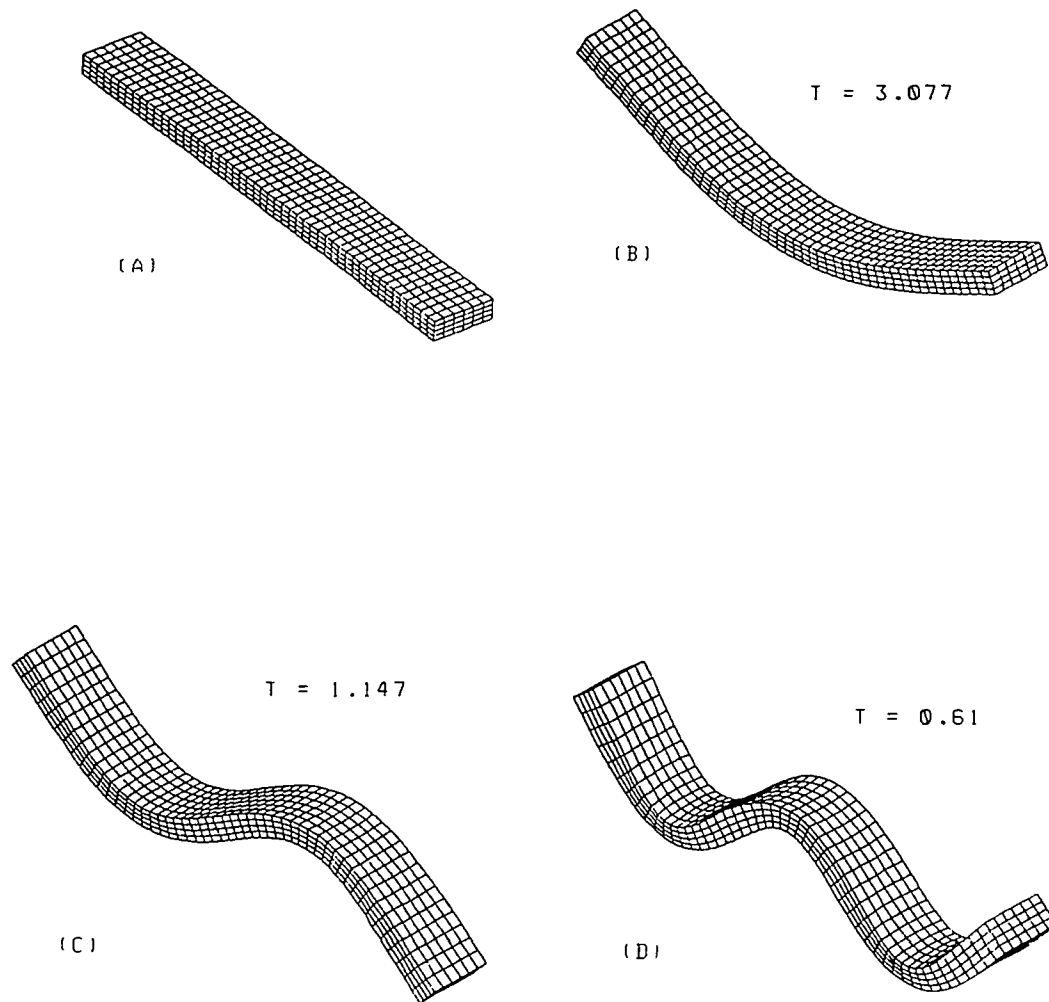


Fig. 6.2 Normal modes of the test box. (A)-rigid mode, (B)-first bending mode, (C)-second bending mode, (D)-third bending mode, T-natural period in seconds.

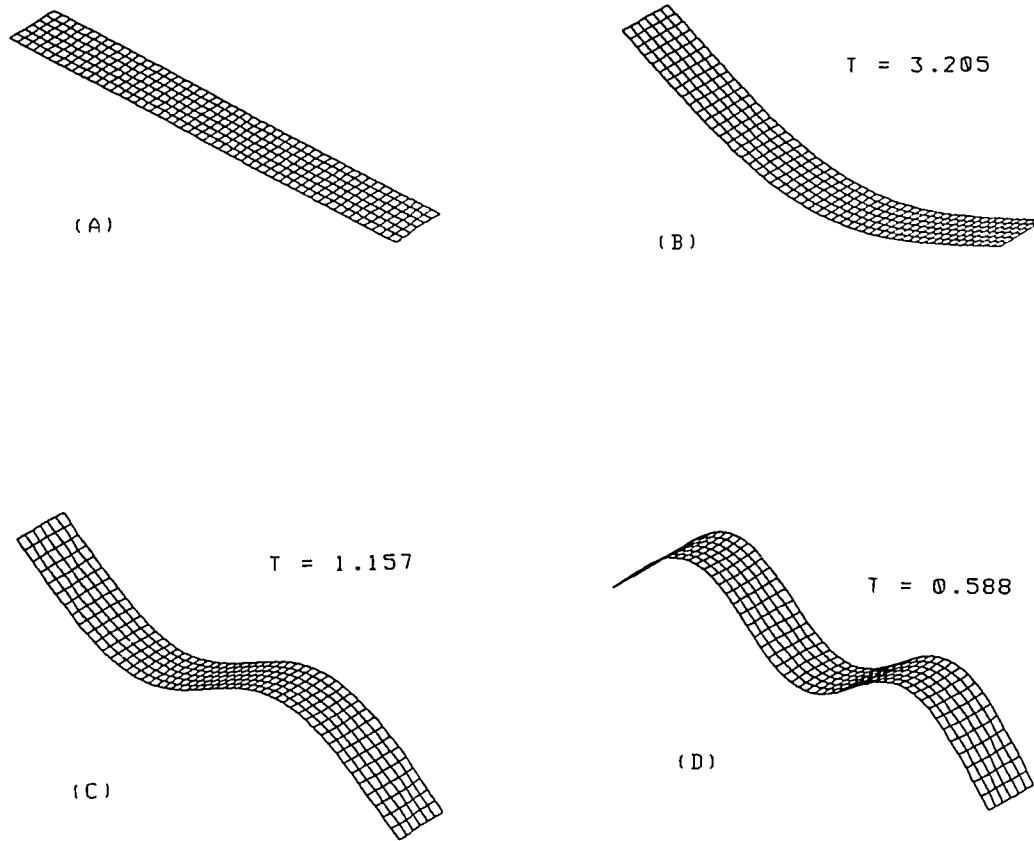


Fig. 6.3 Normal modes of the equivalent plate. (A)-rigid mode, (B)-first bending mode, (C)-second bending mode, (D)-third bending mode, T-natural period in seconds.

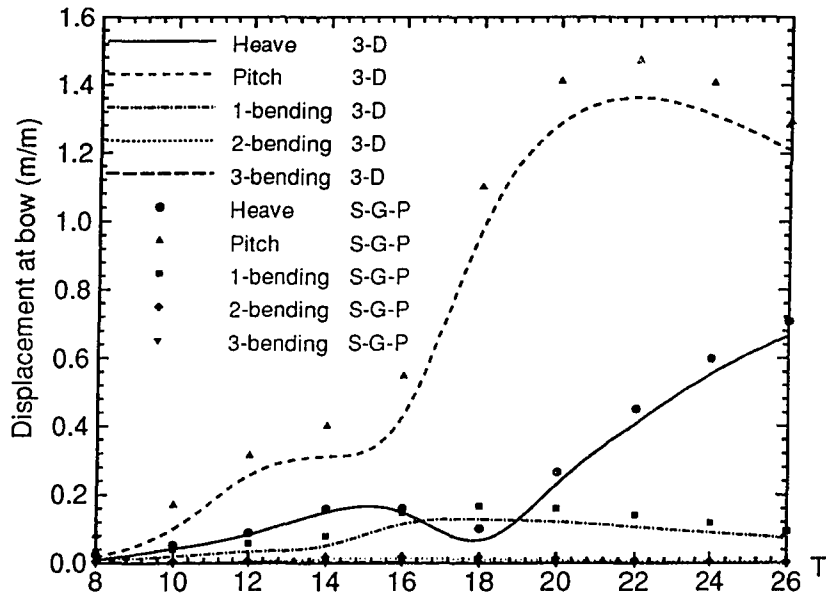


Fig. 6.4 Vertical displacement amplitude transfer function of the box (500*60*20 m³)

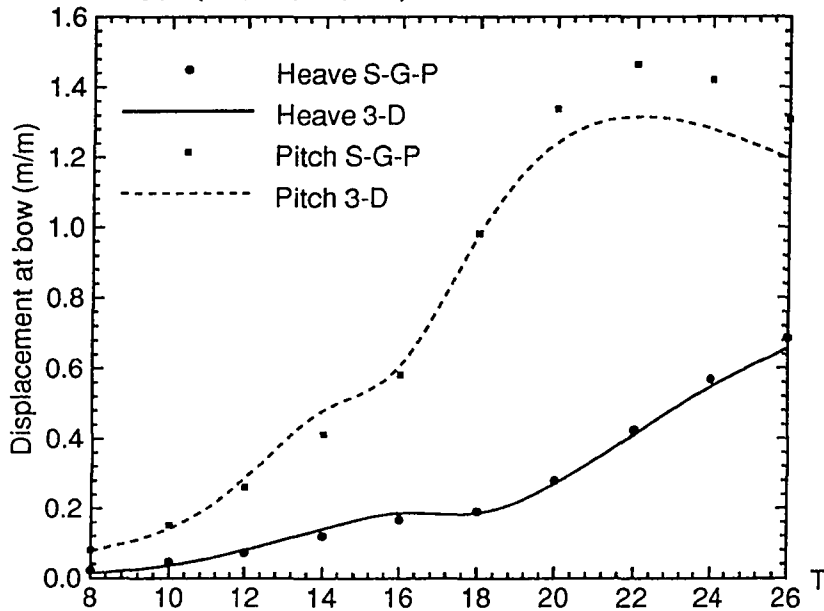


Fig. 6.5 Vertical displacement amplitude transfer function of the box (500*200*20 m³)

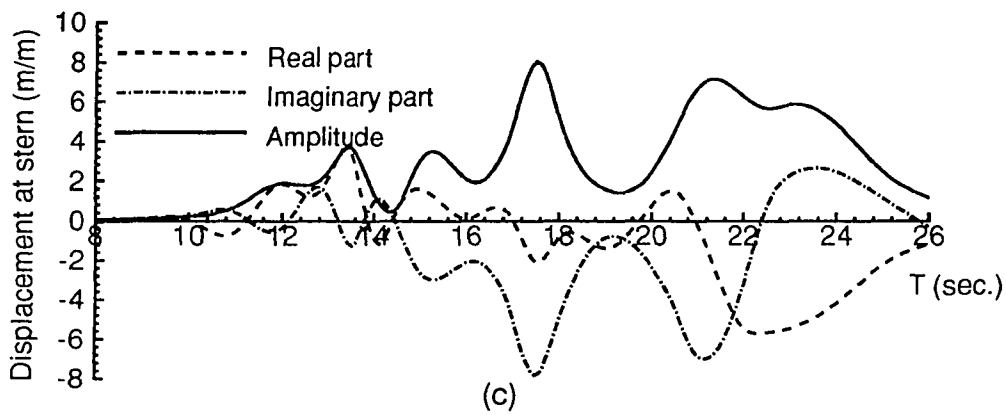
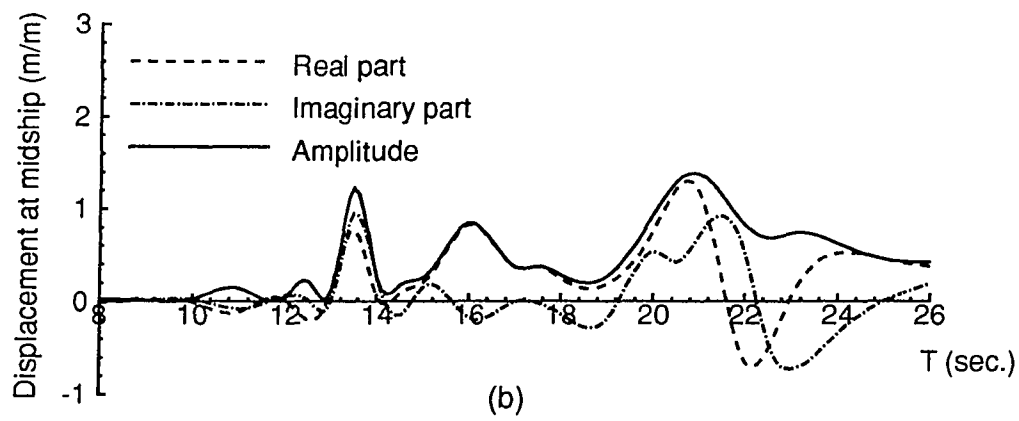
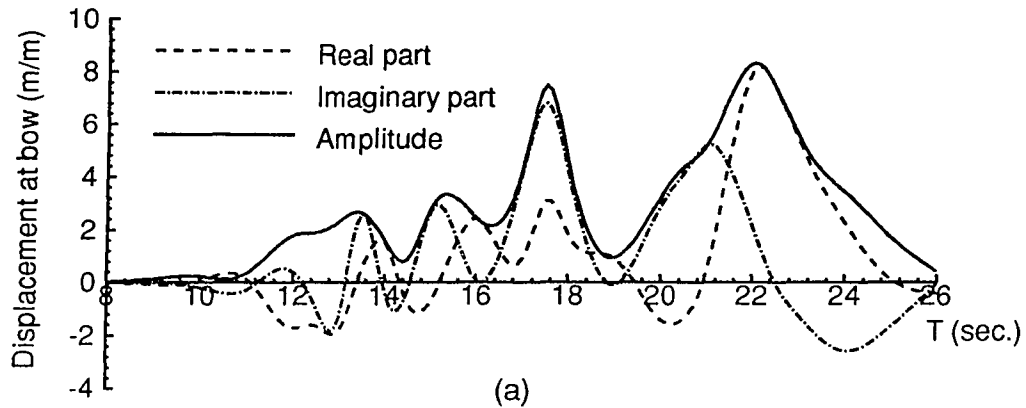
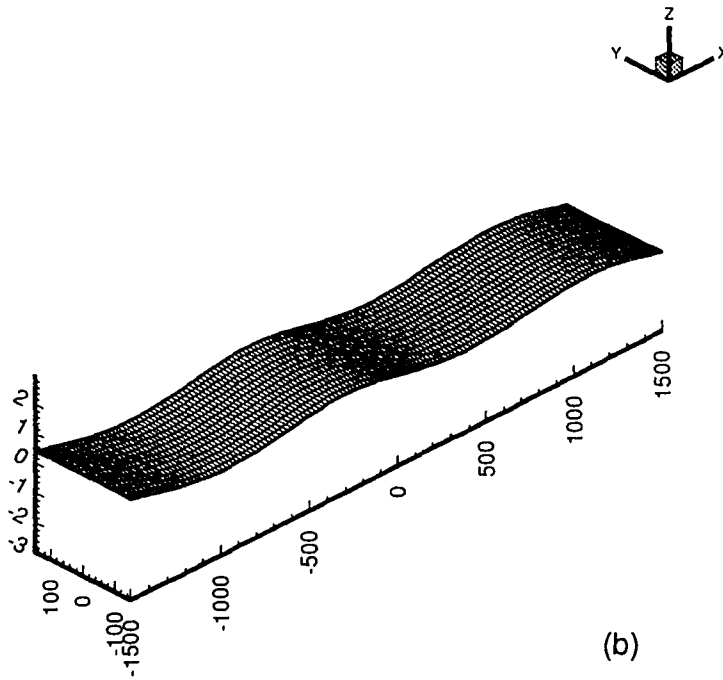
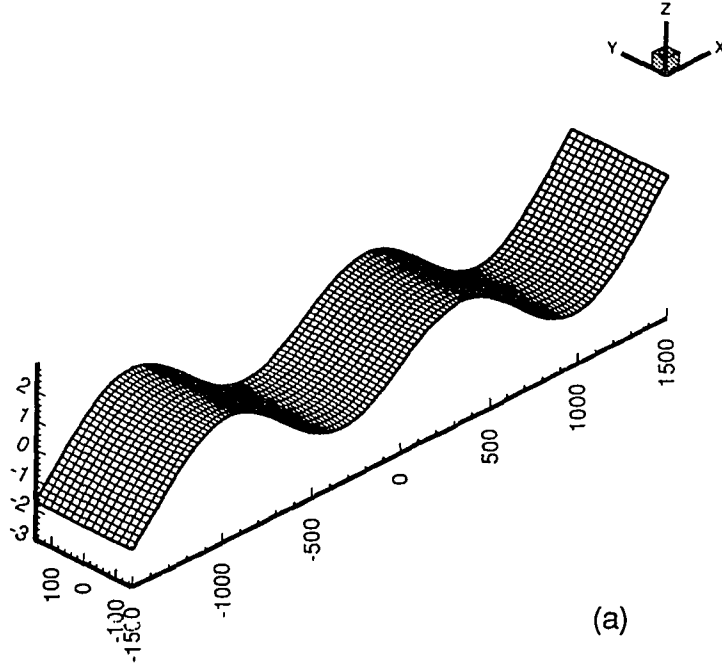
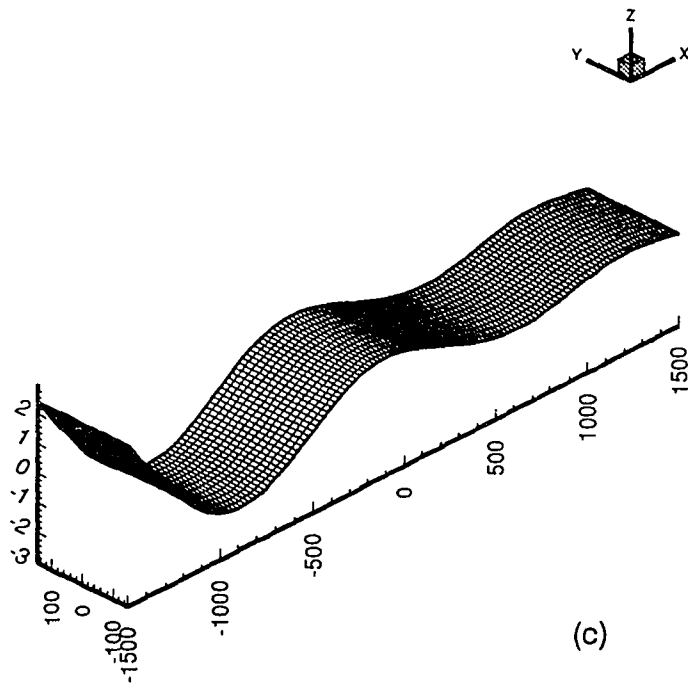
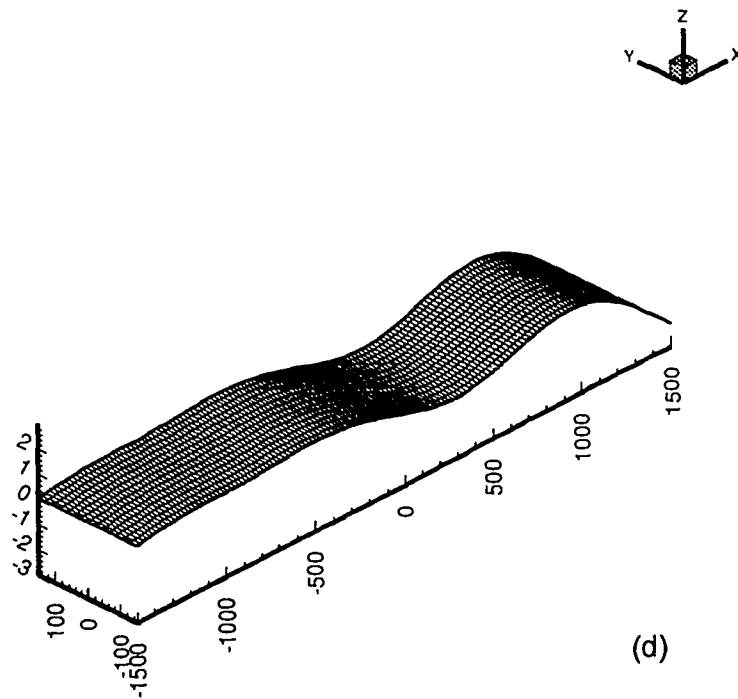


Fig. 6.6 Vertical displacement transfer functions of the runway of 3000m*300m*25m (d=15m), (a) bow, (b) midship, (c) stern

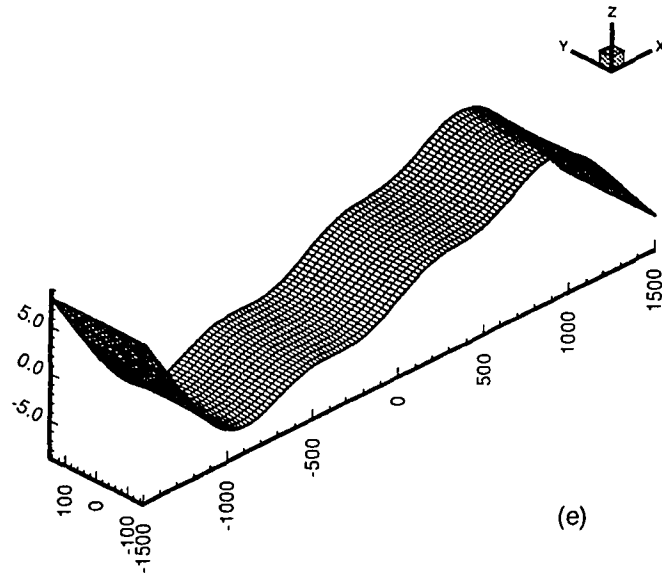




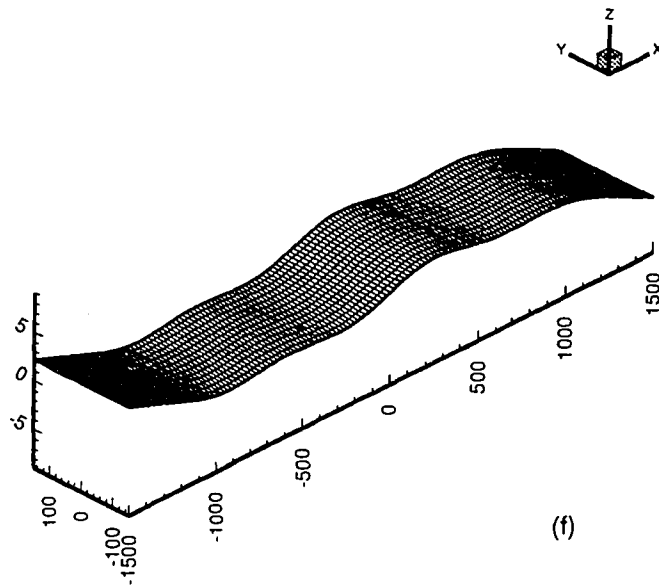
(c)



(d)



(e)



(f)

Fig. 6.7 Vertical displacement transfer functions of the runway of 3000m*300m*25m (d=15m). (a)-real and (b)-imaginary part for a 12 second wave, (c)-real and (d)-imaginary part for a 16 second wave, (e)-real and (f)-imaginary part for a 22 second wave.

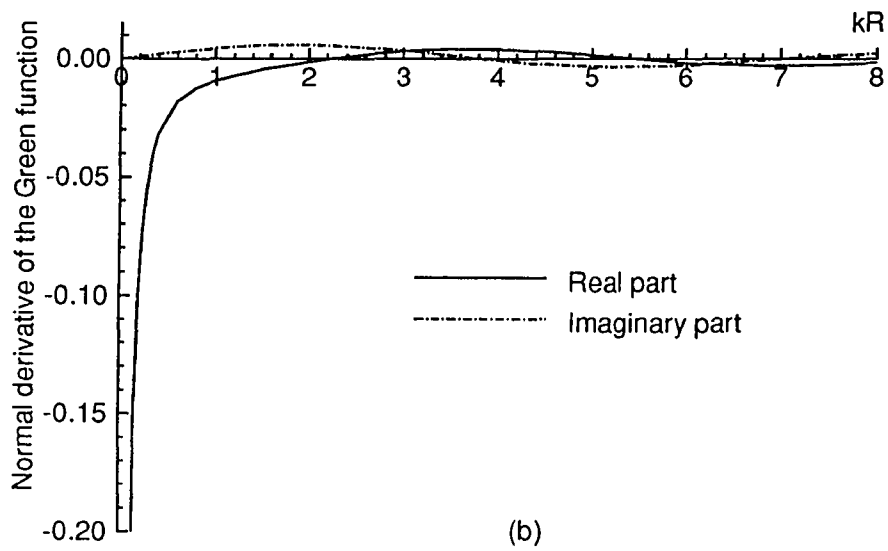
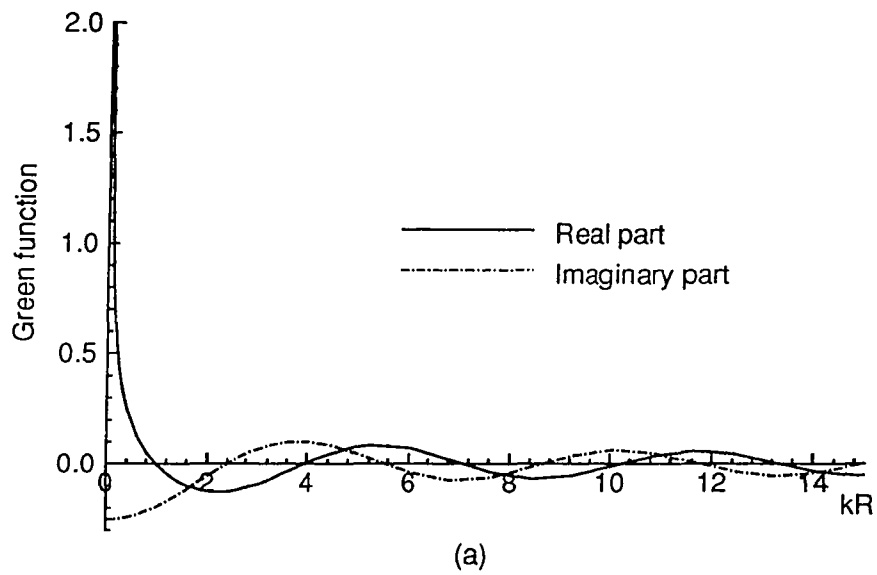


Fig. 7.1 (a) The Green function, (b) its normal derivative

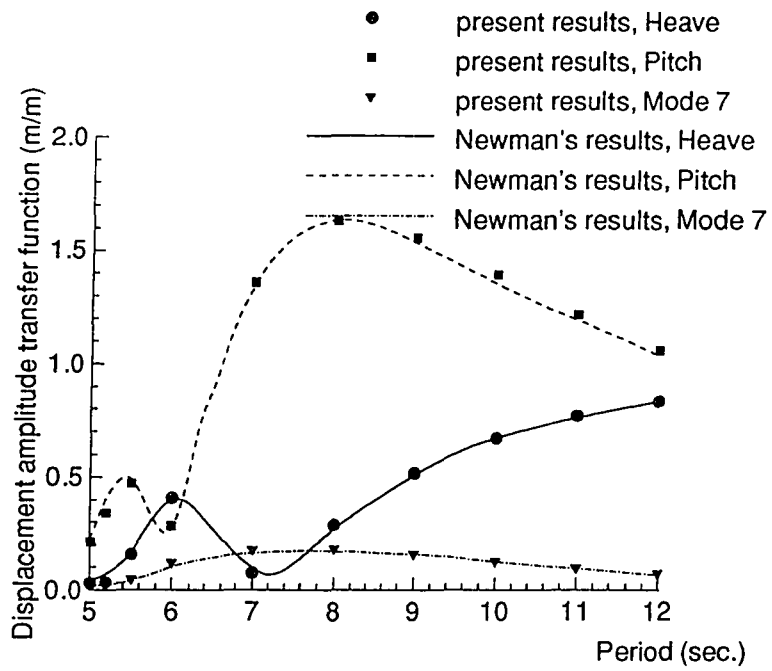
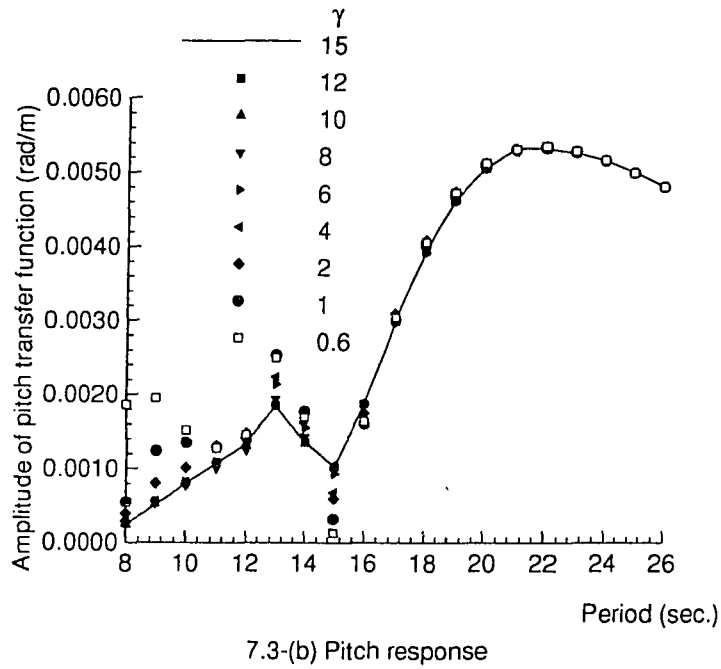
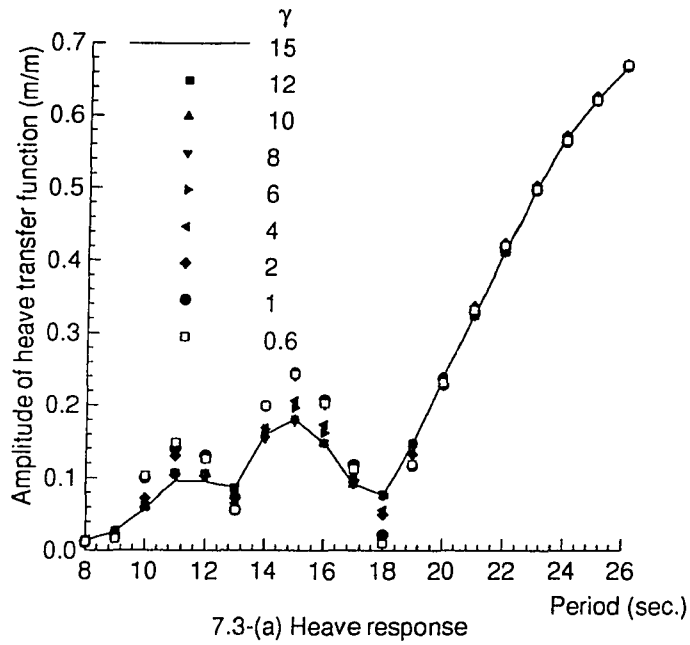
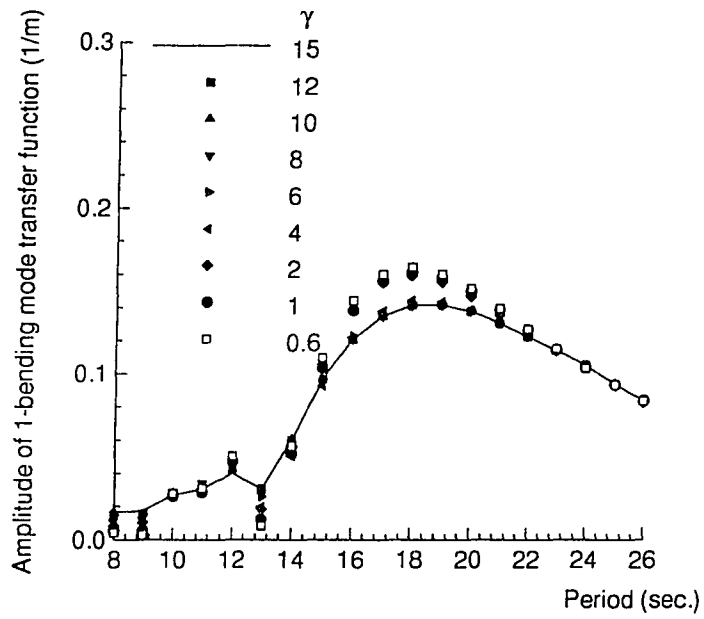
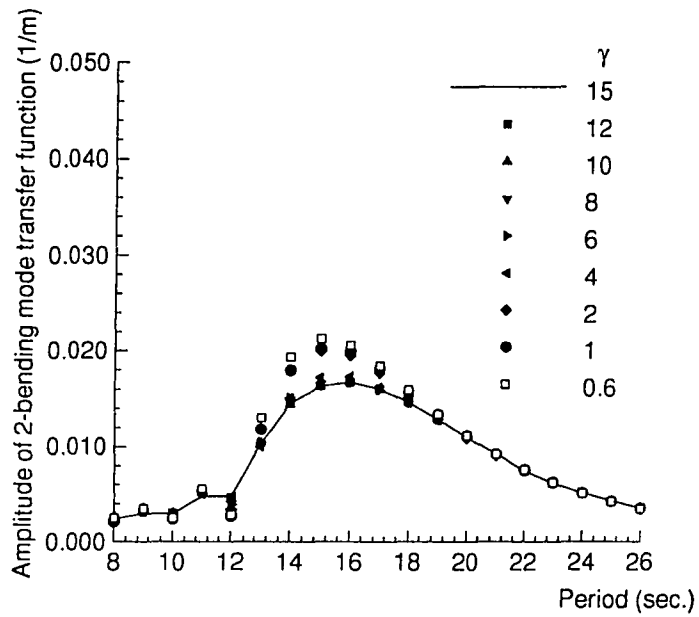


Fig. 7.2 Displacements at bow of the box
(80m*10m*10m)





7.3-(c) Response of the first-bending mode



7.3-(d) Response of the second-bending mode

Fig. 7.3 Responses of the box using different criteria (500m*60m*20m)

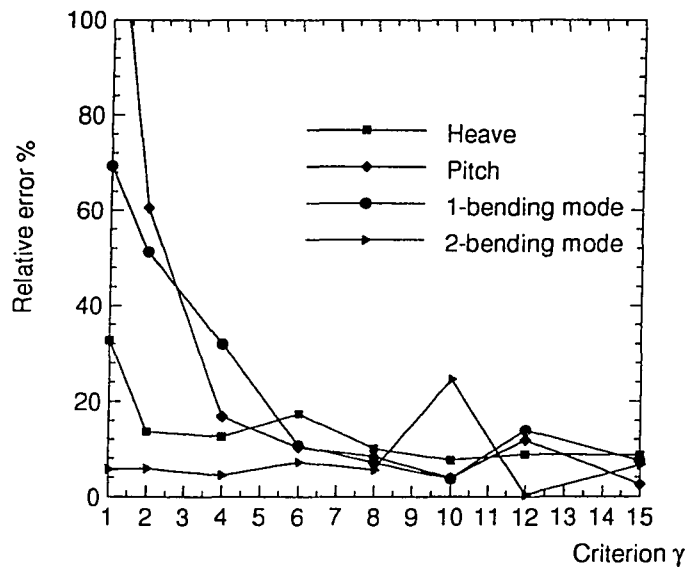


Fig. 7.4 Relative errors of the responses
(period = 8 sec)

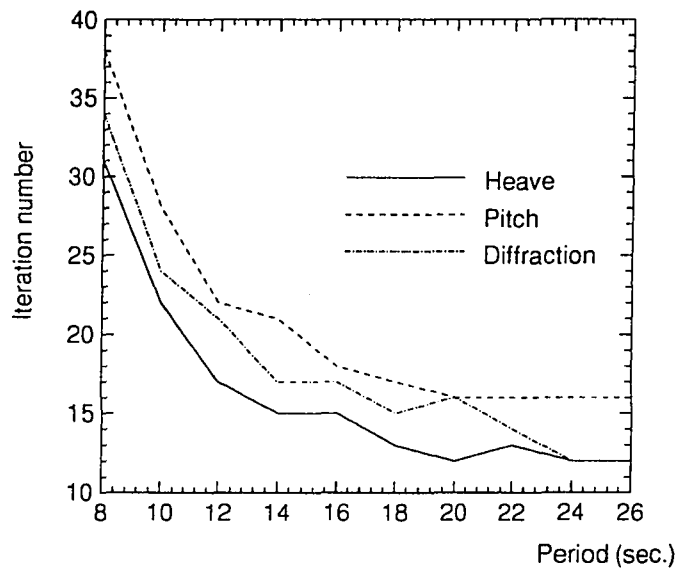


Fig. 7.5 Number of iterations in solving
Eq. (7.7) (number of panel is 936)

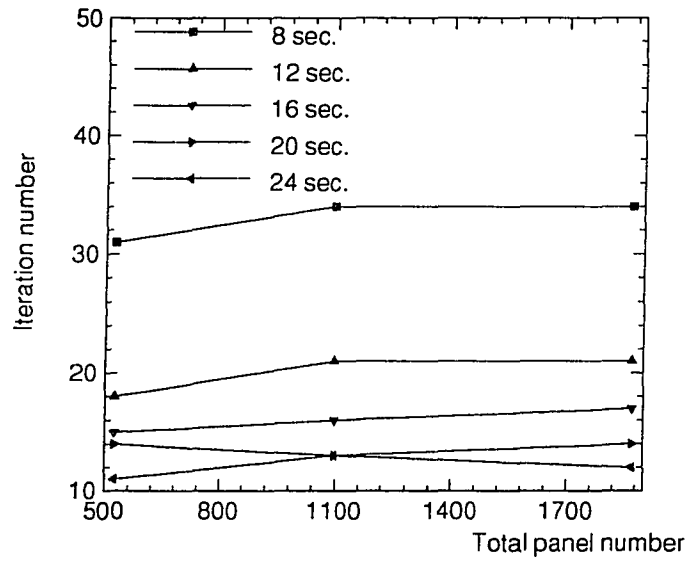


Fig. 7.6 Number of iterations in solving Eq. (7.7) for diffraction source strengths

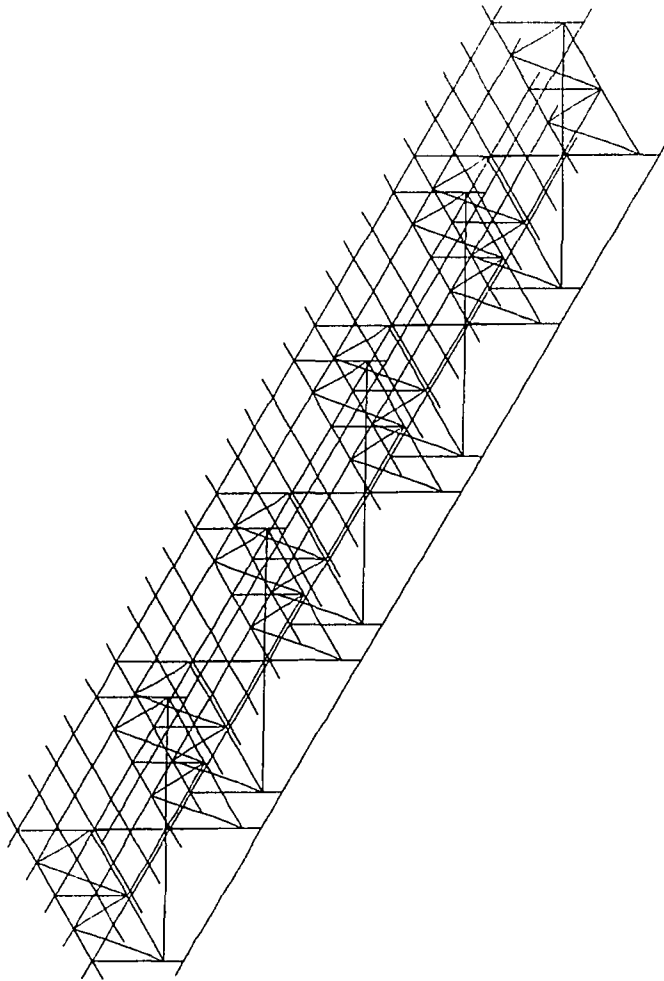


Fig. 8.1 Finite element model of 5-module semi-submersible

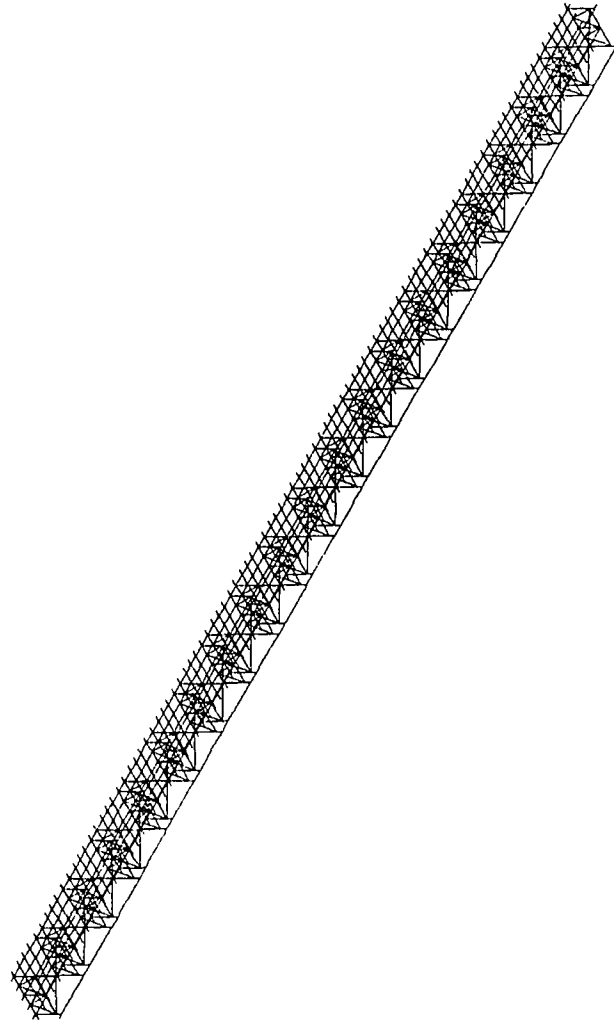


Fig. 8.2 Finite element model of 20-module semi-submersible

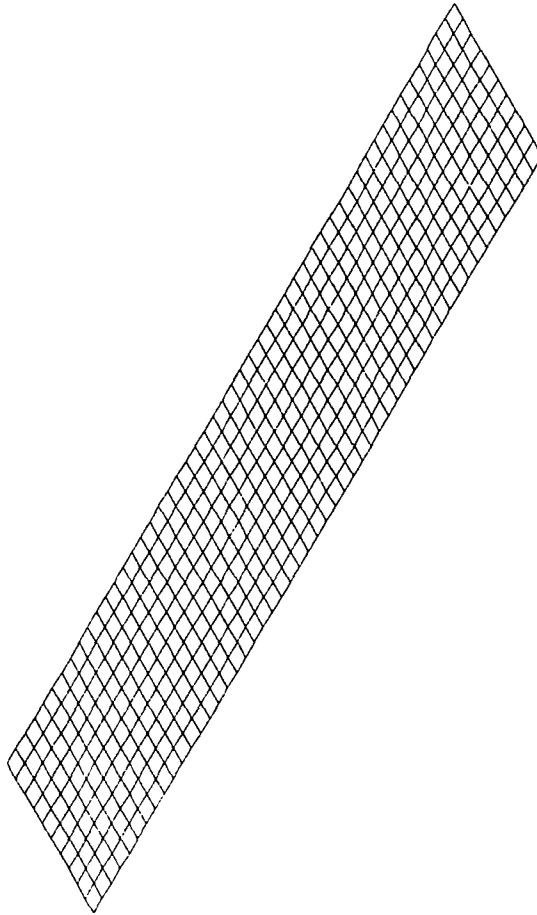


Fig. 8.3 Finite element model of 5-module mat-like VLFS

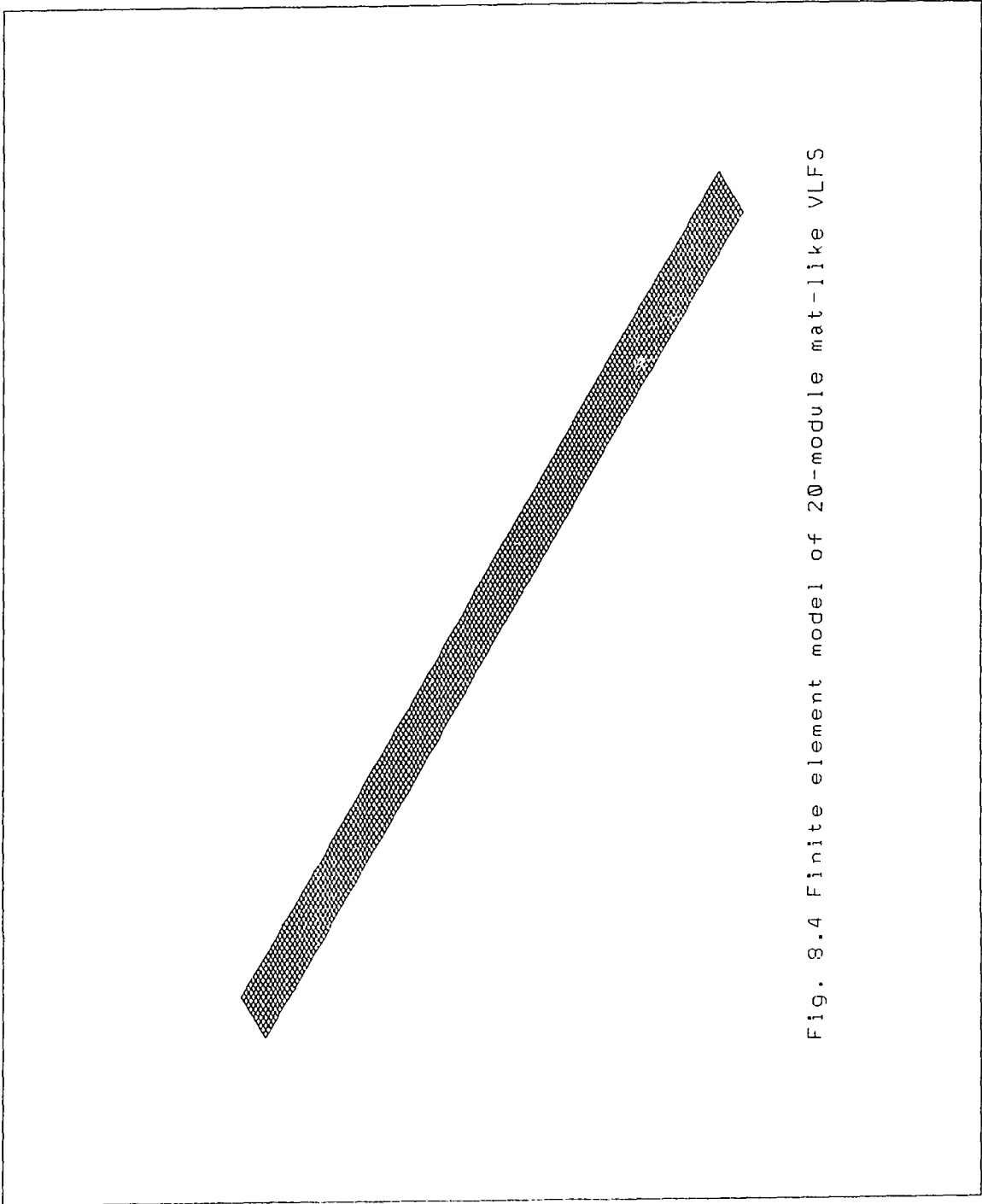
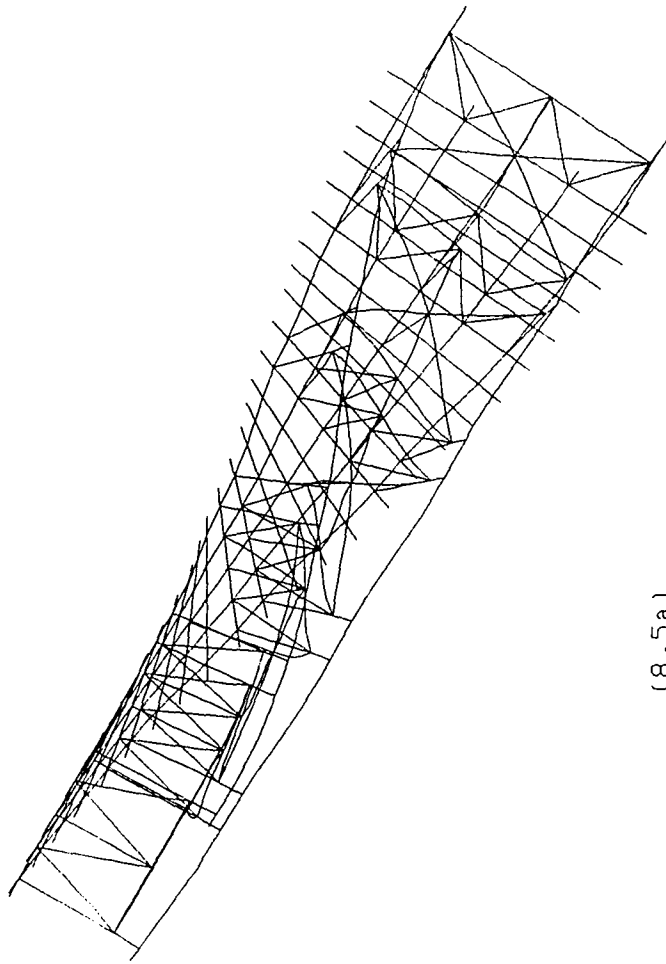


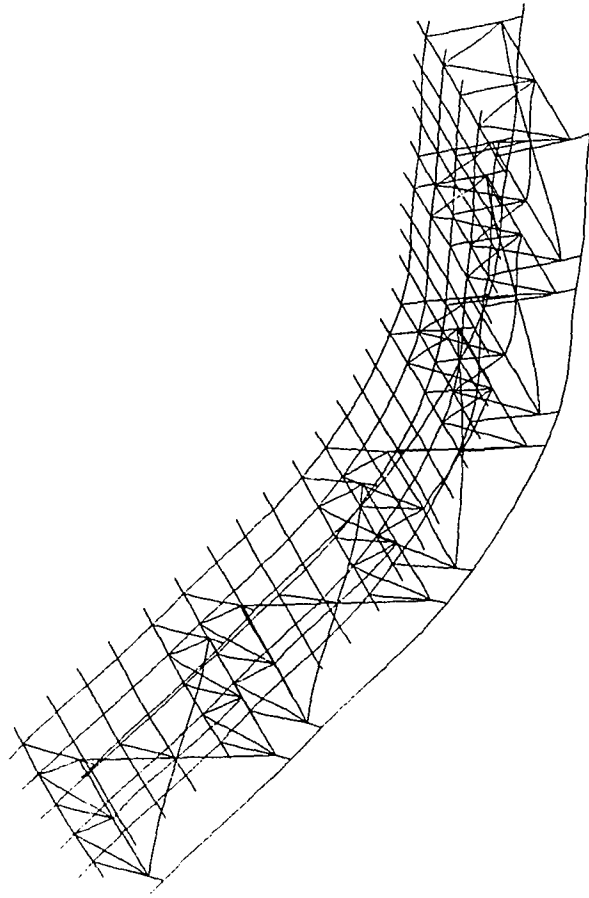
Fig. 8.4 Finite element model of 20-module mat-like VLF

F_Mode=7 0.475 Hz

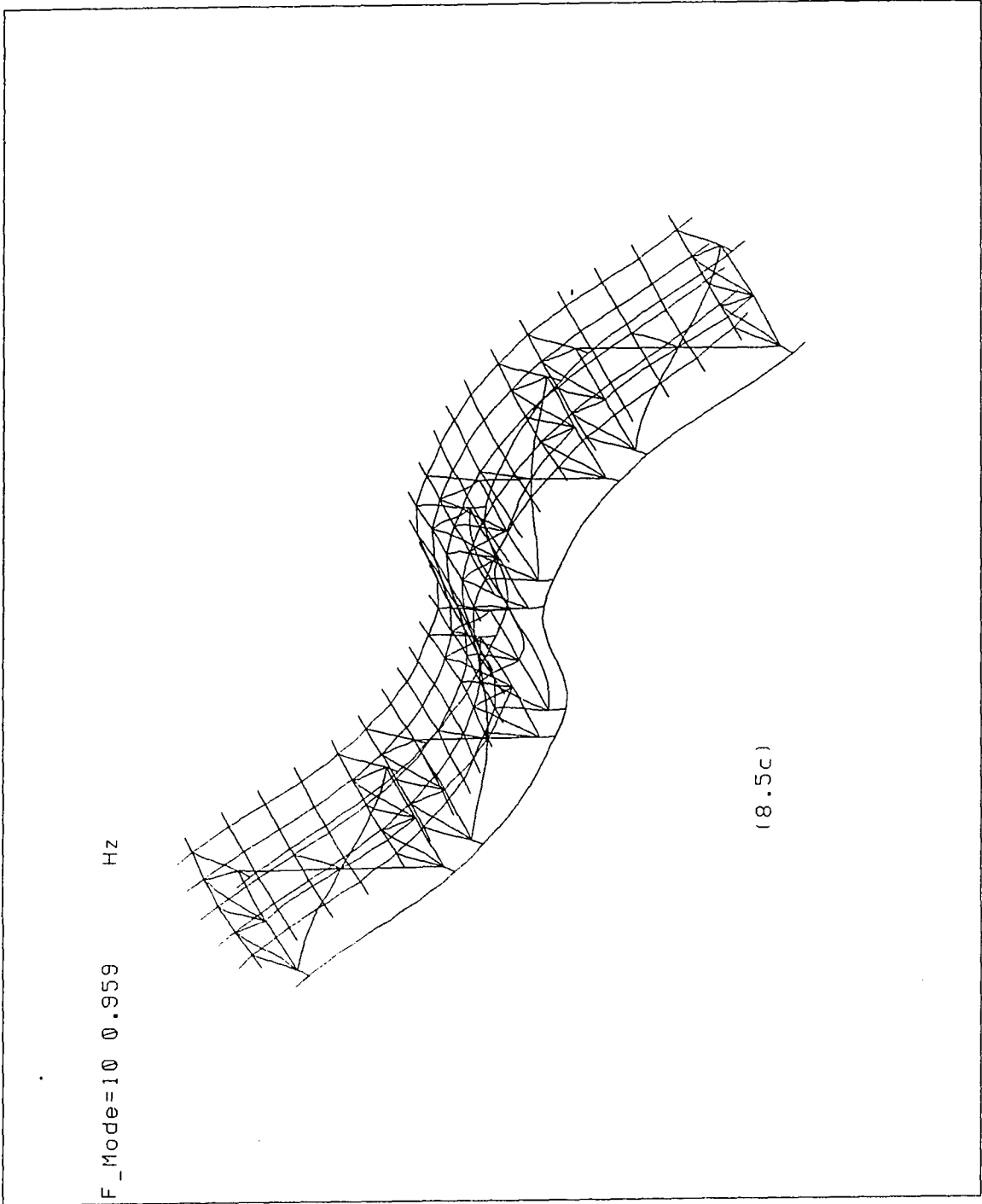


(8.5a)

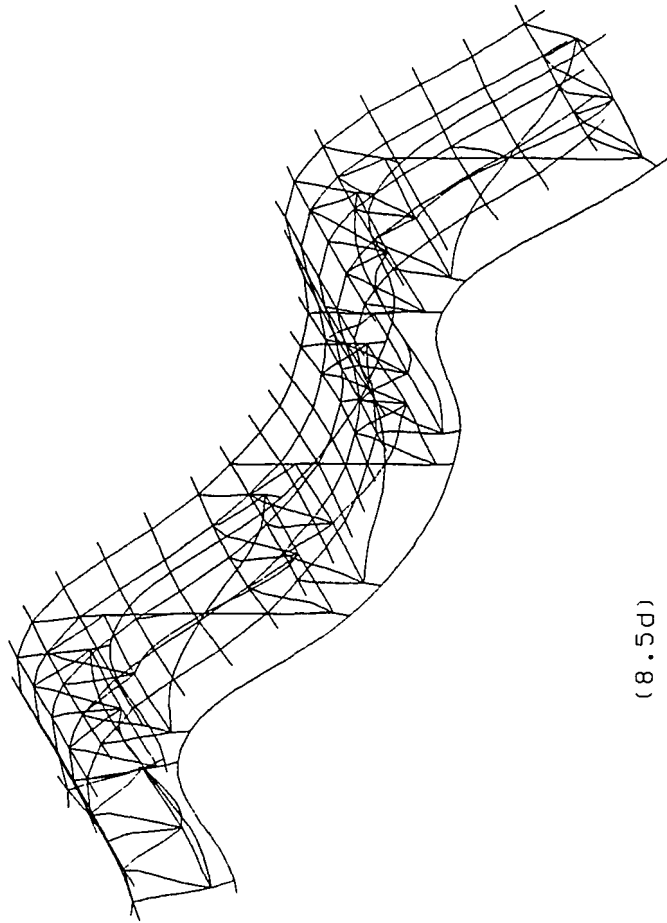
F_Mode=8 0.507 Hz



(8.5b)



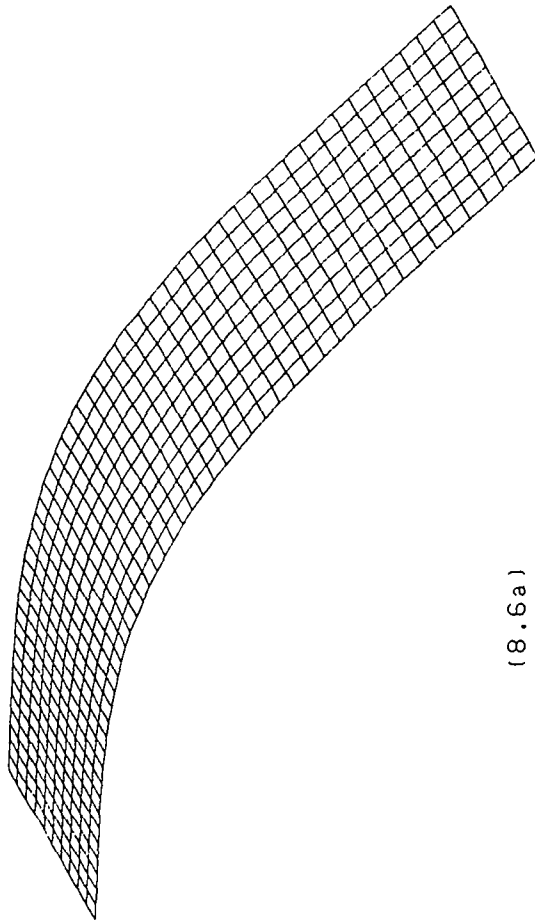
F_Mode=13 1.43 Hz



(8.5d)

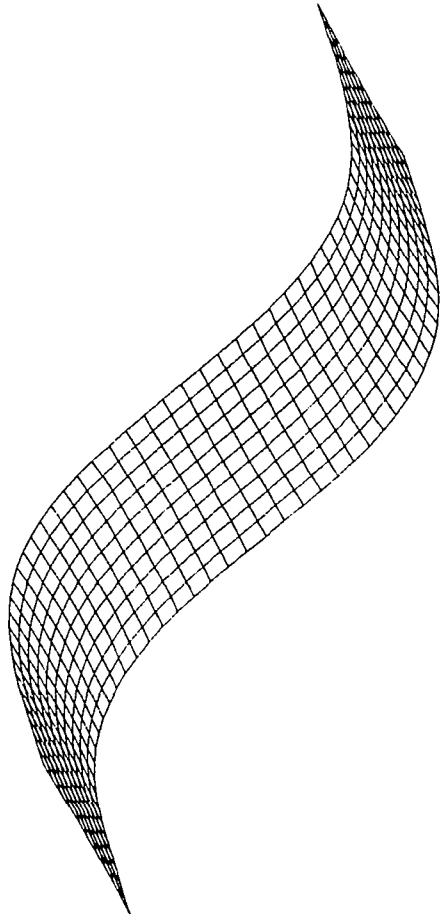
Fig. 8.5 Normal modes of 5-module semi-submersible

F_Mode=8 0.251 Hz



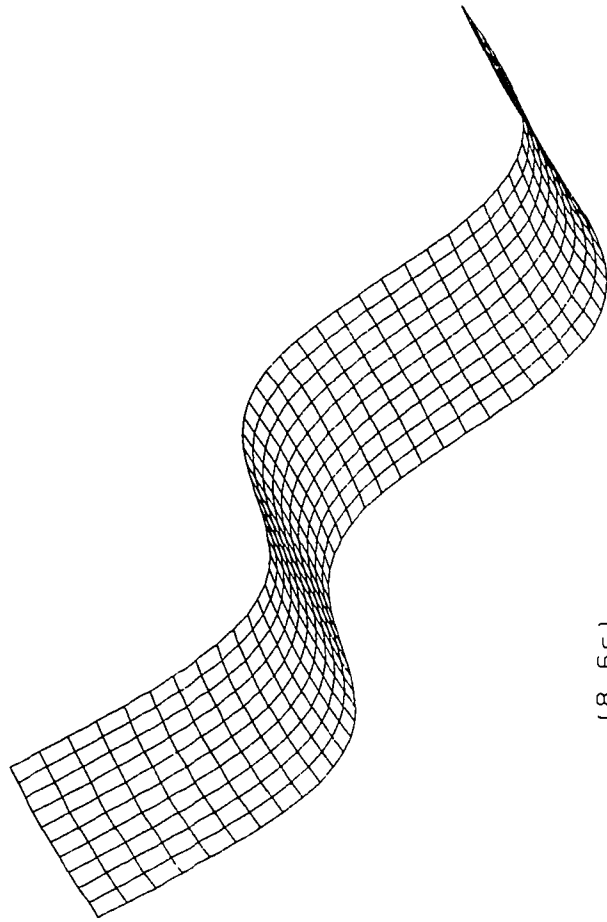
(8.6a)

F_Mode=9 0.695 Hz



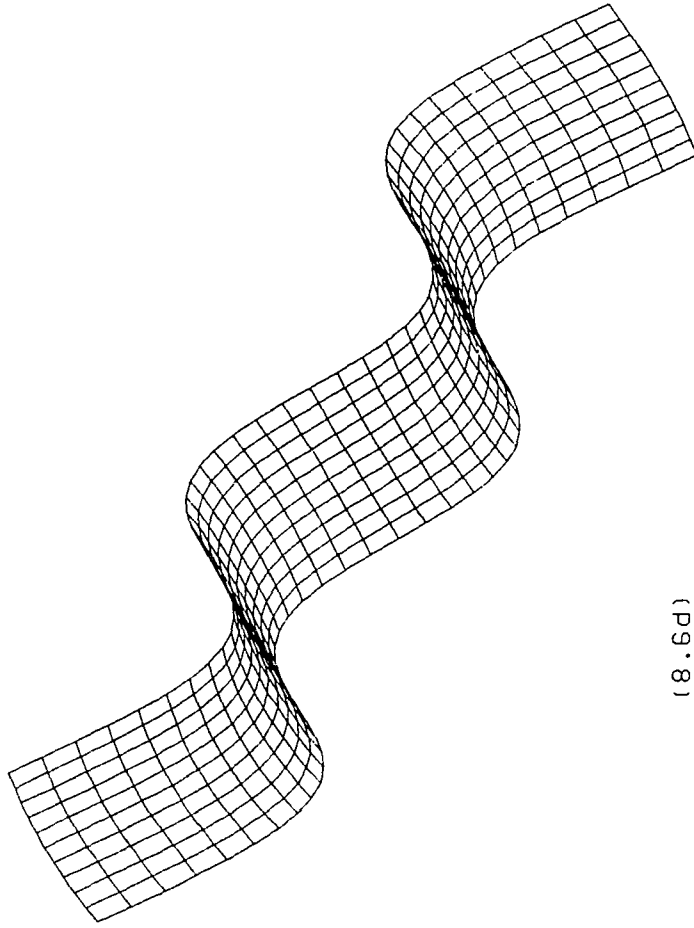
(8.6b)

F_Mode=11 1.37 Hz



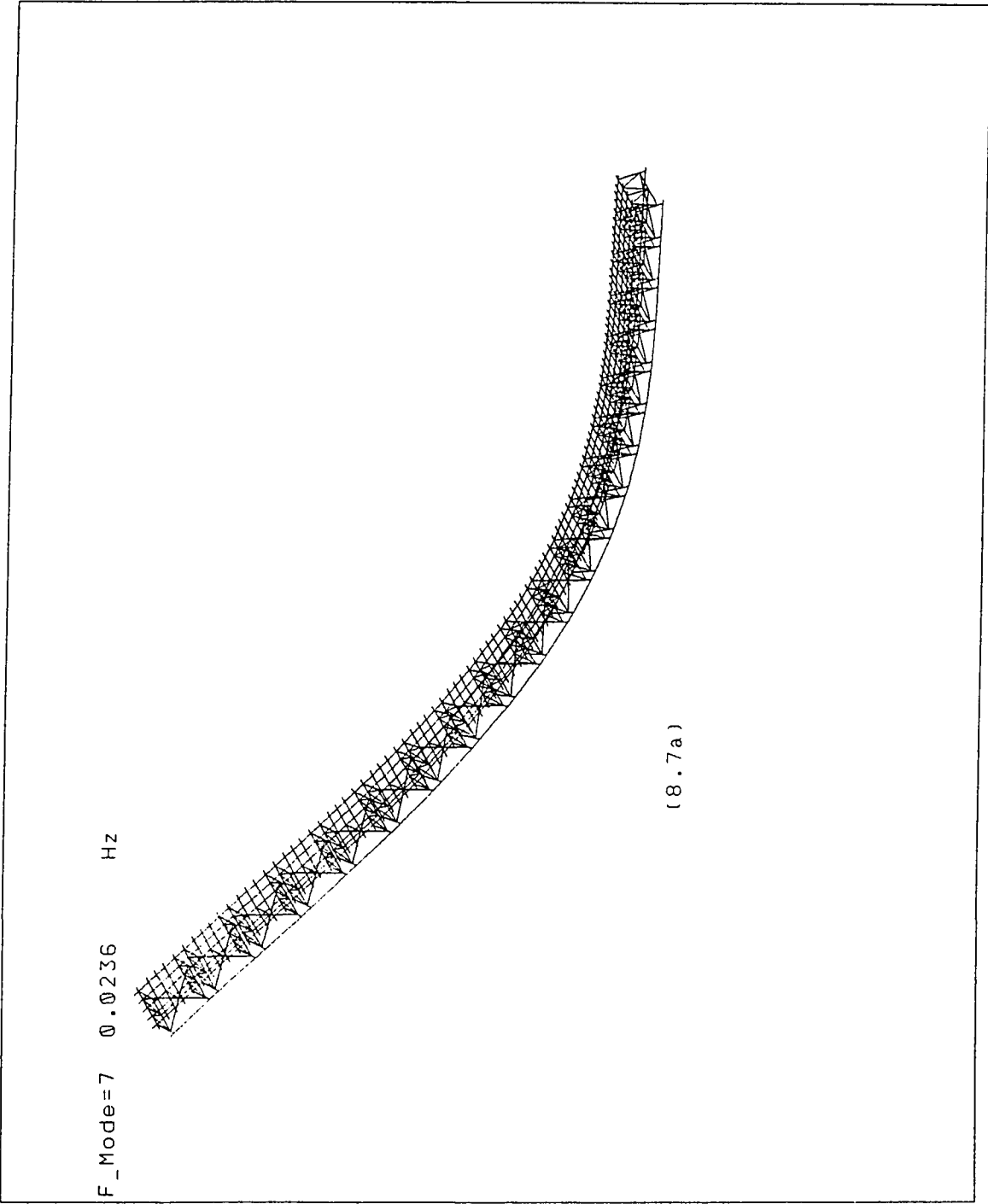
(8.6c)

F_Mode=13 2.26 Hz

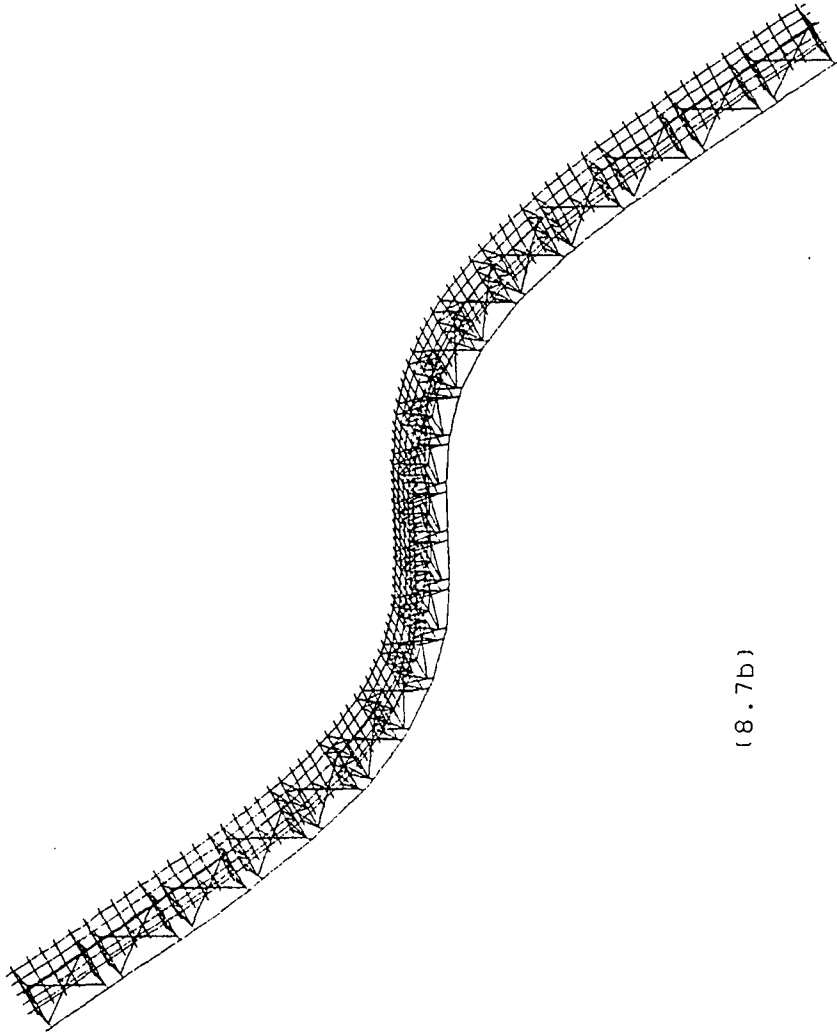


(8.6d)

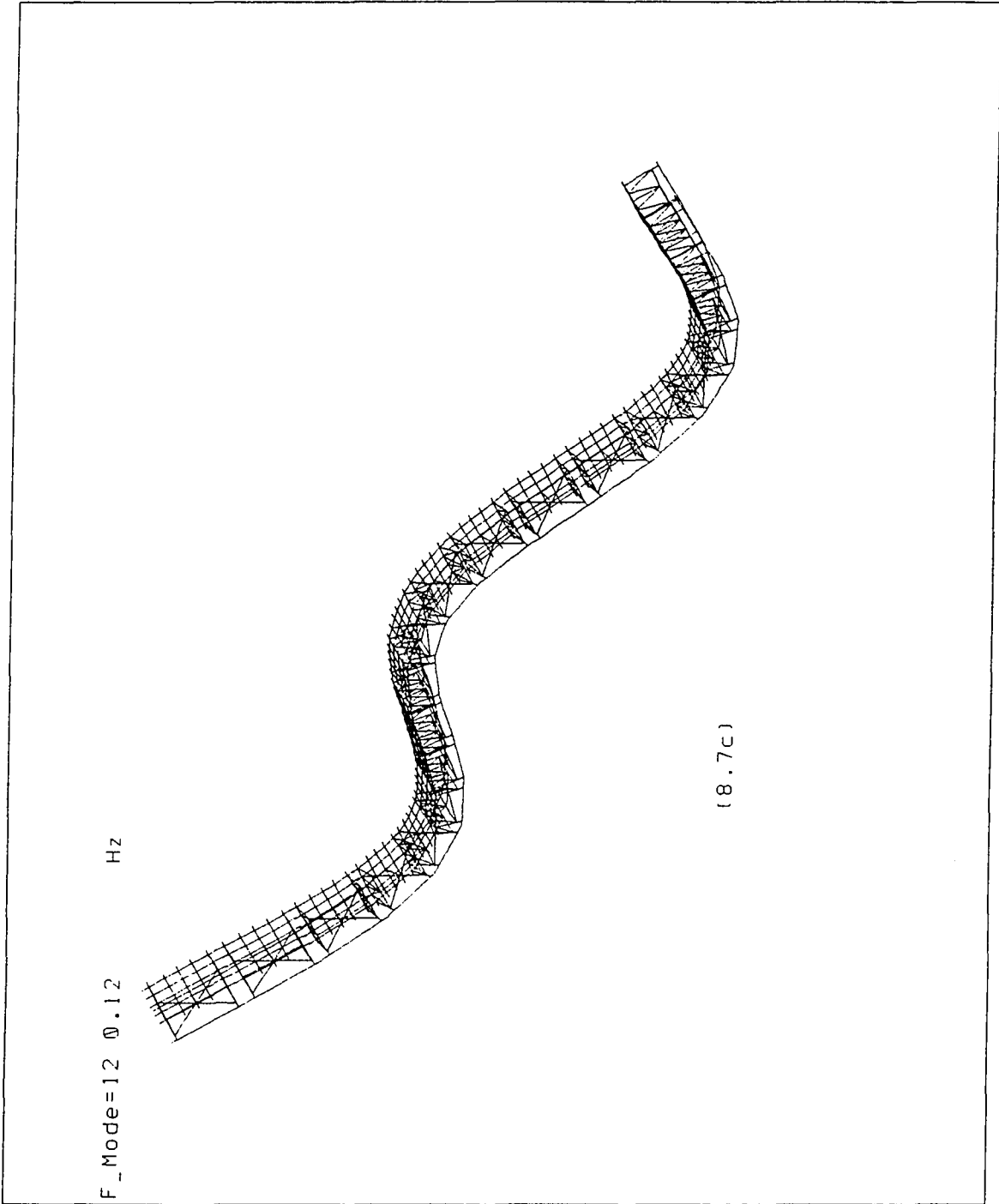
Fig. 8.6 Normal modes of 5-module mat-like VLFS



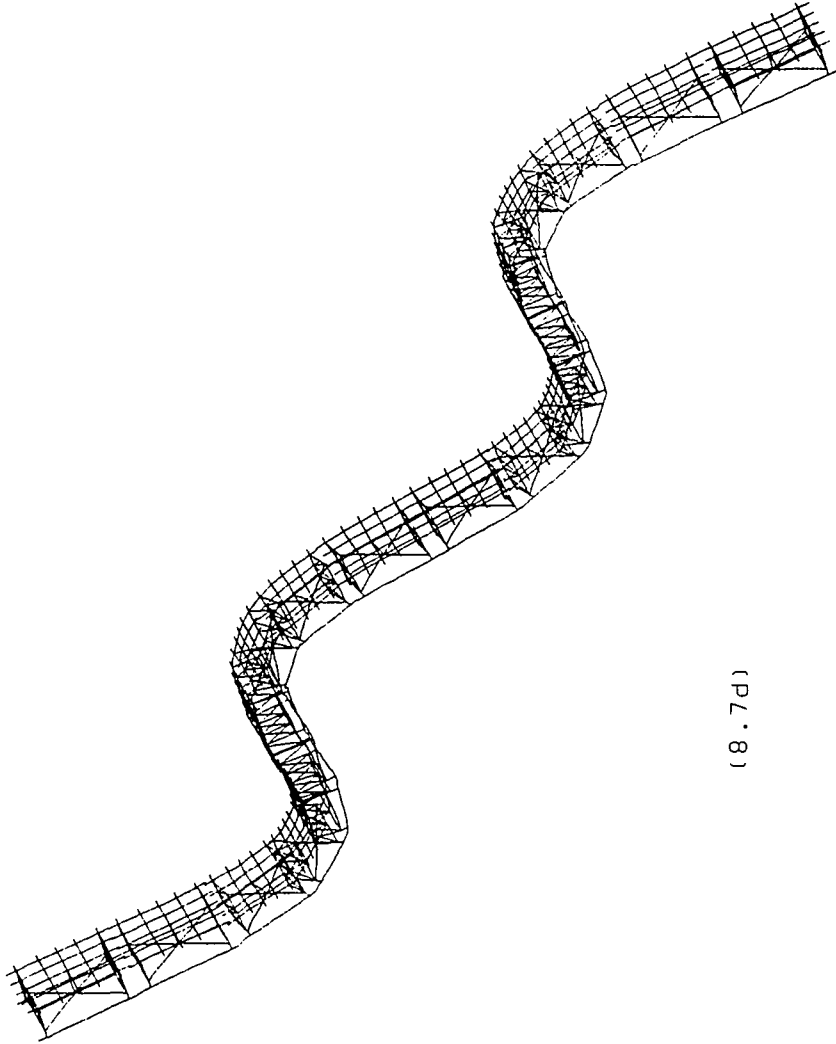
F_Mode=9 0.0636 Hz



(8.7b)

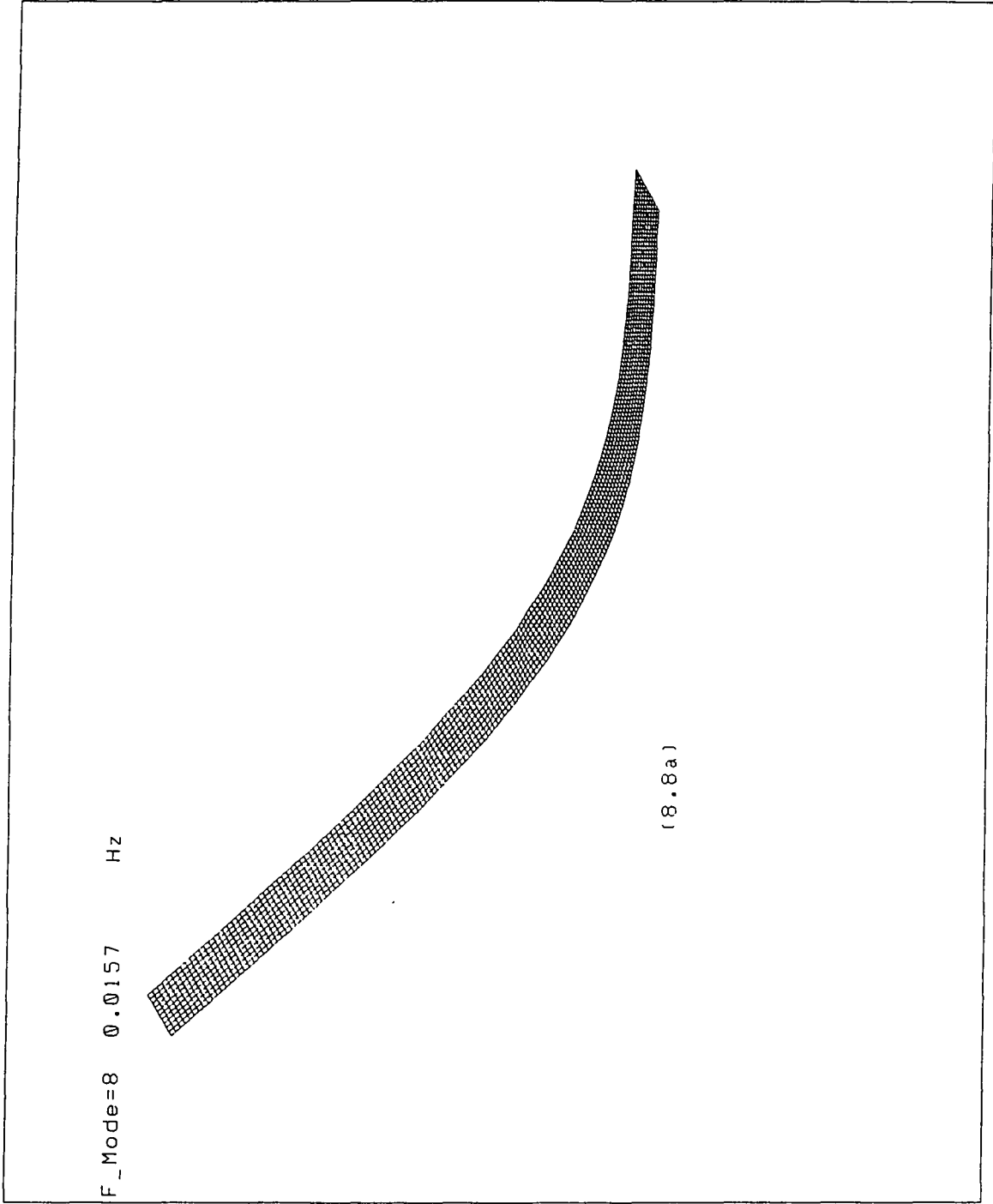


F_Mode=14 0.19 Hz

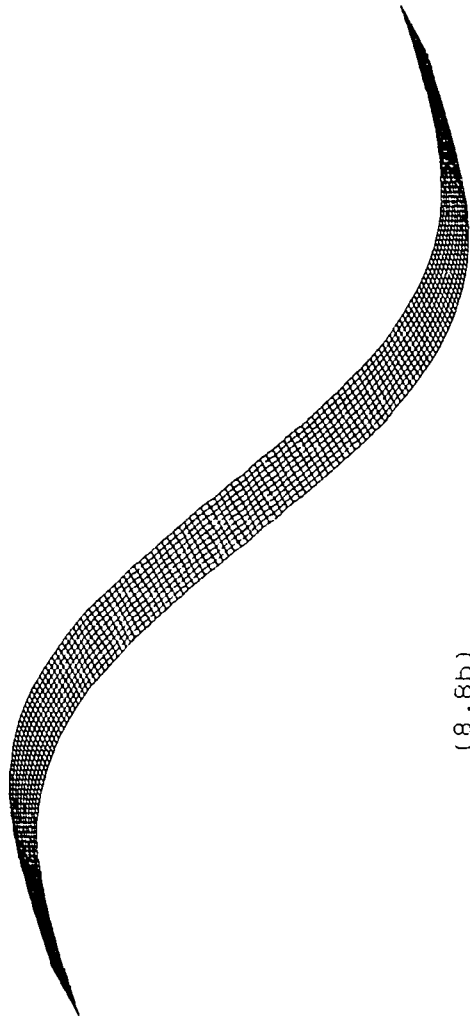


(8.7d)

Fig. 8.7 Normal modes of 20-module semi-submersible

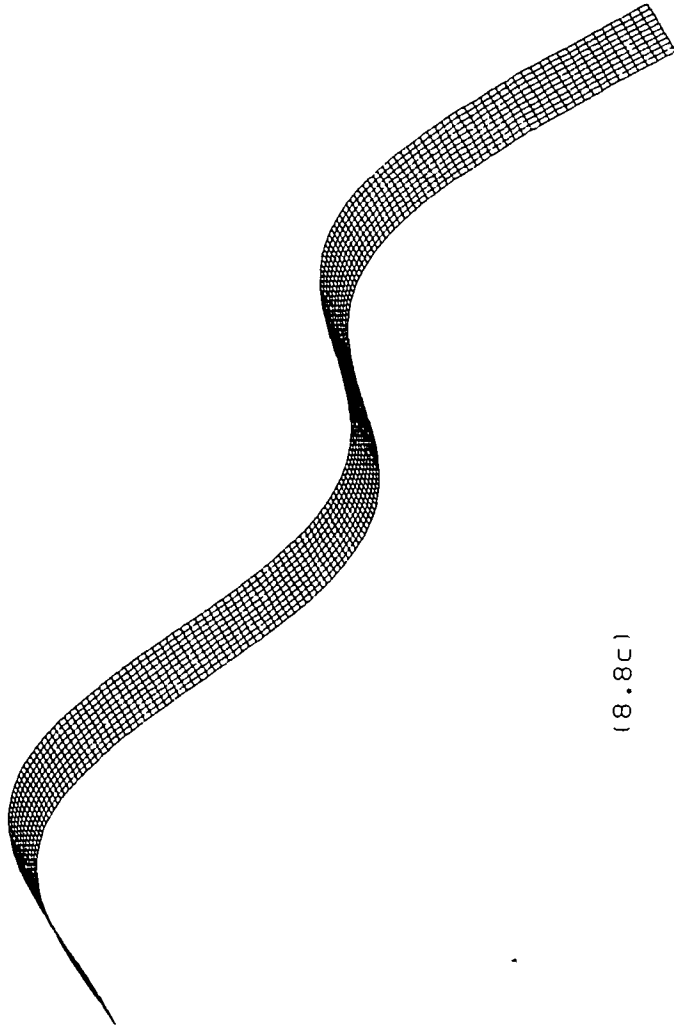


F_Mode=9 0.0433 Hz



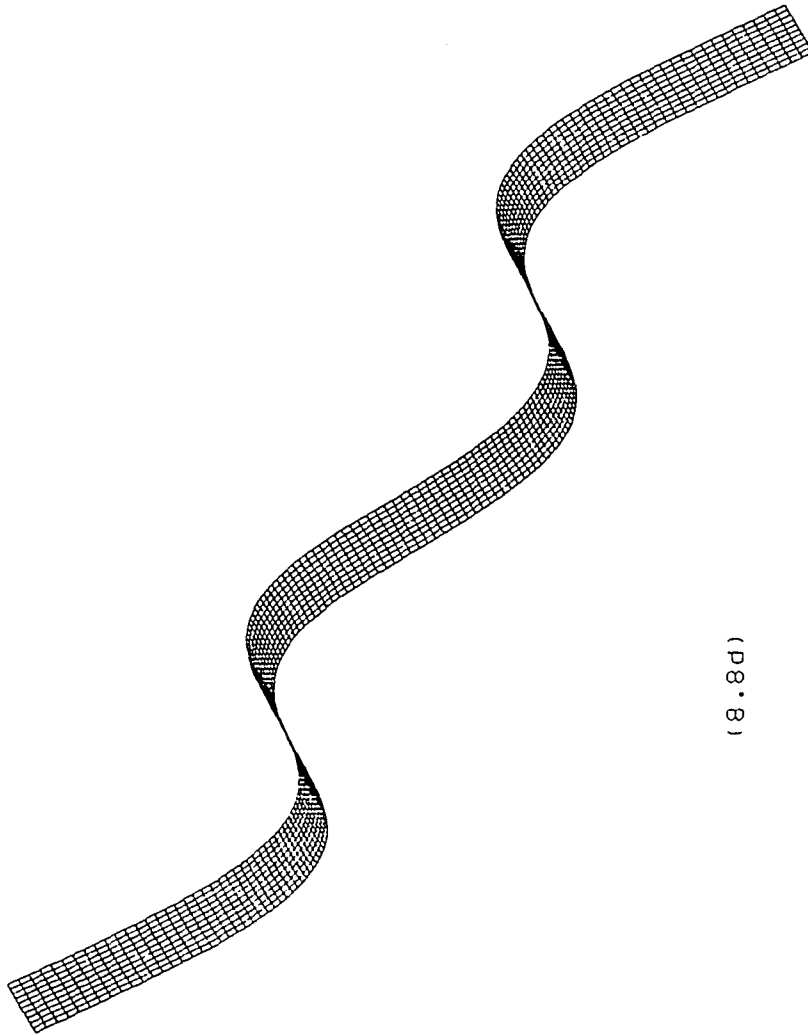
(8.8b)

F_Mode=10 0.085 Hz



(8.8c)

F_Mode=11 0.141 Hz



(8.8d)

Fig. 8.8 Normal modes of 20-module mat-like VLFS

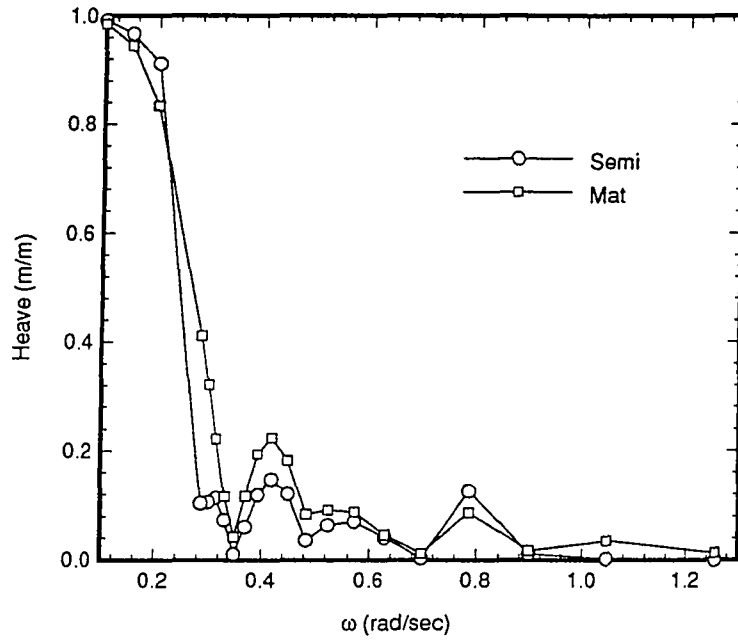


Fig. 8.9 Heave response of 5-module VLFS

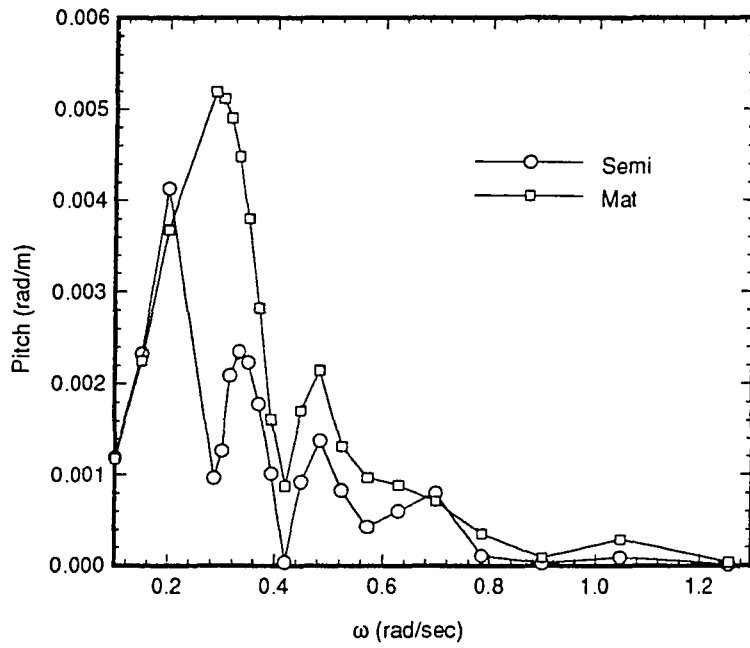


Fig. 8.10 Pitch response of 5-module VLFS

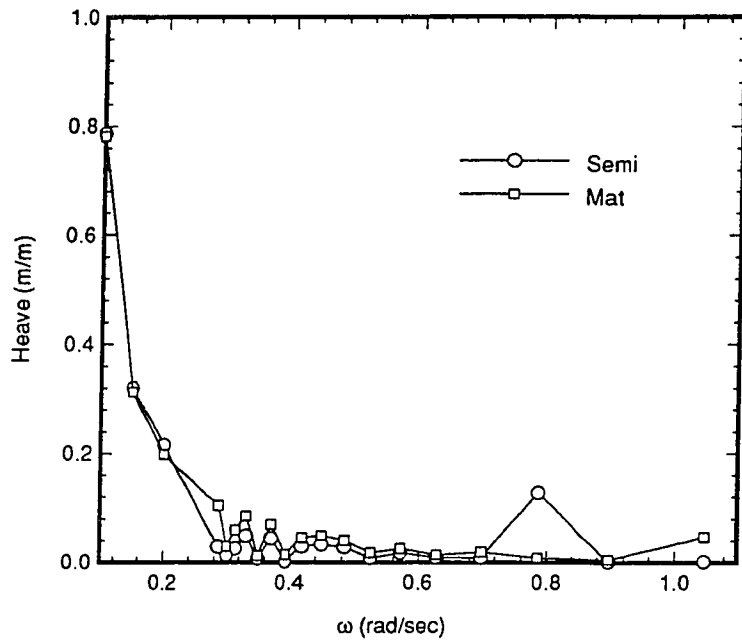


Fig. 8.11 Heave response of 20-module VLFS

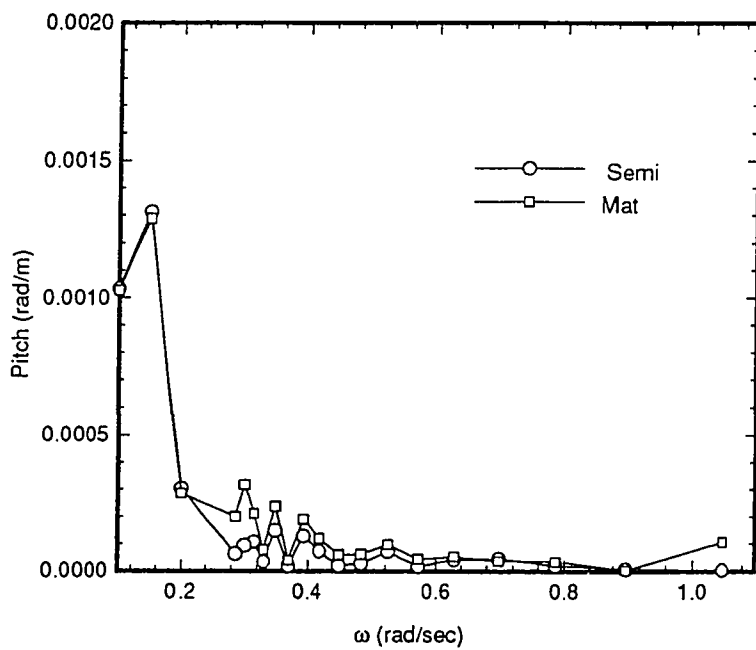
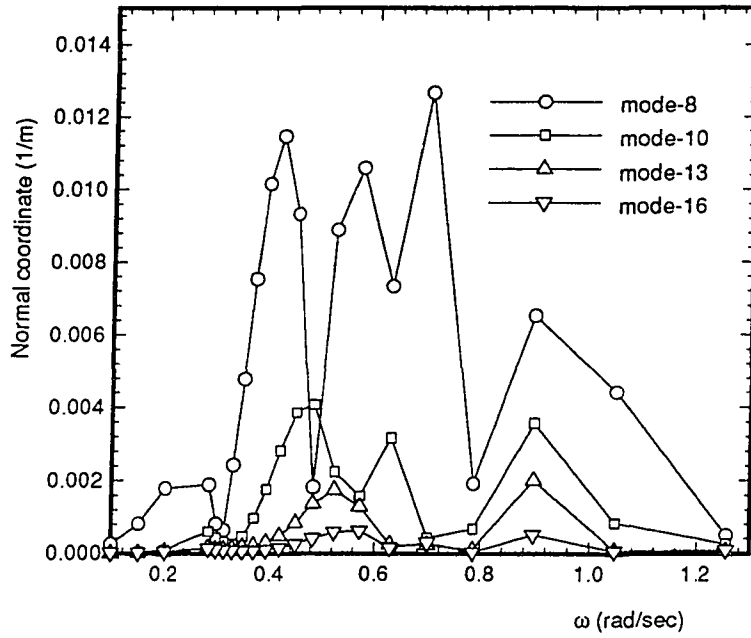
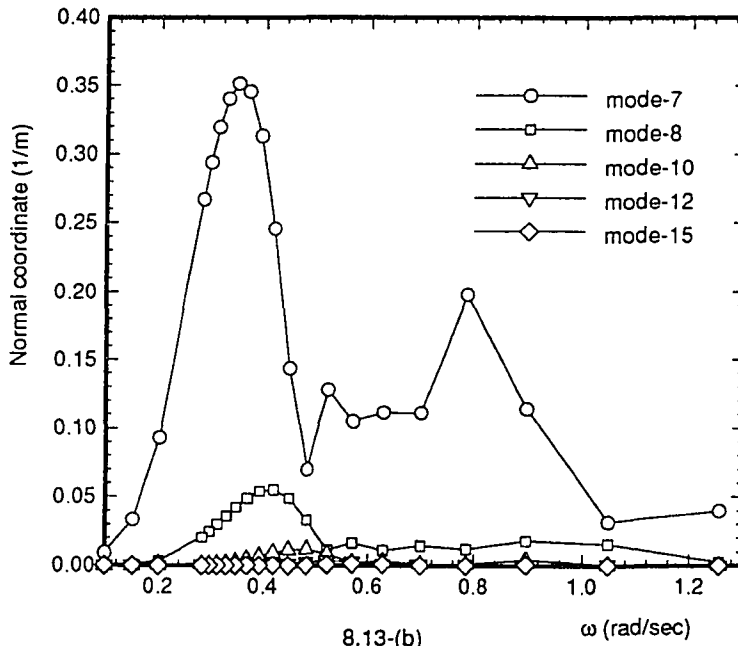


Fig. 8.12 Pitch response of 20-module VLFS



8.13-(a)



8.13-(b)

Fig. 8.13 Normal coordinates of 5-module VLFS, (a)-Semi, (b)-Mat.

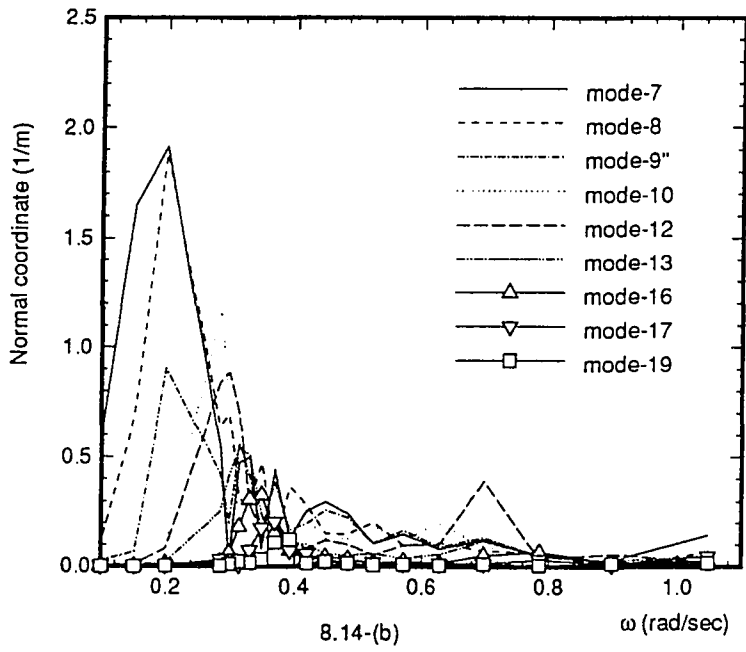
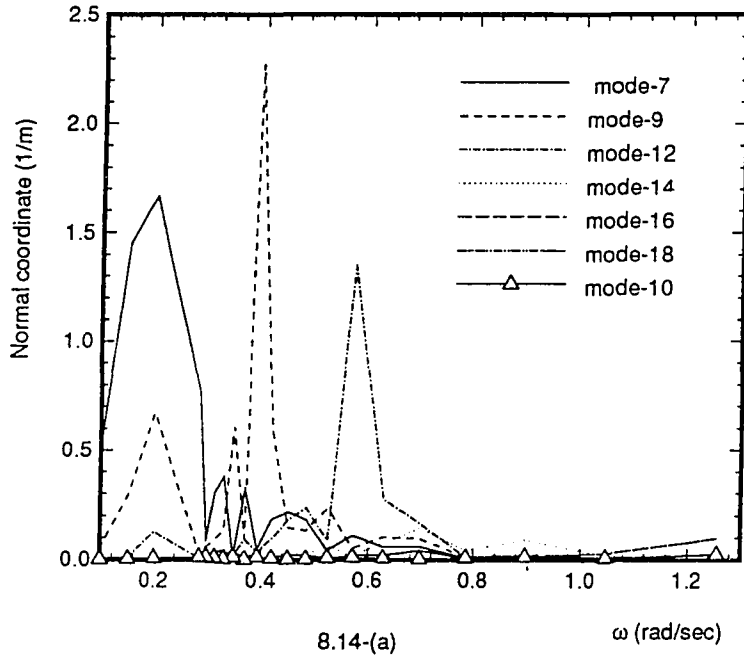


Fig. 8.14 Normal coordinates of 20-module VLFS, (a)-Semi, (b)-Mat.

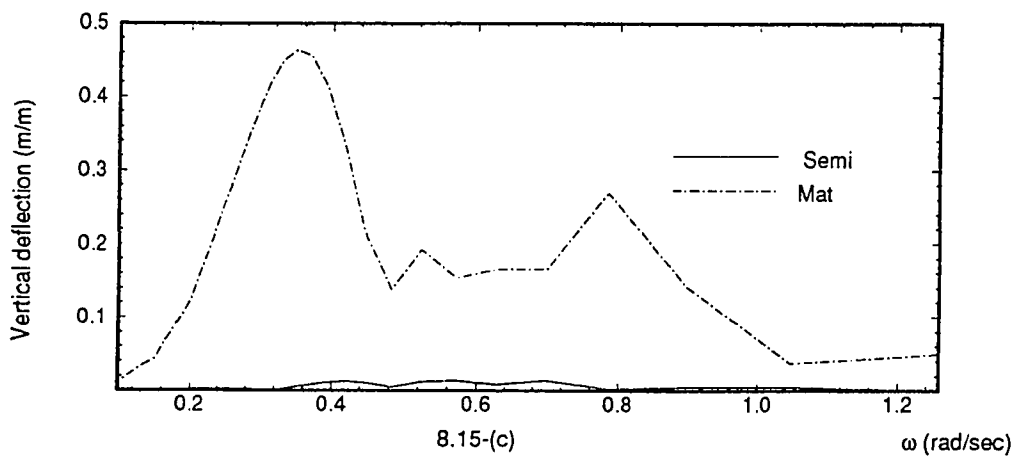
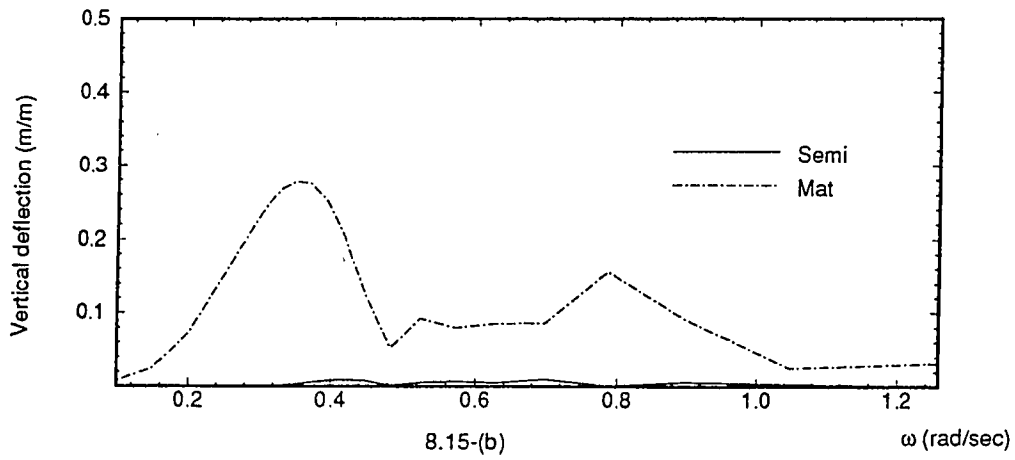
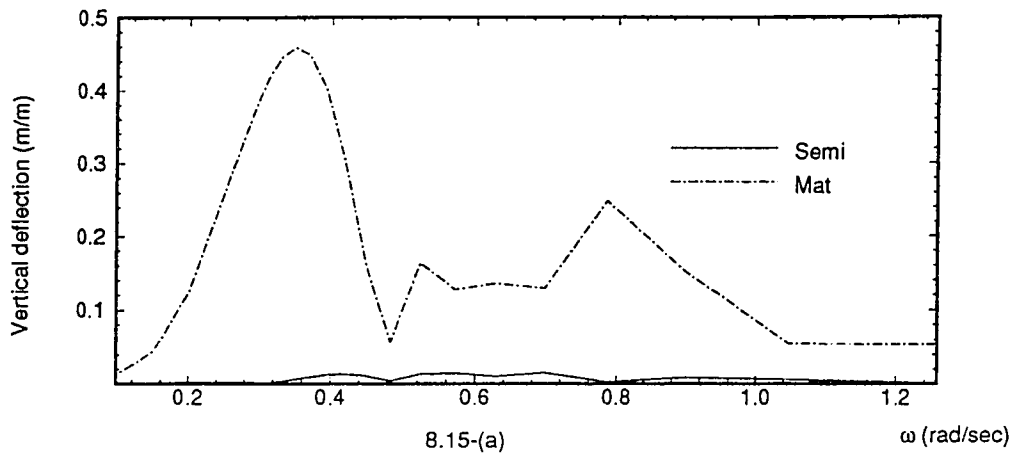


Fig. 8.15 Vertical deflection of 5-module VLFS, (a)-bow, (b)-middle, (c)-stern.

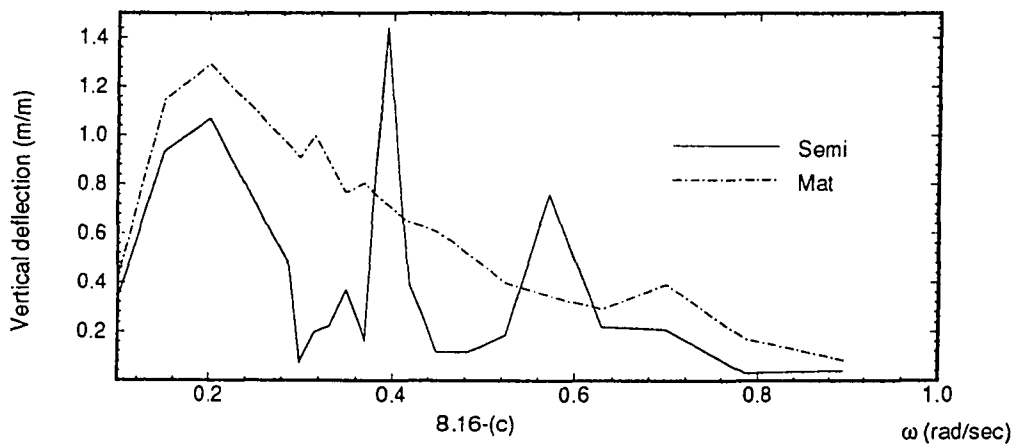
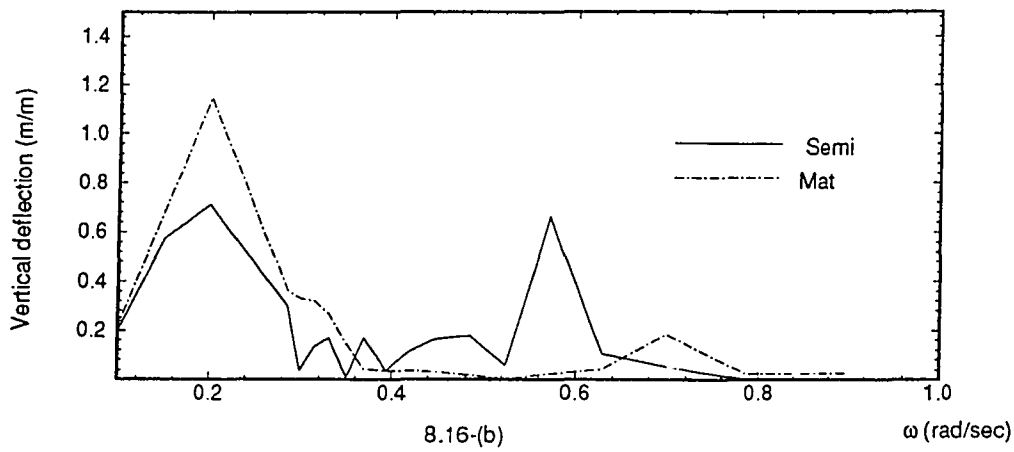
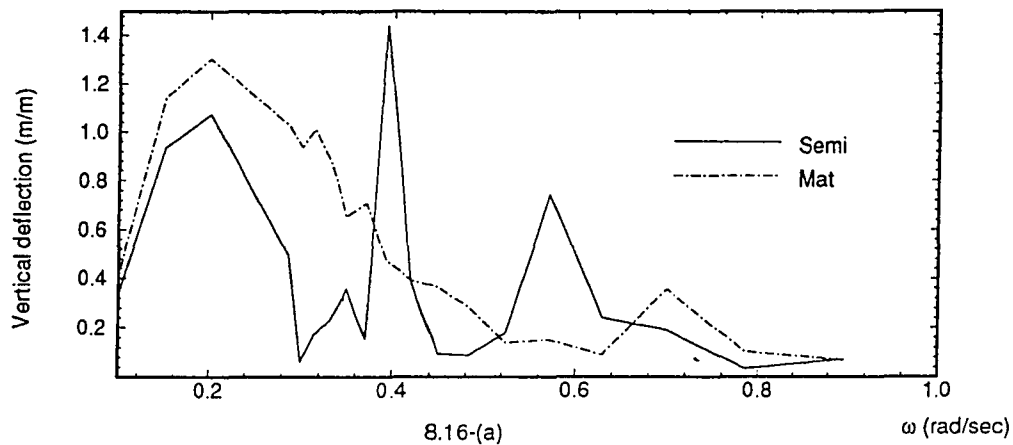


Fig. 8.16 Vertical deflection of 20 module VLFS, (a)-bow, (b)-middle, (c)-stern

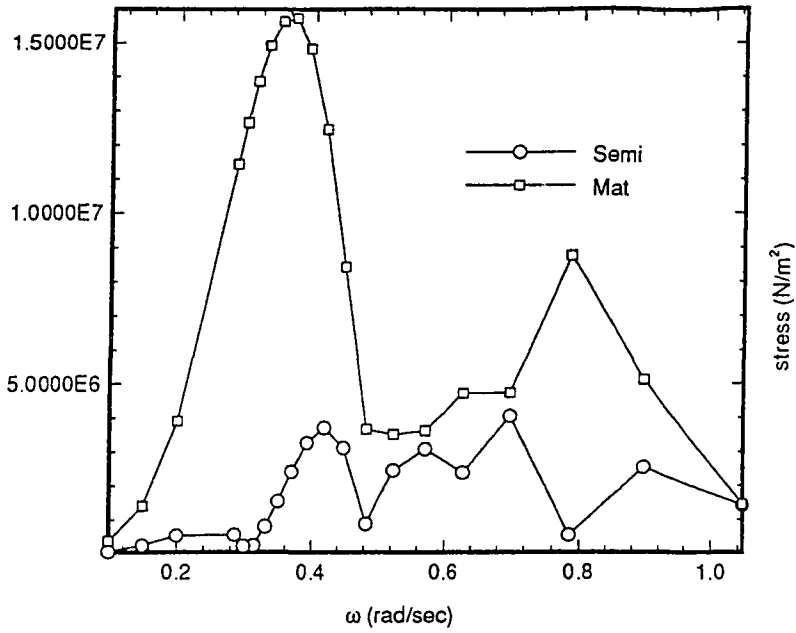


Fig. 8.17 Maximum stresses of 5-module VLFS

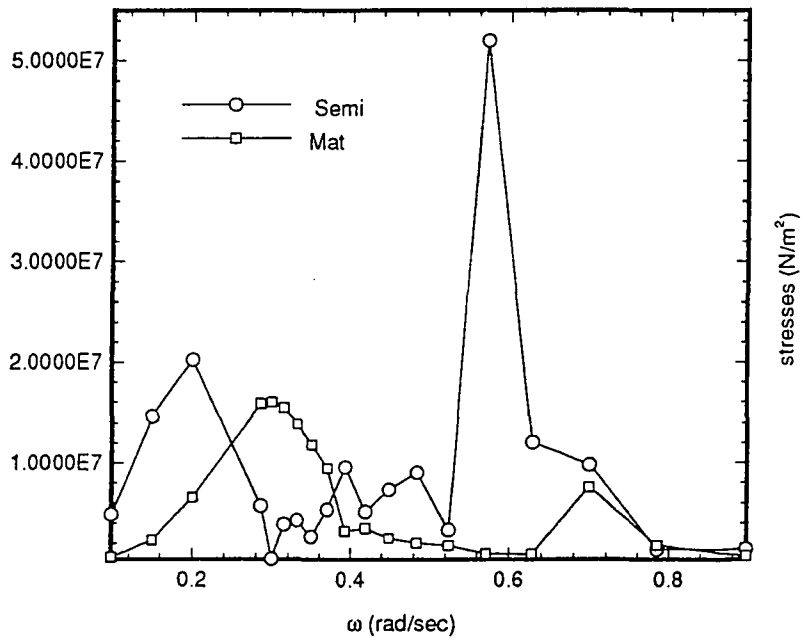


Fig. 8.18 Maximum stresses of 20-module VLFS

APPENDIX A
FRAME AND SHELL ELEMENT

A.1 Two-node frame element

The shape function $[N]$ for a frame element can be written as

$$[N] = [N_{at}] + [N_b] \quad (A.1)$$

where $[N_{at}]$ is a 6×12 matrix of interpolation functions for axial and torsional degrees of freedom:

$$[N_{at}] = \begin{bmatrix} N_1 & 0 & 0 & 0 & 0 & 0 & N_7 & 0 & 0 & 0 & 0 & 0 \\ 0 & 0 & 0 & 0 & 0 & 0 & 0 & 0 & 0 & 0 & 0 & 0 \\ 0 & 0 & 0 & 0 & 0 & 0 & 0 & 0 & 0 & 0 & 0 & 0 \\ 0 & 0 & 0 & N_4 & 0 & 0 & 0 & 0 & 0 & N_{10} & 0 & 0 \\ 0 & 0 & 0 & 0 & 0 & 0 & 0 & 0 & 0 & 0 & 0 & 0 \\ 0 & 0 & 0 & 0 & 0 & 0 & 0 & 0 & 0 & 0 & 0 & 0 \end{bmatrix} \quad (A.2)$$

in which $N_4 = N_1$ and $N_{10} = N_7$. N_1 and N_7 are for axial effects, and are given by

$$N_1 = 1 - \frac{x}{L}; \quad N_7 = \frac{x}{L} \quad (A.3)$$

where L is the beam element length, and x is the local x -coordinate.

N_b is a 6 x 12 matrix of interpolation functions for transverse displacements,

$$[N_b] = \begin{bmatrix} 0 & 0 & 0 & 0 & 0 & 0 & 0 & 0 & 0 & 0 & 0 & 0 \\ 0 & N_2 & 0 & 0 & 0 & N_6 & 0 & N_8 & 0 & 0 & 0 & N_{12} \\ 0 & 0 & N_3 & 0 & N_5 & 0 & 0 & 0 & N_9 & 0 & N_{11} & 0 \\ 0 & 0 & 0 & 0 & 0 & 0 & 0 & 0 & 0 & 0 & 0 & 0 \\ 0 & N_2 & 0 & 0 & 0 & N_6 & 0 & 0 & 0 & 0 & 0 & N_{12} \\ 0 & 0 & N_3 & 0 & N_5 & 0 & 0 & 0 & N_9 & 0 & N_{11} & 0 \end{bmatrix} \quad (A.4)$$

where the components $N_2, N_3, N_5, N_6, N_8, N_9, N_{11}$ and N_{12} are for deflection effects.

They are given

$$N_2 = N_3 = 1 - 3\left(\frac{x}{L}\right)^2 + 2\left(\frac{x}{L}\right)^3 \quad (A.5)$$

$$N_6 = 3\left(\frac{x}{L}\right)^2 - 2\left(\frac{x}{L}\right)^3 \quad N_5 = -N_6 \quad (A.6)$$

$$N_8 = N_9 = x\left(1 - \frac{x}{L}\right)^2 \quad (A.7)$$

$$N_{12} = \frac{x^2}{L}\left(\frac{x}{L} - 1\right) \quad N_{11} = -N_{12} \quad (A.8)$$

A.2 Four-node shell element

Many offshore structures are of tubular construction having a large volume of wetted surface to provide the required buoyancy. To model such structures, the use of thin shell or plate elements is very useful, especially when a three-dimensional

analysis is to be carried out. Such an element is shown in Fig. A.1, where (x, y, z) is the global coordinate system and the local coordinate system is denoted by $(\bar{x}, \bar{y}, \bar{z})$.

The quadrilateral thin shell element used here has the capability to resist both membrane and bending loads. At each of the four nodes of the element, there are six degree of freedom, three translational and three rotational (see Fig. A.2). The 24×1 vector of element nodal displacements, $\{d\}$, can be represented in the local coordinate system by:

$$\{d\} = \{u_1, v_1, w_1, \theta_{x1}, \theta_{y1}, \theta_{z1}, u_2, v_2, \dots, u_4, v_4, w_4, \theta_{x4}, \theta_{y4}, \theta_{z4}\}^T, \quad (A.9)$$

where $u_i, v_i, i = 1, 2, 3, 4$ refer to the in-plane displacements, and $w_i, \theta_{xi}, \theta_{yi}$ $i = 1, 2, 3, 4$ refer to the transverse displacements. The displacement field within the element, $\{u\}$, is interpolated from the nodal displacements by

$$\{d\} = [N]\{u\}, \quad (A.10)$$

where $[N]$ is a 3×24 matrix of interpolation functions. The natural and Cartesian coordinates are related through the interpolation functions as (Che, 1993):

where (\bar{x}_i, \bar{y}_i) are the local coordinates of the i -th node, $i = 1, 2, 3, 4$, and the interpolation functions are defined as:

$$N_i = \frac{1}{4}(1 + \xi \xi_i)(1 + \eta \eta_i), \quad i = 1, 2, 3, 4. \quad (A.12)$$

(ξ_i, η_i) , $i = 1, 2, 3, 4$ are the natural coordinates of the 4 nodes of the element given by:

$$\begin{bmatrix} \bar{x} \\ \bar{y} \end{bmatrix} = \begin{bmatrix} N_1 & 0 & N_2 & 0 & N_3 & 0 & N_4 & 0 \\ 0 & N_1 & 0 & N_2 & 0 & N_3 & 0 & N_4 \end{bmatrix} \begin{bmatrix} \bar{x}_1 \\ \bar{y}_1 \\ \bar{x}_2 \\ \bar{y}_2 \\ \bar{x}_3 \\ \bar{y}_3 \\ \bar{x}_4 \\ \bar{y}_4 \end{bmatrix}, \quad (\text{A.11})$$

$$\begin{aligned} (\xi_1, \eta_1) &= (-1, -1), & (\xi_2, \eta_2) &= (1, -1), \\ (\xi_3, \eta_3) &= (1, 1), & (\xi_4, \eta_4) &= (-1, 1). \end{aligned} \quad (\text{A.13})$$

There are a number of formulations available for the bending displacements, which can be interpolated from the nodal vertical displacements and rotations (Cook et al., 1989; Rao, 1989). Hence, the total displacement field can now be written as

$$\{\mathbf{d}\} = \begin{Bmatrix} \mathbf{u} \\ \mathbf{v} \\ \mathbf{w} \end{Bmatrix} = [\mathbf{N}]\{\mathbf{u}\}, \quad (\text{A.14})$$

where the 3 x 24 matrix of the interpolation functions is given by (Che, 1993):

$$[\mathbf{N}] = \begin{bmatrix} N_1 & 0 & 0 & 0 & 0 & 0 & N_2 & 0 & 0 & 0 & 0 & 0 \\ 0 & N_1 & 0 & 0 & 0 & 0 & 0 & N_2 & 0 & 0 & 0 & 0 \\ 0 & 0 & N_{11} & N_{12} & N_{13} & 0 & 0 & 0 & N_{21} & N_{22} & N_{23} & 0 \\ N_3 & 0 & 0 & 0 & 0 & 0 & N_4 & 0 & 0 & 0 & 0 & 0 \\ 0 & N_3 & 0 & 0 & 0 & 0 & 0 & N_4 & 0 & 0 & 0 & 0 \\ 0 & 0 & N_{31} & N_{32} & N_{33} & 0 & 0 & 0 & N_{41} & N_{42} & N_{43} & 0 \end{bmatrix}, \quad (\text{A.15})$$

where N_1, N_2, N_3, N_4 have been defined before and the other interpolation functions are given as:

$$\begin{aligned}
 N_{11} &= -\frac{1}{8}(-1+\xi)(-1+\eta)(-2+\xi+\xi^2+\eta+\eta^2) \\
 N_{21} &= \frac{1}{8}(1+\xi)(-1+\eta)(-2-\xi+\xi^2+\eta+\eta^2) \\
 N_{31} &= -\frac{1}{8}(1+\xi)(1+\eta)(-2-\xi+\xi^2-\eta+\eta^2) \\
 N_{41} &= \frac{1}{8}(-1+\xi)(1+\eta)(-2+\xi+\xi^2-\eta+\eta^2)
 \end{aligned} \tag{A.16}$$

$$\begin{aligned}
 N_{12} &= -\frac{1}{8}(-1+\xi)^2(1+\xi)(-1+\eta) \\
 N_{22} &= -\frac{1}{8}(-1+\xi)(-1+\xi)^2(-1+\eta) \\
 N_{32} &= \frac{1}{8}(-1+\xi)(1+\xi)^2(1+\eta) \\
 N_{42} &= \frac{1}{8}(-1+\xi)^2(1+\xi)(1+\eta)
 \end{aligned} \tag{A.17}$$

$$\begin{aligned}
 N_{13} &= -\frac{1}{8}(-1+\xi)(-1+\eta)^2(1+\eta) \\
 N_{23} &= \frac{1}{8}(1+\xi)(-1+\eta)^2(1+\eta) \\
 N_{33} &= \frac{1}{8}(1+\xi)(-1+\eta)(1+\eta)^2 \\
 N_{43} &= -\frac{1}{8}(-1+\xi)(-1+\eta)(1+\eta)^2
 \end{aligned} \tag{A.18}$$

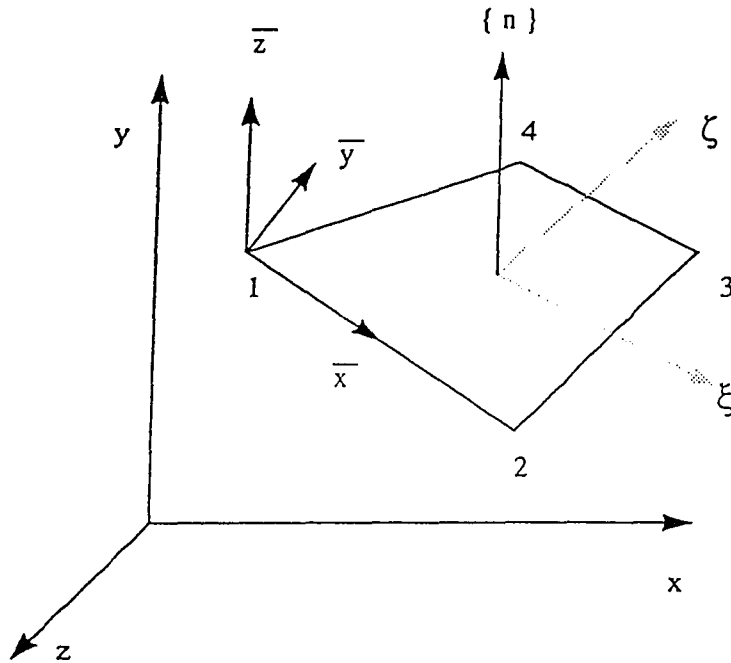


Fig. A.1 Global, local and natural coordinate system for a quadrilateral shell element

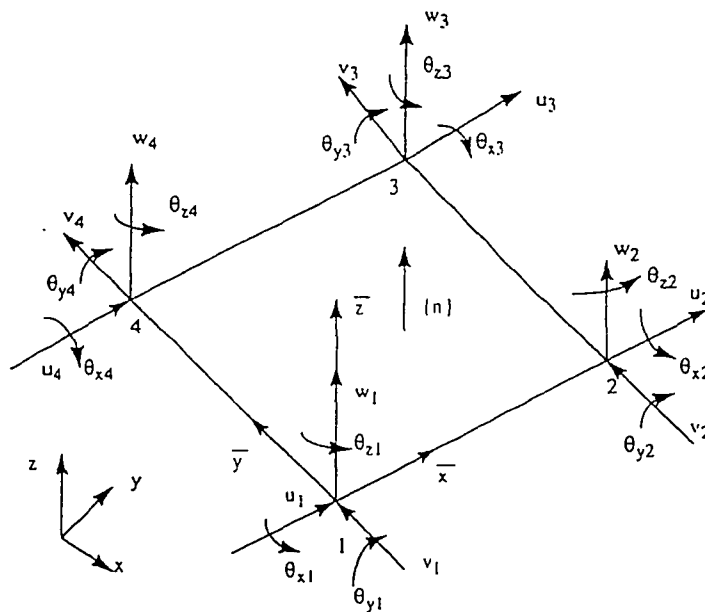


Fig. A.2 Quadrilateral thin shell element

APPENDIX B

CALCULATION OF PANEL NORMALS

Four-node quadrilateral panels are used to discretize the geometry of the structural wetted surface. The nodes, on each panel, are described in a clockwise fashion, as seen from the fluid domain, looking into the structure. This convention is used so that the normal in the subsequent formulation is directed into the structure and out of the fluid.

If (x_i, y_i, z_i) , $i = 1, 2, 3, 4$ are the coordinates of the four corners of the fluid panel, given in the global coordinate system, then a vector from node i to node j , $\{r_{ij}\}$ can be represented by:

$$\{r_{ij}\} = \{(x_j - x_i), (y_j - y_i), (z_j - z_i)\}^T, \quad i \neq j, \quad i, j = 1, 2, 3, 4. \quad (\text{B.1})$$

The normal to the fluid panel, $\{n\} \equiv n_x \hat{i} + n_y \hat{j} + n_z \hat{k}$, assumed to be directed into the body, can be written as:

$$\{n\} = \frac{\{r_{13}\} \times \{r_{24}\}}{\|\{r_{13}\} \times \{r_{24}\}\|}. \quad (\text{B.2})$$

The arithmetic mean position of the fluid panel is

$$\{r_o\} = \frac{1}{4}(\{r_1\} + \{r_2\} + \{r_3\} + \{r_4\}). \quad (\text{B.3})$$

In the above equation, $\{r_i\}$, $i = 1, 2, 3, 4$, is the position vector of the corresponding corner of the fluid panel. The area of the panel can be calculated as

the sum of the areas of the two triangles formed by a diagonal of the panel. The area of the triangle formed from the corners 1, 2 and 4 is:

$$A_{124} = \sqrt{s(s-s_{12})(s-s_{24})(s-s_{14})} , \quad (\text{B.4})$$

where

$$\begin{aligned} s_{12} &= |\{\mathbf{r}_2\} - \{\mathbf{r}_1\}| , \\ s_{24} &= |\{\mathbf{r}_4\} - \{\mathbf{r}_2\}| , \\ s_{14} &= |\{\mathbf{r}_4\} - \{\mathbf{r}_1\}| , \\ s &= \frac{1}{2}(s_{12} + s_{24} + s_{14}) . \end{aligned} \quad (\text{B.5})$$

The centroidal location for the triangle is given as the arithmetic mean of the corner points, namely:

$$\{\mathbf{r}_{c124}\} = \frac{1}{3}(\{\mathbf{r}_1\} + \{\mathbf{r}_2\} + \{\mathbf{r}_4\}) . \quad (\text{B.6})$$

The area and the centroidal location for the other triangle, formed from corners 2, 3 and 4 can be similarly evaluated. The total area for the panel, A_n , and its centroidal location, $\{\mathbf{r}_c\} \equiv (x_c, y_c, z_c)$, is then given by:

$$\begin{aligned} A_n &= A_{124} + A_{234} , \\ \{\mathbf{r}_c\} &= \frac{(\{\mathbf{r}_{c124}\}A_{124} + \{\mathbf{r}_{c234}\}A_{234})}{(A_{124} + A_{234})} . \end{aligned} \quad (\text{B.7})$$

APPENDIX C
HYDROSTATIC RESTORING COEFFICIENTS OF
RIGID BODY MODES

By using the rigid body modes defined by Eq. (2.31), the restoring coefficients have the following form:

$$\mathbf{K}_{fjk}^* = \begin{bmatrix} 0 & 0 & 0 & 0 & 0 & 0 \\ 0 & 0 & 0 & 0 & 0 & 0 \\ 0 & 0 & \rho g S_w & \rho g S_2 & -\rho g S_1 & 0 \\ 0 & 0 & \rho g S_2 & \rho g [S_{22} + \nabla(z'_B - z'_G)] & -\rho g S_{12} & 0 \\ 0 & 0 & -\rho g S_1 & -\rho g S_{12} & \rho g [S_{11} + \nabla(z'_B - z'_G)] & 0 \\ 0 & 0 & 0 & 0 & 0 & 0 \end{bmatrix}, \quad (\text{C.1})$$

where

$$S_j = \iint_{S_w} x'_j dx' dy', \quad S_{jk} = \iint_{S_w} x'_j x'_k dx' dy', \quad (\text{C.2})$$

$$\mathbf{x}' = (x', y', z') = (x'_1, x'_2, x'_3), \quad j, k = 1, 2, 3,$$

and (x'_B, y'_B, z'_B) , (x'_G, y'_G, z'_G) are the coordinates of the center of buoyancy

and the center of gravity respectively, in the body fixed coordinate system. It can be seen that:

$$\frac{1}{\nabla} S_{22} + (z'_B - z'_G) = \overline{GM}_T \quad (\text{C.3})$$

and

$$\frac{1}{\nabla} S_{11} + (z'_B - z'_G) = \overline{GM}_L. \quad (\text{C.4})$$

REFERENCES

- Abramowitz, M. and Stegun, I. A. (1964). *Handbook of mathematical functions*. National Bureau of Standards, Washington, D.C.
- Baschieri, M. and Bellincioni, P. (1991). "Prestressed concrete floating airport." *Proceedings, First International Workshop on Very Large Floating Structures*, University of Hawaii, Honolulu, 421-436.
- Bathe, K. J. and Wilson, E. L. (1976). *Numerical methods in finite element analysis*. Prentice-Hall, Inc., Englewood Cliffs, New Jersey, 528 pp.
- Betts, C. V., Bishop, R. E. D. and Price, W. G. (1977). "The symmetric generalized fluid forces applied to a ship in a seaway." *Trans. RINA*, Vol. 119, 265-278.
- Bishop, R. E. D. (1971). "On the strength of large ships in heavy seas." *South African Mechanical Engineer*, Vol. 126, 153-166.
- Bishop, R. E. D. and Taylor, R. (1973). "On wave-induced stress in a ship executing symmetric motions." *Phil. Trans. Royal Soc., London*, A257, 1-32.
- Bishop, R. E. D. and Price, W. G. (1974). "On modal analysis of ship strength." *Proc. Royal Soc., London*, A342, 121-134.
- Bishop, R. E. D. and Price, W. G. (1976). "On the relationship between 'dry modes' and 'wet modes' in the theory of ship response." *Journal of Sound and Vibration*, 45, No. 2, 157-164.
- Bishop, R. E. D., Price, W. G. and Tam, P. K. Y. (1977). "A unified dynamic analysis of ship response to waves." *Trans. RINA*, Vol. 119, 363-390.

- Bishop, R. E. D. and Price, W. G. (1979). *Hydroelasticity of Ships*. Cambridge University Press, Cambridge, U.K.
- Blagoveshchensky, S. N. (1962). *Theory of ship motion*, Dover Publications Co., New York.
- Brahtz, J. F. P. (1989). "Modularized ocean basing system: A United States option in a strategy of discriminate deterrence (circa 2000)." Rep. No. TR928, Naval Civil Engrg. Lab., Port Heuneme, California, Nov.
- Bretz, G. (1988). "Development of deployable ports may prove vital to U. S. Navy." *Sea Technology*, Sept., p. 12.
- Bryndum, M. B., Bonde C., Tura, F. and Monseti, M. (1989). "Long free spans exposed to current and waves: model tests." *Proc Offshore Technology Conference*, 1-4 May, Houston, Texas, No. 6153, 317-336.
- Burke, B. G. (1969). "The analysis of semi-submersible drilling vessels in waves." *Proc. 1st Int. Offshore Tech. Conf.*, Houston, May, I-235 to I-241.
- Chang, M. S. (1977). "Computations of three-dimensional forces on a body moving beneath a free surface." *Proc. 2nd Int. Conf. on Num. Ship Hydrodynamics*, 124-135.
- Che, X. L., Wang, D. Y., Wang, M. L. and Xu, Y. F. (1992). "Two-dimensional hydroelastic analysis of very large floating structures." *Marine Technology*, 29, 1, Jan., 13-24.
- Che, X. L. (1993). *Techniques for Hydroelastic analysis of very large floating structures*. Ph.D. Dissertation, University of Hawaii at Manoa, Honolulu.

- Che, X. L., Riggs, H. R. and Ertekin, R. C. (1994). "Composite 2D/3D hydroelastic analysis method for floating structures." *Journal of Engineering Mechanics*, Transactions of ASCE, **120**, No. 7, July, 1499-1520.
- Chen, L. H. and Pierucci, M (1977). "Underwater fluid-structure interaction. Part I: Introduction and scope; Part II: Mechanically-applied forces; Part III: Acoustically-applied forces." *Shock and Vibration Digest*, Vol. 9, No. 8, 36, Vol. 9, No. 8, 41.
- Chitrapu, A. S., Ertekin, R. C. and Paulling, J. R. (1993). "Viscous drift forces in regular and irregular waves." *Ocean Engineering*, Vol. 20, No. 1, 33-55.
- Chitrapu, A. S. and Ertekin, R. C. (1995). "Time-domain simulation of large-amplitude response of floating platforms." *Ocean Engineering*, Vol. 22, No.4, 367-386.
- Clough, R. W. and Penzien, J. (1975). *Dynamics of Structures*, McGraw-Hill, 634 pp.
- Cook, R. D., Malkus, D. S. and Flesha, M. E. (1989). *Concepts and applications of finite element analysis*. John Wiley & Sons Inc., New York, 630pp.
- Dean, R. G. and Dalrymple, R. A. (1984). *Water wave mechanics for engineers and scientists*."
- Du, S. X. and Ertekin, R. C. (1991). "Dynamic response analysis of a flexibly joined, multi-module Very Large Floating Structure." *Proc. of the Oceans '91 Conference*, IEEE, Honolulu, October, Vol. 3, 1286-1293.

- Ertekin, R. C., Riggs, H. R., Seidl, L. H. and Wu, Y. S. (1990). The design and analysis of very large floating structures (VLFS): Vol. 2 - Analysis. Rep. No. UHMOE-90106, Dept. of Ocean Engrg., Univ. of Hawaii at Manoa, June.
- Ertekin, R. C., Wang, M. L. and Riggs, H. R. (1991). "Response of flexible floating structure modules in regular and irregular waves." *Proc. of the Int. Symp. on Marine Structures*, ISMS 1991 (ISSC '91 Pre-Congress Symp.), Ed. Xinsen Lu, Sept. Shanghai, 75-80.
- Ertekin, R. C., Riggs, H. R., Che, X. L. and Du, S. X. (1993). "Efficient methods for hydroelastic analysis of very large floating structures." *Journal of Ship Research*, 37, 1, March, 58-76.
- Ertekin, R. C. (1994). "Current and future directions in Very Large Floating Structure research and development." *Proc. Intl. Symp. Techno-Ocean 94*, Oct, 26-29, Kobe, Japan, 23-29.
- Ertekin, R. C., Wang, S. Q. and Riggs, H. R. (1994). "Hydroelastic response of a floating runway." *Proc. of the Intl. Conf. on Hydroelasticity in Marine Technology*, Eds. Faltinsen et al., May 25-27, Trondheim, Norway, 389-400.
- Ertekin, R. C., Wang, S. Q., Che, X. L. and Riggs, H. R. (1995). "On the application of the Haskind-Hanaoka relations to hydroelasticity problems." To appear in *Marine Structures*.
- Faltinsen, O. M. and Michelsen, F. C. (1974). "Motions of large structures in waves at zero Froude number." *Intl. Symp. on Dynamics of Marine Vehicles and Structures in Waves*, Paper No. 11, Institution of Mechanical Engineers, 99-113.

- Frank, W. (1967). "Oscillation of cylinders in or below the free surface of deep fluids." NSRDC Report 2375, Naval Ship R &D Center, Bethesda, Md.
- Froude, W. (1861). "On the rolling of ships." *Trans. Institute of Naval Architects*, Vol. 2.
- Garrison, C. J. (1977). *Hydrodynamic interaction of waves with a large displacement floating body*. Rep. No. NPS-69Gm77091, Naval Postgraduate School, Monterey, California, 159pp.
- Georgiadis, C. (1981). "Wave induced vibrations of continuous floating structures." Ph.D. Dissertation, University of Washington, Seattle, WA.
- Garrison, C.J. (1984). "Wave-structure interaction." *Proc. the specialty Conf. on Computer Methods in Offshore Engineering*, Halifax, Nova Scotia, Canada, May 23, 1-48.
- Goo, J-S and Yoshida, K. (1990). "A numerical method for huge semi-submersible responses in waves." *Transactions, SNAME*, **98**, 365-387.
- Hackbusch, W. (1994). *Iterative Solution of Large Sparse Systems of Equations*, Springer-Verlag, 429 pp.
- Hamida, M. B. and Webster, W. C. (1991). "The motions of large floating flexible structures." *Proceedings, First International Workshop on Very Large Floating Structures*, University of Hawaii, Honolulu, 331-(1)-331-(16).
- Hartz, B. J. (1981). "Dynamic response of Hood canal floating bridge." *Proc. Dynamic Response of Structures*, ASCE, 1981, 16-28.

- Hartz, B. J. and Georgiadis, C. (1982). "A finite element program for dynamic response of continuous floating structures in short-crested waves." *Proc. International Conf. on Finite Element Methods*, Shanghai. 493-498.
- Havelock, T. H. (1942). "The damping of the heaving and pitching motion of a ship." *Phil. Mag*, Vol. 33, 666-673.
- Heller, S. R. and Abramson, H. N. (1959). "Hydroelasticity: A new naval science." *Journal of American Soc. of Naval Engineers*, 71, No. 2, 205-209.
- Hess, J. L. and Smith, A. M. O. (1964). "Calculation of non-lifting potential flow about arbitrary three-dimensional bodies." Rep. No. E. S. 40622, Douglas Aircraft Division, Long Beach, California.
- Hirayama, T., Ma, N. and Ueno, S. (1994). "Influence of flexibility on the motions and deflections of an airport-oriented floating long offshore structure." *Proc. of the Intl. Conf. on Hydroelasticity in Marine Technology*, Eds. Faltinsen et al., May 25-27, Trondheim, Norway, 377-387.
- Inglis, R. B. and Price, W. G. (1982). "A three dimensional ship motion theory- Calculation of wave loading and response with forward speed." *Trans. RINA*, Vol. 124, 183-192.
- John, F. (1950). "On the motion of floating bodies." *Comm. Pure Appl. Math.*, Vol. 3, 45-101.
- Kagemoto, H. and Yue, D. K. P. (1993). "Hydrodynamic interaction Analysis of very large floating structures." *Marine Structures*, 6(2-3): 295-322.

- Kim, W. D. (1963). "On the Forced Oscillations of Shallow-Draft Ships." *J. of Ship Research*, Vol. 7, No. 3, 7-18.
- Kinsman, B. (1965). *Wind waves*. Prentice-Hall, New Jersey.
- Korvin-Kroukovsky, B. V. and Jacobs, W. R. (1957). "Pitching and heaving motions of a ship in regular waves." *Trans. SNAME*, Vol. 65, 1957.
- Krylov, A. (1896). "A new theory of the pitching motion of ships on waves and of the stresses produced by this motion." *Trans. Institute of Naval Architects*, Vol. 37.
- Lamb, H. (1932). *Hydrodynamics*. 6th Edition, Dover Publications, New York, 738pp.
- Langen, I. and Sigbjornesson, R. (1983). "On stochastic dynamics of floating bridges." *Engineering Structures*, Vol. 2, 209-216.
- Lemke, E. (1987) Floating Airports. *Concrete International*, May, 37-41.
- Liu, Y. H., Xie, G. and Lou, J. Y. K. (1991). "The effect of large structural deformation on hydrodynamic loads for a huge floating platform." *Proc. of the first Int. workshop on Very Large Floating Structures*, University of Hawaii, Honolulu, 23-38.
- Lundgren, J., Price, W. G. and Wu, Y (1988). "A hydroelastic investigation into the behavior of a floating 'dry' dock in waves." Spring Meetings 1988, Paper No. 1, The Royal Institution of Naval Architects, London, U. K.
- Mac Camy, R.C. and Fuchs, R. A. (1954). "Wave forces on piles: a diffraction theory." *Tech. Memo. No. 69, Beach Erosion Board*, Coastal Eng. Res. Center, U.S. Army, Washington, D.C.

- Maeda, H, and Eguchi, S (1976). "On the Hydrodynamic Forces for Shallow Draft Ships in Shallow Water (2nd Report), " *J. of the Society of Naval Architects of Japan*, Vol. 139.
- Maeda, H., Maruyama, S., Inoue, R., Watanabe, K., Togawa, S. and Suzuki, F. (1979). "On the motions of a floating structure which consists of two or three blocks with rigid or pin joints. *Journal of Soc. of Naval Arch. of Japan*, **145**, 75-82.
- Mamidipudi, P. and Webster, W.C. (1994). "The Motion Performance of a Mat-Like Floating Airport." *Proc. Int. Conf. on Hydroelasticity in Marine Technology*, Trondheim, Norway, pp 363-375.
- Masuda, K., Maeda, H., Usui, M. and Kato, W. (1987). "Dynamic response by shallow draft floating elastic structures in head waves." *Proceedings, 6th Offshore Mech. & Arctic Engrg. Conf.*, ASME, Houston, 337-344.
- Morison, J. R., O'Brien, M. P., Johnson, J. W. and Schaff, S. A. (1950). "The force exerted by surface waves on piles." *Petroleum Transactions*, AIME, Vol. 189, 149-154.
- Newman, J. N. (1977). *Marine Hydrodynamics*. The MIT Press, Cambridge, Massachusetts, 402pp.
- Newman, J. N. (1978). "The theory of ship motions." *Advances in Applied Mechanics*, **18**, 221-283.
- Newman, J. N. (1985). "Algorithms for the free surface Green function." *Journal of Engineering Mathematics*, **19**, 57-67.

- Newman, J. N. and Sclavounos, P. D. (1986). User manual for FINGREEN. Dept. of Ocean Engineering, M.I.T., Cambridge, Massachusetts, U. S. A.
- Newman, N. J. (1994). "Wave effects on deformable bodies." *Applied Ocean research*, **16**, 47-59.
- Nojiri, N. (1981). "A Study of Hydrodynamic Pressures and Wave Loads on Three-Dimensional Floating Bodies," *IHI Engineering Review* (Japan), Vol. 14, No. 2, April, pp. 6-20.
- Ogilvie, T. F. and Tuck, E. O. (1969). "A rational strip theory of ship motions, Part I." Interim Technical Report No. 013, Dept. of Naval Arch. and Marine Eng., University of Michigan.
- Ogilvie, T.F. (1963). "First- and second-order forces on a cylinder submerged under a free surface." *J. Fluid Mechanics*, **16**: 451-472.
- Okamoto, K., Masuda, K., and Kato, W. (1985). "Hydroelastic response analysis for large floating structures." *Proceedings Intl. Symp. on Ocean Space Utilization '85*, Ed. W. Kato, Tokyo, June 1985, 275-281.
- Paulling, J. R. (1970). "Wave induced forces and motions of tubular structures." *Proc. 8th Symp. on Naval Hydrodynamics*, Pasadena, California, 1083-1110.
- Paulling, J. R. and Tyagi, S. (1991). "Multi-module floating ocean structures." *Marine Structures*, Vol. 6, 187-205.
- Price, W. G. and Wu, Y. S. (1983). "Fluid interaction in multi-hull structures travelling in waves." *Proc. Int. Symp. on the Practical Design of Ship (PRADS 83)*, Tokyo & Seoul, 251-263.

- Rao, S. S. (1989) *The finite element method in engineering*. 2nd Ed., Pergamon Press, 643 pp.
- Reilly, E. T., Shin, Y. S. and Kottte, E. H. (1988). "A prediction of structural load and response of a SWATH ship in waves." *Naval Engineers Journal*, 251-264.
- Riggs, H. R. (1991). "Current efforts in technology development for Very Large Floating Structures." *Proceedings, OCEANS '91 Conference, IEEE, Honolulu, Oct. 3, Vol. 1, 201-206.*
- Riggs, H. R., Che, X. L. and Ertekin, R. C. (1991). "Hydroelastic response of Very Large Floating Structures." *Proc. 10th Intl. Conf. on Offshore Mech. and Arctic Engrg.*, Stavanger, ASME, 1A, 291-300.
- Riggs, H. R. and Ertekin, R. C. (1993). "Approximate methods for dynamic response of multi-module floating structures." *Marine Structures*, 6, 117-141.
- Salvesen, N., Tuck, E. O. and Faltinsen, O. (1970). "Ship motions and sea loads." *Trans SNAME*, Vol. 78, 250-278.
- Seidl, L. H. (1991). "Iterative source distribution technique." *Proceedings First International Workshop on Very Large Floating Structures*, University of Hawaii, Honolulu, 171-190.
- Takarada, N. (1984). "Floating runway for night landing practice of carrier-borne planes." Rep. of Tech. Sub-Committee of The Shipbuilders' Association of Japan.

- Tangirala, A. (1995). "Efficient 3-D Hydroelastic Analysis of Very Large Floating Structures," M.S. Thesis, Dept. of Ocean Engineering, University of Hawaii, Honolulu.
- Wang, D. Y., Riggs, H. R. and Ertekin, R. C. (1991a). "Three-dimensional hydroelastic response of a very large floating structure." *Int. J. Offshore and Polar Engineering*, Vol. 1, No. 4, December, 307-316.
- Wang, M. L. (1991). "A hybrid approach to the hydroelastic analysis of very large floating structures." MS Thesis, Dept. of Ocean Eng., Univ. of Hawaii at Manoa, Honolulu, 191 pp.
- Wang, M. L., Du, S. X. and Ertekin, R. C. (1991b). "Hydroelastic response and fatigue analysis of a multi-module very large floating structure." *Proceedings, Intl. Symp. on Fatigue and Fracture in Steel and Concrete Structures, ISFF '91*, Eds. A. G. M. Rao and T. V. S. R. A. Rao, Madras, India, Dec., Oxford & IBH Pub. Co., Bombay, 2, 1277-1291.
- Wang, S., Ertekin, R. C. and Riggs, H. R. (1993). Hydroelastic analysis of Very Large Floating Structures: EMFC method with frequency-dependent coefficients. Rep. No. UHMOE-93112, Dept. of Ocean Engineering, Univ. of Hawaii at Manoa, Honolulu, Hawaii, December, 57pp.
- Wang, S., Ertekin, R. C., Stiphout, A.T.F.M. and Ferrier, P.G.P. (1995a). "Hydroelastic-response analysis of a box-like floating airport of shallow draft." *Proc. of the Fifth Int. Offshore and Polar Engineering Conference*, The Hague, The Netherlands, June 11-16, Vol. 1, 145-152 (submitted to IJOPE).

- Wang, S., Ertekin, R. C. and Riggs, H. R. (1995b). "On Increasing Computational Efficiency in Hydroelasticity of VLFS," *Proc. 14th Int. Conf. on Offshore Mech. & Arctic Engineering*, Copenhagen, Denmark, June 18-22, Vol. 1-A, 455-463 (Submitted to Computers and Structures journal).
- Webster, W. C. (1991). "Considerations for the design of floating airport." UJNR Meeting, Tokyo, Japan.
- Wehausen, J. V. and Laitone, E. V. (1960). "Surface Waves." Ed. S. Flüge, *Handbuch der Physik*, Band 9, Springer-Verlag, 446-776.
- Wilkins, G. A., Ertekin, R. C. and Riggs, H. R., Editors, (1992). "Future directions in VLFS research and development." *Proc. 1st. Int. Workshop on Very Large Floating Structures, VLFS '91*, Vol. 2, University of Hawaii at Manoa, Honolulu, January, 42 pp.
- William, H. P., Saul, A. T., William, T. V. and Brian, P. F. (1992). "Numerical Recipes in Fortran," Cambridge University Press, 961 pp.
- Winkler, R. S., Seidl, L. H., Riggs, H. R., Ertekin, R. C. and Wilkins, G. A. (1990). The design and analysis of very large floating structures (VLFS): Vol. 1 - Design. Rep. No. UHMOE-90105, Dept. of Ocean Engrg., Univ. of Hawaii, June.
- Wu, X. J. and Price, W. G. (1986). "A Method to Analyses Shallow Draft Offshore Structures with Six Modes of Motion," *Proc. 5th Int. Conf. on Offshore Mech. & Arctic Eng.*, Tokyo, Vol. 1, pp 476-482.

- Wu, Y. S. (1984) *Hydroelasticity of floating bodies*. Ph. D. Dissertation, Brunel University, U. K.
- Wu, Y. S., Wang, D., Riggs, H. R. and Ertekin, R. C. (1993). "Composite singularity distribution method with application to hydroelasticity." *Marine Structures*, **6**, 143-163.
- Yeung, R. W. (1973). "A singularity distribution method for free surface flow problem." Rep. No. NA-73-6, Dept. of Naval Architecture, University of California, Berkeley, vi + 124 pp.